

STUDIA
UNIVERSITATIS BABEȘ-BOLYAI

PHYSICA

38(1)

1993

CLUJ-NAPOCA

REDACTOR ȘEF: **Prof. A. MARGA**

REDACTORI ȘEFI ADJUNCȚI: **Prof. N. COMAN, Prof. A. MAGYARI, Prof. I. A. RUS,
Prof. C. TULAI**

COMITETUL DE REDACȚIE AL SERIEI FIZICĂ: **Prof. E. BURZO (redactor
coordonator), Prof. I. ARDELEAN, Prof. O. COZAR, Prof. S. SIMON, Prof. E.
TĂTARU, Conf. A. NEDA, Cercet. șt. II S. COLDEA (secretar de redacție)**

S T U D I A

UNIVERSITATIS BABEŞ-BOLYAI

PHYSICA

1

Redacția 3400 CLUJ-NAPOCA str. M. Kogălniceanu nr. 1 ▶ Telefon 116101

SUMAR - CONTENTS - SOMMAIRE

Molecular Physics and Spectroscopy

P. ARDELEAN, F. DUNCA, C. CUNA, D. IOANOVICIU, A. PAMULA, C. ARDELEAN, I. MALZ, Medium Size Normal Circle Bounded Homogeneous Magnetic Field Single Focusing Mass Spectrometer with Improved Resolution	3
M. CIULEA, N. PALIBRODA, S. NICOARĂ, O. COZAR, I. OPREAN, I. FENEŞAN, Electron Impact Fragmentation of Some Thionic-Dioxaphosphorinan-Arylsulphonamide Derivatives	11
T. ILIESCU, S. SIMON, I. ARDELEAN, N. MARTON, Raman Spectroscopic Study of the Structure of $B_2O_3-Li_2O-CuO$ Glasses	23
G. V. DAMIAN, Comparison of Interaction Energies for Methane Using Buckingham and Lennard-Jones Potentials	31

Plasma Physics

S. D. ANGHIEL, A RF Generator for Capacitively coupled Plasma at Atmospheric Pressure	39
S. COLDEA, Application of the Simulation Method for a Gyrotron Amplifier	53

Theoretical Physics

D. JALOBEANU, L. TĂTAR, The BRST-BV Symmetry in Classical Mechanics	63
I. ARDELEAN, Thermodynamic Theory of Cross-Polarization in a NMR-Moist Experiment	69
S. CODREANU, The Reconstruction of the State Space from Chaotic Time Series	75
A. MIHÁLY, The Behaviour of the Nucleon Spin in a Periodic Phase of the Nuclear Matter	89



MEDIUM SIZE NORMAL CIRCLE BOUNDED HOMOGENEOUS MAGNETIC FIELD SINGLE FOCUSING MASS SPECTROMETER WITH IMPROVED RESOLUTION

P.ARDELEAN*, F.DUNCA*, C.CUNA*, D.IOANOVICHU*, A.PAMULA*, C.ARDELEAN**, L.MALZ*

Received 10.04 1993

ABSTRACT. - A 90° deflection normal circle sector homogeneous magnetic field mass spectrometer was constructed and tested. The instrument was designed for a mean ion path radius of 100 mm. The mass spectrometer main parts are described. A peak half height resolution of 1570 was obtained at an ion current of 0.16×10^{-12} A for a final accelerating slit of 0.02 mm. For a slit 0.03 mm wide the resolution was 1410 while the ion current increased to 0.85×10^{-12} A. The instrument was operated at even higher intensities, currents of 0.9×10^{-10} A being collected with resolutions over 200, the final accelerating slit width being set to 0.5 mm.

1. Introduction. The mass spectrometer was designed for isotopic concentration analysis. It can be used for gases and volatile liquids, by covering the mass range from 1 to 200 mass units.

The design with circular boundaries, normal beam entry and exit was found to be the most appropriate for our purposes. An ion main path radius of 100 mm was selected to satisfy both resolution and sensitivity requirements simultaneously without excessive instrument size and weight increase.

2. Description The main parts of the mass spectrometer (Fig 1) are the sample inlet system (IS) with its own vacuum system, the ion source (S), the analyzer (A), the detection

* *Institute of Isotopic and Molecular Technology, P O Box 700, 3400 Cluj-Napoca, Romania*

** *Technical University, Department of Automatisation and Computers, 3400 Cluj-Napoca, Romania*

system (D) and the main vacuum system

The sample introduction system is a standard one, allowing the simultaneous attachment of two samples. The valves ensure the separation of the two introduction ways, and the separate introduction of the samples into the expanding container. These valves also allow the evacuation of the introduction system after the end of the analysis.

From the container, the sample to be analysed is admitted by a capillary tube into the ion source.

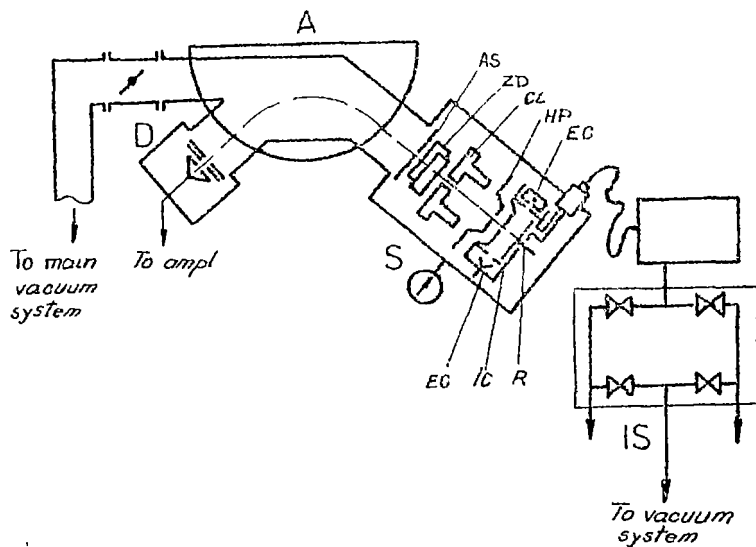


Fig 1 A schematic diagram of the mass spectrometer

The introduction system is evacuated by a 4m³/h rotary pump

The ion source of the mass spectrometer was derived from the modified Nier design [1]. It consists (Fig 1) from an ionization chamber (IC) with the electron gun (EG) and ion repeller (IR), the half plates (HP), the cylindrical lens (CL), the z deflectors (ZD) and the final ion beam accelerating slit (AS). The electrodes were manufactured from nonmagnetic

MEDIUM SIZE NORMAL CIRCLE

stainless steel, and are aligned by ceramic spacers and supported by a system of iron rods. The electrons are collected by an electron collector (EC) housed in the ionisation chamber, the collector field being screened by a shield with a slit for the electrons.

The energy of the ionizing electrons produced by a rhenium filament is usually of 60-100 eV [2]. The value of the ionizing current measured on the electron collector (EC) is stabilized on the range 10-70 μA .

An auxiliary collimating magnetic field of 100 Oe ensures the electronic beam focusing. To this value must be added a small component due to the stray field of the main analyzer.

The optimum potential of the repeller related to the ionization chamber was established experimentally to be around +1.8 V to maximize the resolution and keeping a good sensitivity.

The analyzer is a 90° normal circle homogeneous magnetic sector field. The mean ion path curvature radius is of 100 mm. The second order focusing properties of this design allowed us to obtain a good resolution for a relatively small curvature radius.

In this respect it was possible to use a radius of 100 mm, and to keep the instrument global size between limits acceptable for usual research work [3]. The magnetic sector position can be regulated by a screw and it was accurately located between the ion source final slit and the collector, accounting for the fringing field effects [4, 5]. The magnetic sector is provided with magnetic screens.

The magnetic circuit of "C" type design was made from Armco iron with the coil on the central yoke section.

The ion collection system consists of a grounded variable slit, an antidynatron slit and

a Faraday cage connected to an electrometer amplifier

The main vacuum system consisting of a PVDIF-04-100 type oil diffusion pump, provided with a liquid nitrogen cod trap designed especially for the efficient retention of the oil vapours permitted to obtain a pressure under 10^{-6} torr in the absence of the sample

The vacuum valves are electrically acted by the control and protection unit which closes them and disconnects the heater of the diffusion pump, the high voltage unit and also the electron gun supply in case of vacuum system failure

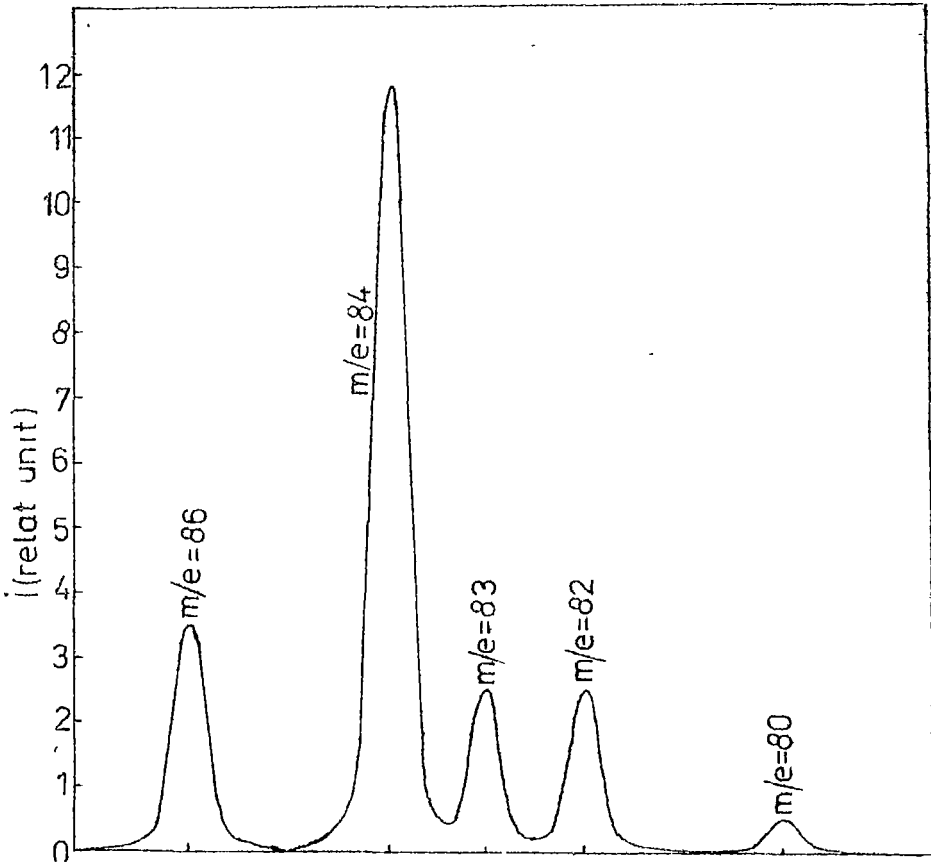


Fig 2 The mass spectrum of the Kr obtained for a final slit width of 0.5 mm

3. Experimental results and discussion. The measurements were performed on the isotopic peaks of Krypton. By using a large 0.5 mm wide final accelerating slit a resolution R_s of 210 at 50 % peak height (Fig 2) was obtained at $m/e = 80$ to $m/e = 86$ the ion current intensity being 0.9×10^{-10} A. The intensity of the ionizing current was 25 μ A.

An accelerating voltage of 2.1 kV was applied on the ion source.

To calculate the resolution at peak half height from the mass spectrum the following formula was used

$$R_s = m_M L / (n \Delta l) \quad (1)$$

where m_M is the average value of the masses $m_M = (m_1 + m_2)/2$ in u, Δl is the width of the greatest peak at half height in mm, L is the distance on the spectrum between the peak centroids also in mm, n is the distance between the m_1 and m_2 in mass units(u).

A resolution R_s as peak half height of 350 for a final ion beam accelerating slit of 0.25 mm at an ion current intensity of 0.7×10^{-10} A was measured. The resolution increased to 840 at an ion current intensity of 1.5×10^{-12} A for an accelerating slit of 0.07 mm.

In the case of a final ion source slit reduced to 0.03 mm (Fig 3) the value of the resolution was 1410 at an ion current intensity of 0.85×10^{-12} A.

The best resolution 1570 was reached for an accelerating slit width of 0.02 mm at a current of 0.16×10^{-12} A (Fig 4).

The theoretical peak half height resolution can be estimated with the formula

$$R_t = [s/C + \Delta U_s / U + \Delta U_f / U + 2 \Delta I_m / I_m]^{-1} \quad (2)$$

where s is the width of the final source slit, C the ion main path radius, $e\Delta U_s$ the difference between the energies of the ions formed at the same point of the source at different instants, produced by high voltage short time instabilities or noise, in our case 1×10^{-3} of the value of

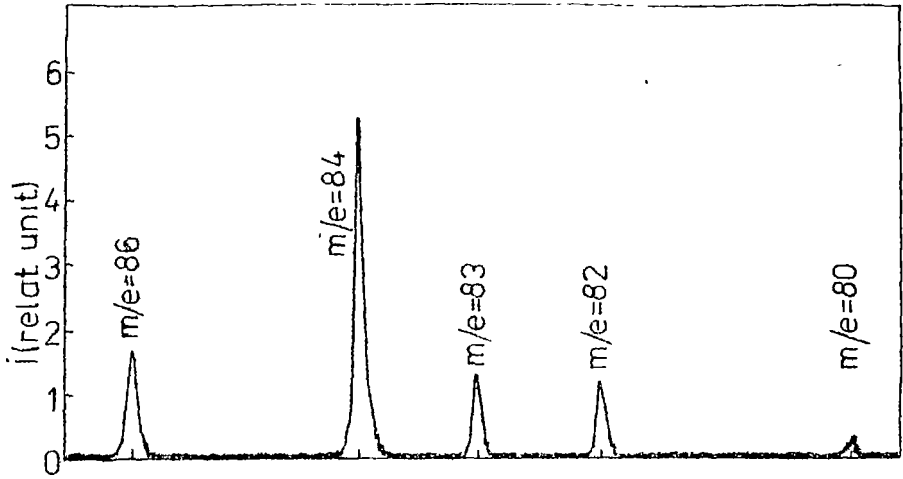


Fig 3 The mass spectrum of the Kr for a final ion source slit of 0.03 mm

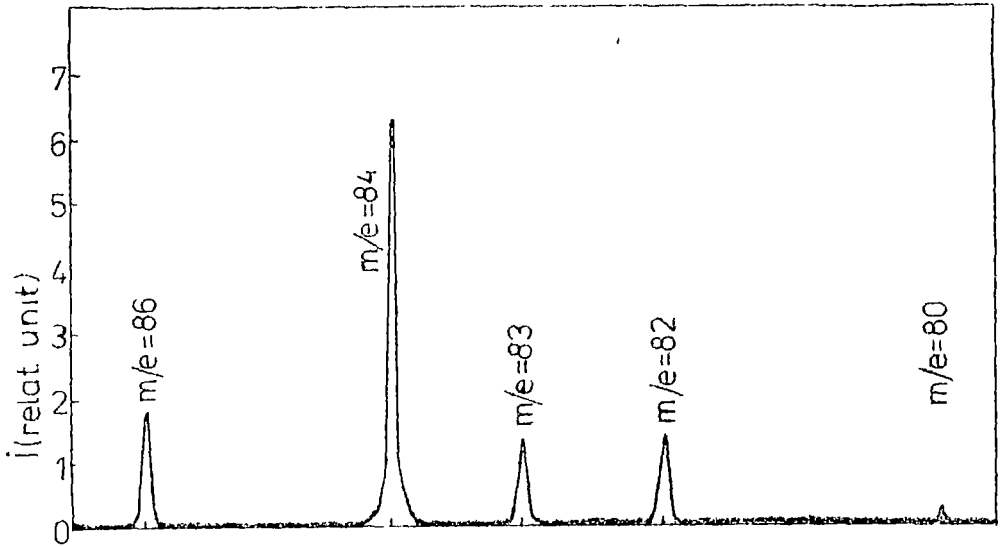


Fig 4 The mass spectrum for a final ion source slit width of 0.02 mm

the ion accelerating voltage U , $e\Delta U_i$ the beam energy spread due to the thickness of the ionization region, typically 0.5 eV, ΔI_m the instability or noise of the magnet current supply, in our case also 1×10^{-5} and e the ion electric positive charge

In Fig 5 two $R_i = f(s)$ curves are given for instabilities of 1×10^{-4} and 2×10^{-4} respectively. The open dots are the values obtained experimentally, quite close by the

MEDIUM SIZE NORMAL CIRCLE

theoretical values

As it can be seen, for wider final ion accelerating slits the resolutions practically coincide with the theoretical values indicating a good focusing of the ion beam. The size of the ion-optical object is equal or in the case of 0.5 mm slit a little bit thinner than the width of the final accelerating slit.

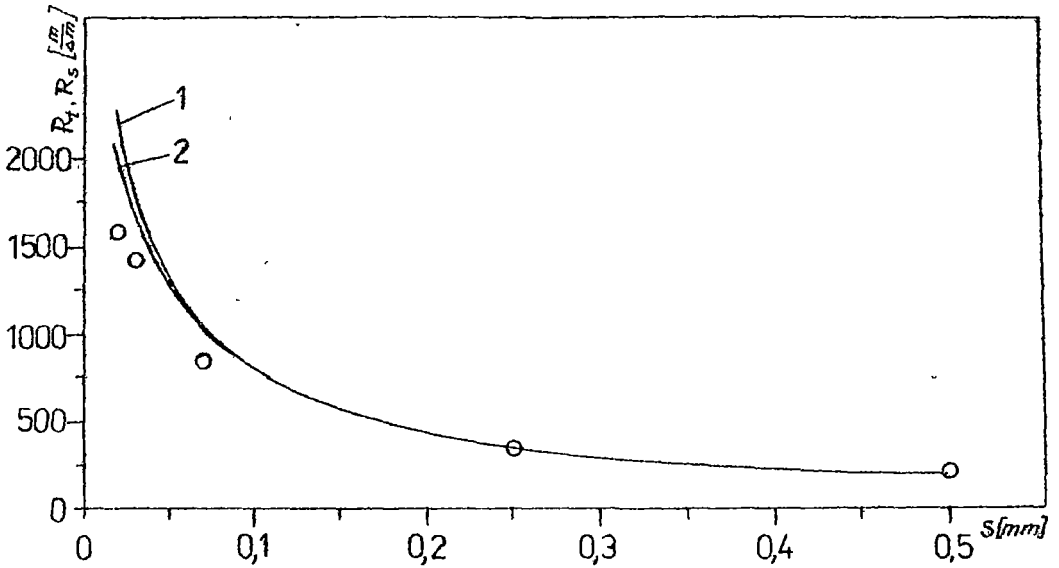


Fig 5. The calculated resolution $R_y = f(s)$ 1 - calculated for an instability of 1×10^{-5} , 2 - for an instability of 2×10^{-5} , o - the data obtained from spectra (R_s)

It is also possible that the beam energy spread caused by the ionization region thickness is smaller than the value 0.5 eV usually assumed, and this could also be responsible for the good resolution obtained.

For 0.07 mm, 0.03 mm and 0.02 mm final accelerating slit widths the experimental resolution is close to the theoretical values indicating that the focusing properties of the ion source using cylindrical lenses enabled to deliver a well focused ion beam.

The position of the analyzer sector, as well as the position of the magnetic screens is quite critical and any small displacement affects the instrument resolution

Acknowledgements. The authors thank Prof Dr V Grecu, Dr N Palibroda and Dr D Ursu for helpful discussions

R E F E R E N C E S

- 1 J Barnard, *Modern Mass Spectrometry*, The Institute of Physics, London, 1953, p 60.
- 2 V Mercea, P Ardelean, D Ioanoviciu, A Pamula, D Ursu, *Introducere in Spectrometria de Masa*, Edit Tehnica, Bucuresti, 1978, p 43
- 3 C A McDowell, *Mass Spectrometry*, McGraw-Hill Book Comp Inc , 1963, p 104
- 4 H Matsuda and H Wollnik, *Nucl Instrum Methods*, 77, 50 (1969)
- 5 H A Enge, *Rev Sci Instrum* , 35 278 (1961)

ELECTRON IMPACT FRAGMENTATION OF SOME THIONIC-DIOXAPHOSPHORINAN-ARYLSULPHONAMIDIC DERIVATIVES

M.CULEA*, N.PALIBRODA*, S.NICOARĂ**, O.COZAR***, I.OPREAN****, I.FENEŞAN****

Received 19 11 1993

ABSTRACT. - The mass spectra and the fragmentation pathways obtained by electron impact of Phenyl- (1), 2-p-methyl- (2), 2-p-fluorine- (3), 2-p-chlorine- (4), 2-p-bromide- (5), and 2-p-methoxy- (6) -phenylsulphonamido-2-thiono-5, 5-dimethyl-1,3,2-dioxaphosphorinanes are presented. Accurate mass measurements and metastable transitions detection for compound (1) were used to elucidate the proposed fragmentation reactions

Introduction. Organophosphorus compounds are widely used as pesticides, therapeutic and plastifying agents, due to their structure and biological potential. Their thioderivatives were increasingly studied lately /1-8/

The articles on the mass spectrometry of these compounds outline that the fragmentation mechanisms depend on the nature of the atoms bonded to the P atom /7/

The aim of this work is to interpret the mass spectra and the fragmentations under 70 eV electron impact of some [(1)-(6)]2-arylsulphonamido-2-thiono-5, 5-dimethyl-1,3,2-dioxaphosphorinanes which contain the P=S and P-N bonds /7/ Their structural formula is presented in Fig 1

Experimental. The compounds (1)-(6) were synthesized at the Chemistry Institute

* Institute of Isotopic and Molecular Technology, 3400 Cluj-Napoca, Romania

** Technical University, Department of Physics, 3400 Cluj-Napoca, Romania

*** "Babeş-Bolyai" University, Faculty of Physics, 3400 Cluj-Napoca, Romania

**** Institute of Chemistry, 3400 Cluj-Napoca, Romania

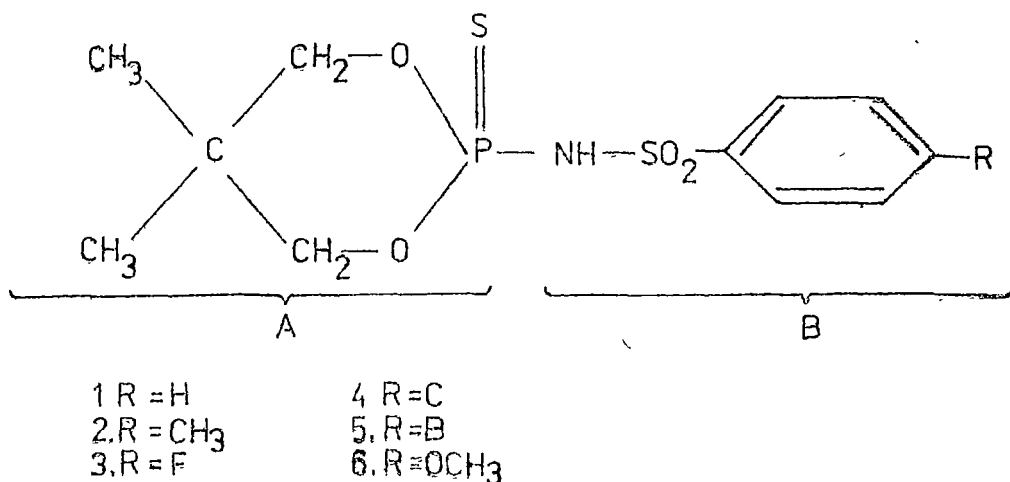


Fig 1 Structural formula of the compounds (1)-(6)

from Cluj-Napoca, Romania, by a substitution reaction between 2-chlorine-2-thiono5, 5-dimethyl-1,3,2-dioxaphosphorinane and the sodium salts, of the corresponding arylsulphonamides [7]

Measurements were made using a MAT 311 mass spectrometer with inverse Nier-Johnson geometry. Standard operating conditions were 70 eV electron energy, 100 μ A emission current, 150°C ion source temperature and 700 resolving power.

The direct inlet system was used at the optimum evaporation temperatures 85°C (1), 95°C (2), 80°C (3), 100°C (4), 120°C (5) and 125°C (6).

Metastable transitions, registered by the HV and MIKE techniques [9,10], confirmed the fragmentations for compound (1). High resolution measurements were used in the peak matching mode, to determine the accurate chemical formulae of the ions [9].

Results and discussion. The 70 eV electrons impact mass spectrum of compound (1) is shown in Fig. 2.

ELECTRON IMPACT FRAGMENTATION

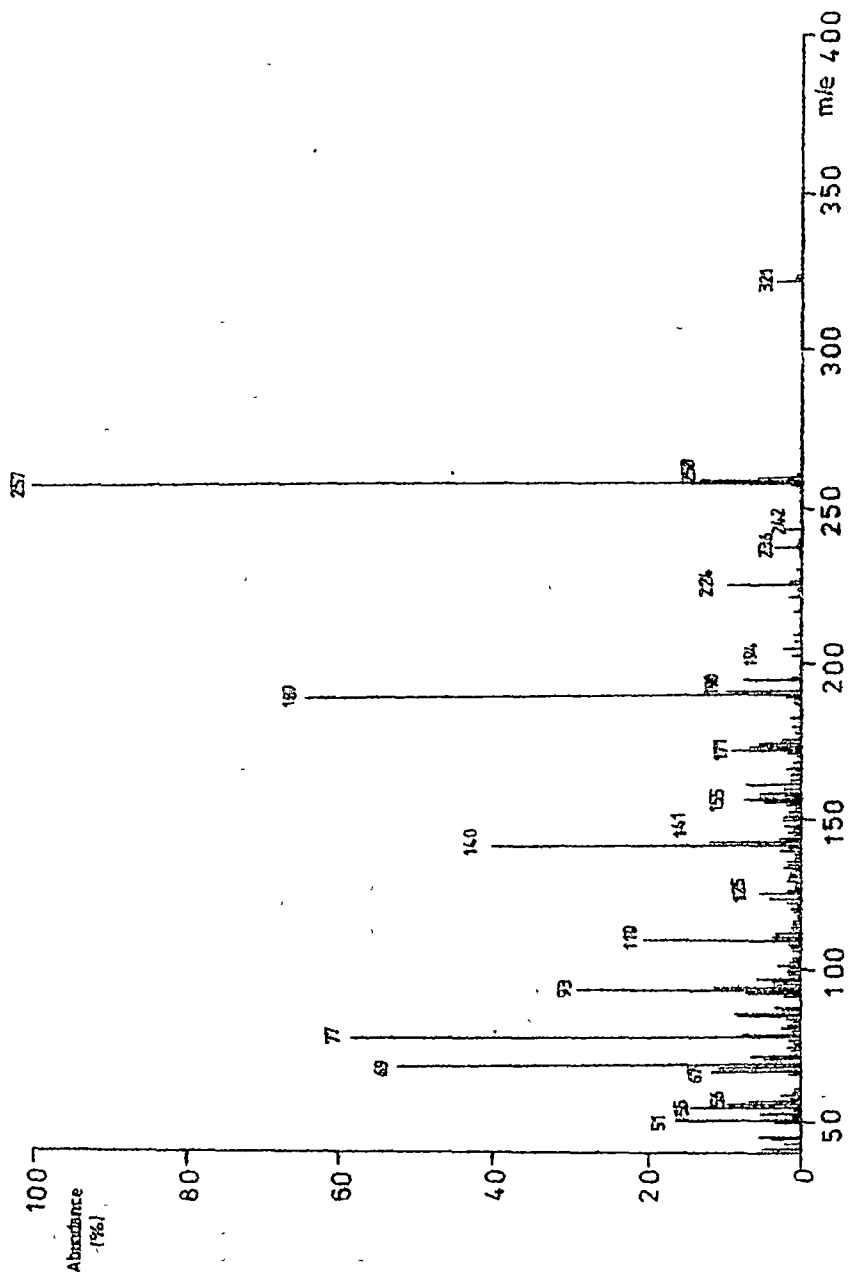


Fig 2 Mass spectrum of compound (1)

Table 1 presents the main fragment ions in the mass spectra of compounds (1)-(6) and

Fig 3-5 show the proposed fragmentations together with the structures of the ions

Ion	(1) m/e(%)	(2) m/e(%)	(3) m/e(%)	(4) m/e(%)	(5) m/e(%)	(6) m/e(%)
M ⁺ (320+R)	321(4)	335(2%)	339(4)	355(2)	399(1)	351(2)
a(236+R)	257(100)	271(100)	275(100)	291(100)	335(100)	287(100)
b(241+R)	242(2.5)	258(2)	260(2)	276(2)	320(1.5)	272(3)
c(207+R)	208(1.5)	222(1)	226(-)	242(1.5)	285(1.5)	238(0.5)
d(223+R)	224(9)	238(9)	242(8)	258(6)	302(3)	254(2)
e(201+R)	202(1.5)	216(2)	220(2)	236(1)	280(1)	232(-)
f(171+R)	172(8)	185(12)	190(6)	206(4)	231(1)	232(5)
g(189+R)	190(10)	204(4)	208(10)	224(8)	268(8)	220(4)
h(188+R)	189(68)	203(36)	207(65)	223(16)	267(44)	219(26)
i(170+R)	171(10)	185(14)	109(8)	205(12)	248(8)	201(21)
j(154+R)	155(8)	169(9)	173(8)	189(8)	233(8)	185(20)
k(224+R)	225(1.5)	239(3)	243(2)	259(1)	303(1)	265(0.5)
l(223+R)	224(10)	238(9)	242(7)	258(6)	302(3)	254(2)
m(193+R)	194(7)	208(7)	212(6)	228(5)	272(1)	224(2)
n(165)	165(3)	165(2)	165(4)	165(3)	165(3)	165(4)
o(133)	133(3)	133(2.5)	133(4)	133(4)	133(3)	133(1.5)
p(140+R)	141(13)	155(12)	159(16)	175(11.5)	201(10)	171(15)
q(124+R)	125(7)	139(8)	143(7)	159(7)	203(5.5)	125(7)
r(92+R)	93(27)	107(21)	111(30)	127(24)	171(20)	127(24)
s(76+R)	77(58)	91(48)	95(46)	111(34)	155(23)	111(34)
t(155+R)	156(4)	170(3)	174(4)	190(2)	234(3)	174(4)
v(235+R)	236(4)	250(3)	254(3)	270(3)	314(3)	236(4)
w(139+R)	140(40)	154(23)	158(39)	174(20)	218(20)	140(40)
z(203+R)	204(2)	218(1.5)	222(5)	238(2)	282(3)	234(2)

Table 1 Mass spectral data for compounds (1)-(6)

In all cases, M⁺ produces low intensity peaks (<2%) and eliminates the neutral molecule SO₂ as reported in similar studies /3,4,11,12/, giving the base peaks at ions *a* (See Fig 3) Afterwards, like other dioxaphosphorinanes /8/, ions *a* loose one CH₃ group, leading to ions *b* and, consequently, to the structures *c* or *d* The latter ions occur by the elimination of the neutral molecules H₂S or H₂O, respectively, processes already encountered for thiophosphororganic molecules containing O /4,12-15/

Ions *a* may also loose the radical C₂H₅ and form the structure *e* in Fig 3 This

ELECTRON IMPACT FRAGMENTATION

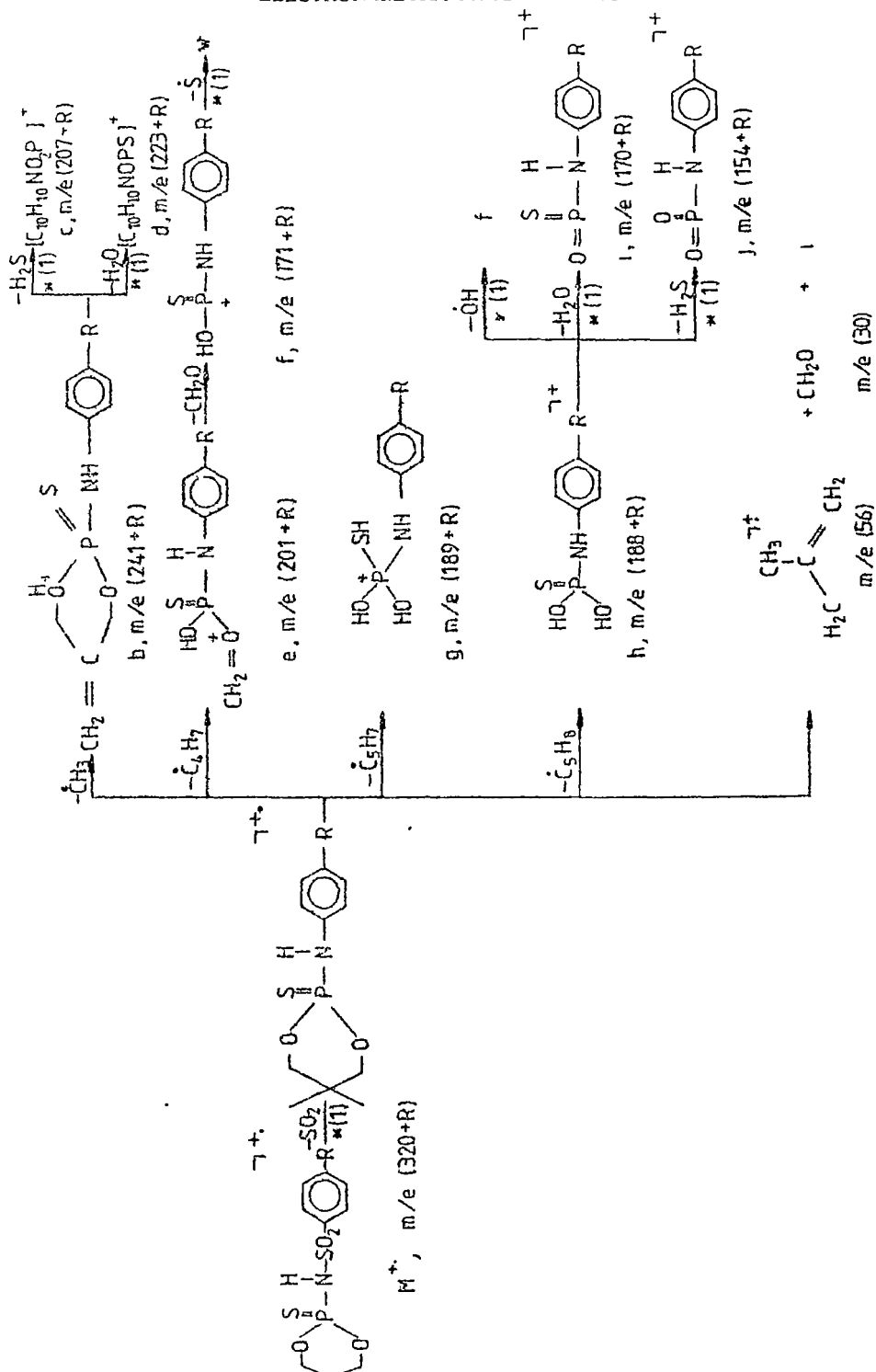


Fig. 3 Reactions starting with the loss of the SO₂ group prior to the heterocycle fission.

fragmentation is produced by the cleavage of the dioxaphosphorinanic cycle (part A of the molecule in Fig 1), which is a frequent process in the organophosphorus compounds with this kind of heterocycle /1,8,16,17/

Ions *e* may eliminate the neutral molecule CH_2O , by the P-O bond fission, as reported in likely situations /12,15/

The ions *W* are produced from the structure *f* by the elimination of the S atom, subsequent to the P=S double bond fission, process confirmed by the metastable transitions and mentioned in other thiophosphororganic compounds /1,15/.

Undergoing a rearrangement process by a five membered transition state, as proposed by Edmundson /8/, ions *a* loose the radical C_3H_7 , and produce ions *g*, in Fig. 3

The cleavage of the dioxaphosphorinanic cycle in ions *a* and the elimination of the radical C_3H_8 probably leads to the structure *h*. Reactions of this kind were formerly reported /8,19,20/

Ions *h* conduct to ions *f*, by loosing one OH side group, as found for similar cases /13,18/

Metastable detections confirmed that ions *h* eliminate a neutral H_2O molecule to produce ions *i* or a neutral H_2S molecule to form ions *j*, processes frequently observed in organic compounds containing O and S /4,12-14,21/

These results concerning the dioxaphosphorinanic cycle cleavage, present an obvious similarity to those already reported /8/

Figure 4 proposes other fragmentations pathways for ions *a*. They may loose S, to form scarcely observed ions *k*, or loose the radical SH and produce important ions *l*. This is opposite to the results mentioned in the literature, on the A type of compounds /8/, but an

ELECTRON IMPACT FRAGMENTATION

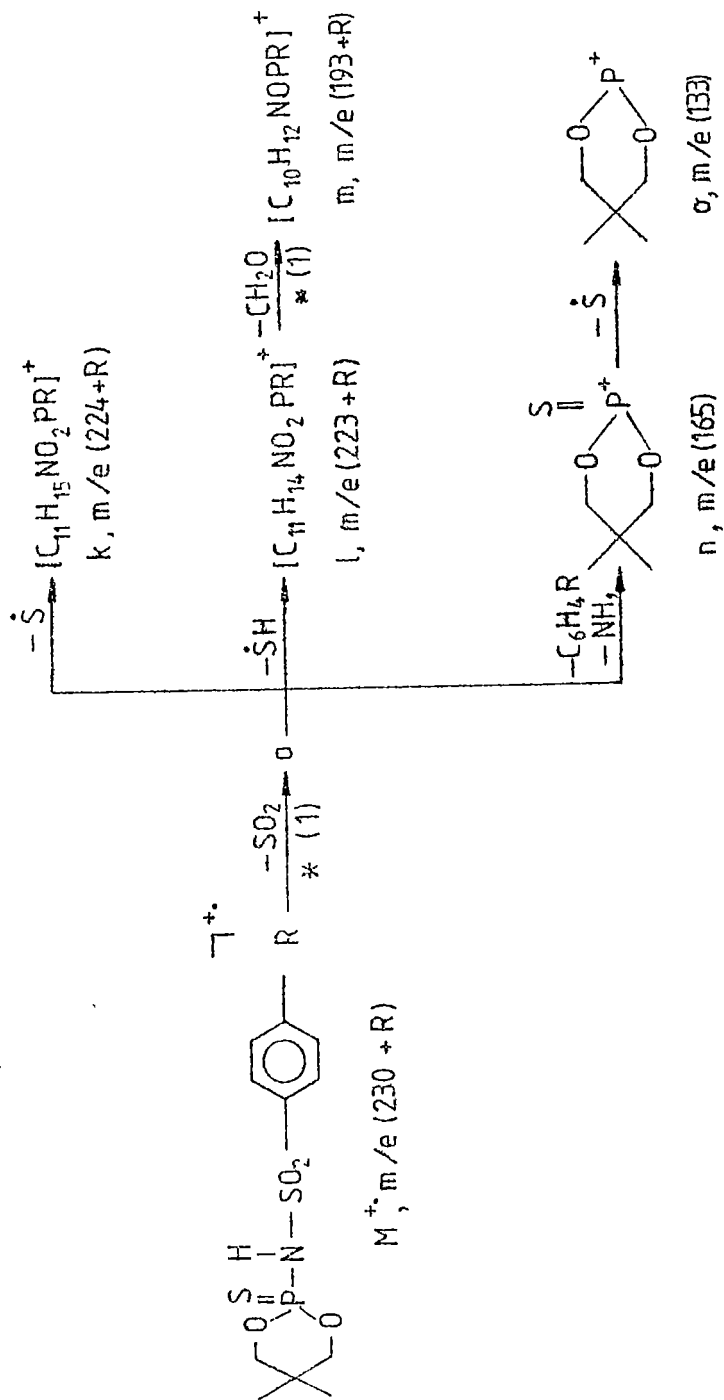


Fig 4 Reactions starting with the loss of the SO₂ group prior to the elimination of neutral radicals or atoms

explanation could be given by considering the increased acidic feature of the amide proton, in our compounds (1)-(6). This does not yet exclude the Edmundson's conclusion /8/ that a methylenic proton from the cycle gives its contribution to the SH elimination.

Metastables detection proved that ions *l* lose CH_2O , as already reported /15,19/, to form ions *m* (See Fig 4).

Finally, producing ions *n*, the ions *a* may eliminate the fragments NH and $\text{C}_6\text{H}_4\text{R}$, other simultaneous losses of more fragments, being sometimes observed /22,23/. Subsequently, ions *n* form the ions *o*, by breaking the double $\text{P}=\text{S}$ bond, as Edmundson also reported. The abundances of ions *n* and *o* are ten times lower for our substances than other data on the A type of compounds /8/. This difference is the different ways that the π electrons distribute between the $\text{P}=\text{S}$ and the $\text{P}-\text{N}$ bonds, inside the molecular ion M^+ , which is an aromatic amide in this case (Fig 1) and an aliphatic amide in the literature.

Figure 5 presents another fragmentation scheme for the molecular ions M^+ . They undergo simple fission of the $\text{N}-\text{S}$ bond and form ions *p* which subsequently may lose one O atom, to give ions *q*, SO , to produce the structure *r*, or SO_2 , to form ions *s*. These eliminations are common for organics containing SO_2 , /3,4,11/.

The simple fission of the $\text{P}-\text{N}$ bond, frequently encountered in phosphororganics with N /22/, produces the ions *t*, from the molecular ions.

The dioxaphosphorinanic cycle may undergo cleavage even in the molecular ions, producing the structure *v* in Fig 5.

Ions *v* eliminate SO_2 to form ions *f* which subsequently lose one S atom and produce ions *w*.

The ions *z* may result from *v*, by the elimination of the S atom and further conduct

ELECTRON IMPACT FRAGMENTATION

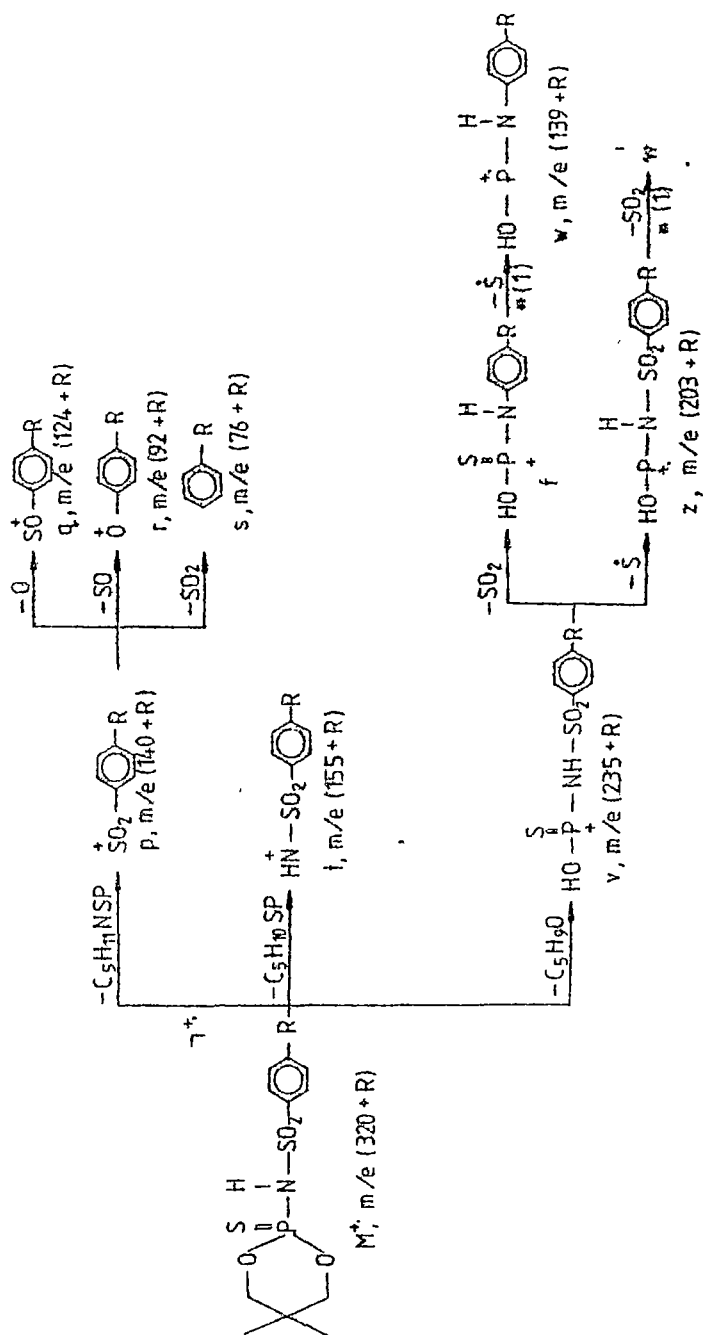


Fig 5 Reactions starting by simple fission or rearrangement of the molecular ion $M^{\bullet+}$

to ions w , by loosing the SO_2 group. Metastable measurements indicated the reaction $f \rightarrow w$, as well as $z \rightarrow w$.

In all spectra, important ions at m/e 77, 56, 55 and 51 are present due to the fragmentation of the aryl group.

Ions at m/e 69, also important in all spectra, result from the fission of the heterocyclic part of the molecular ion M^+ and consist of the fragment having the following elemental formula C_3H_9 .

Conclusions. These compounds mainly pursue fragmentation by the cleavage of both the arylsulphonamidic and the dioxaphosphorinanic sides of the molecules.

All six substances show low molecular ions (<3%) The base peaks, in all spectra, are given by ions a , formed from M^+ which loose SO_2 .

The fragments a undergo rearrangement reactions involving H transfer inside the dioxaphosphorinanic cycle as well as from this cycle to the S atom, subsequently eliminating CH_3 , C_4H_7 , C_5H_7 and C_5H_8 (neutral radicals).

During the fission reactions, the following groups are also eliminated: SO_2 , H_2O , H_2S , CH_2O (neutral molecules) and O, S, SH, OH, SO, NH, $\text{C}_6\text{H}_4\text{R}$, $\text{C}_5\text{H}_9\text{O}$ (neutral atoms or radicals).

REFERENCES

- 1 Z Moldovan, M Culca, N Palibroda, I Fenesan and R Popescu, *Org Mass Spectrom*, **26**, 840(1991)
- 2 Z Moldovan, N Palibroda, M.Culea, I Fenesan and A Hantz, *Org Mass Spectrom*, **24**, 81(1989)
- 3 R Popescu, I Oprean, N Palibroda and Z Moldovan, *Studia Univ "Babeş-Bolyai", Chemia*, XXXIV, **1**(1989)
- 4 R.Popescu, I Oprean, N Palibroda and Z Moldovan, *Studia Univ "Babeş-Bolyai", Chemia*, XXXIII, **1**(1988)
- 5 E J Griffith and M Graison, "Topics in Phosphorus Chemistry", Wiley-Interscience, New-York (1976)
- 6 S Safe and O Hutzinger, "Mass Spectrometry of Pesticides and Pollutants", CRC Press, Cleveland (1976)
- 7 I Fenesan, V Mureşan, A Barabas and M Bogdan, *Rev Roum. Chim.*, **29**, 761(1984)
- 8 R S Edmundson, "Phosphorus and Sulphur", **9**, 307(1981)
- 9 R G.Cooks, J H.Beynon, R.M Caprioli and B R Lester, "Metastable Ions", Elsevier, Amsterdam (1973)
- 10 Z Moldovan, N Palibroda, V Mercea and G Mihailescu, *Org Mass Spectrom*, **20**, 77 (1985)
- 11 J H Bowie and M B Stringer, *Org Mass Spectrom.*, **20**, 138 (1985)
- 12 M C Hamming and N G Foster, "Interpretation of Spectra of Organic Compounds", Academic Press, New-York (1972)
- 13 D V Ramana et al, *Org Mass Spectrom.*, **26**, 303 (1991)
- 14 Pradip R Das et al., *Org Mass Spectrom*, **26**, 703 (1991)
- 15 M Vairamuni et al, *Org Mass Spectrom.*, **26**, 33 (1991)
- 16 E Wyrzykiewicz and W Wysocka, *Org Mass Spectrom*, **25**, 453 (1990)
- 17 A S Płaziak et al, *Org Mass Spectrom*, **26**, 849 (1991)
- 18 D Rasala and R Gavinecki, *Org Mass Spectrom*, **24**, 135 (1989)
- 19 G Sollazzo, R.Tonani and P Taldi, *Org Mass Spectrom*, **23**, 550 (1988)
- 20 A Sturaro et al., *Org Mass Spectrom*, **22**, 462 (1987)
- 21 Z Moldovan, M Culca, N Palibroda, E Gros, R Nutu and I Gros *Org Mass Spectrom*, **21**, 474 (1987)
- 22 M Lozynski et al, *Org Mass Spectrom*, **21**, 33 (1986)
- 23 I Vidawsky et al, *Org Mass Spectrom*, **26**, 287 (1991)
- 24 R G Cooks and A F Gerard, *J Chem Soc B*, 1327 (1968)



RAMAN SPECTROSCOPIC STUDY OF THE STRUCTURE
OF B_2O_3 - Li_2O - CuO GLASSES

T. ILIESCU, S. SIMON, I. ARDELEAN and N. MARTON*

Received 10 03 1993

ABSTRACT. - The influence of the melting temperature (1273 K and 1573 K) and of the CuO content on the network structure in the $(1-x)[2B_2O_3, Li_2O] xCuO$ glasses with $0 \leq x \leq 0.05$ mol % is investigated by Raman spectroscopy. At melting temperature 1573 K the glass network is broken in a larger mode like than at temperature 1273 K. Copper oxide acts as modifier in lithium borate glasses in which are present six membered borate rings with two BO_4 tetrahedra, chain type metaborate group, ortoborate, pyroborate and free BO_4 units.

Introduction. The most common glasses are formed by mixing glass forming oxides (SiO_2 , B_2O_3 , P_2O_5) with modifier metal oxide [1]. The oxygen from the metal oxide becomes part of the covalent glass network by creating new structural units. Raman spectroscopy is a powerful and efficient tool for resolving the structure of local arrangements in glasses.

Raman spectra of binary lithium borate glasses were investigated at different lithium oxide concentration by many authors [2,3]. In the Raman spectra of B_2O_3 glasses there is a specific strong band at 807 cm^{-1} assigned to the boroxol rings in which boron atom is three coordinated [2]. The addition of alkali oxide Li_2O to B_2O_3 determines the appearance in the Raman spectra of a new band about 780 cm^{-1} Brill [4] assigned this peak to the formation of six membered borate rings containing one BO_4 tetrahedron (boron atom is four coordinated). The proportion of boroxol and borate rings depends on the Li_2O content. At a ratio $R > 0.33$ of Li_2O and B_2O_3 concentration there present only borate rings.

By combining the Raman scattering study and NMR investigations, structural groups

* "Babeș-Bolyai" University, Faculty of Physics, 3400 Cluj-Napoca, Romania

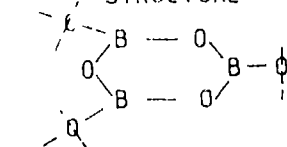
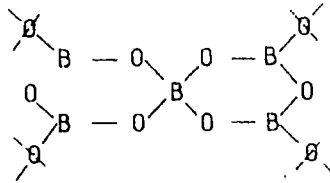
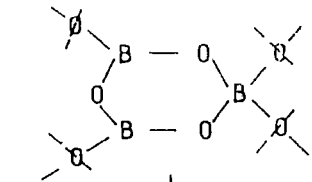
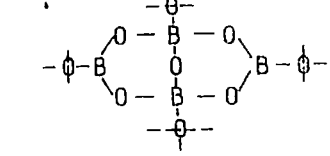
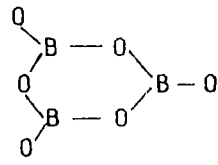
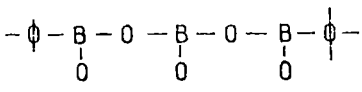
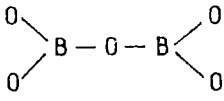
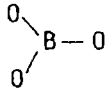
BORATE GROUPS	STRUCTURE	FREQUENCY (cm ⁻¹)
Boraxol ring		806 (vitreous B ₂ O ₃)
Pentaborate group		765 (α-K ₂ O·5B ₂ O ₃) 785 (β-K ₂ O·5B ₂ O ₃)
Triborate group		760 (B ₂ O·3B ₂ O ₃)
Diborate group		730 (Li ₂ O·2B ₂ O ₃)
Ring type metaborate group		630 (Na ₂ O·B ₂ O ₃) 610 (K ₂ O·B ₂ O ₃)
Chain type metaborate group		720 (Li ₂ O·B ₂ O ₃) 735 (CaO·B ₂ O ₃)
Pymborate group		840 (2Na ₂ O·B ₂ O ₃) 850 (2MgO·B ₂ O ₃) 810 (2CaO·B ₂ O ₃)
Orthoborate group		905 (3Na ₂ O·B ₂ O ₃) 920 (3MgO·B ₂ O ₃) 930 (3CaO·B ₂ O ₃)

Fig 1

present in borate glasses have been clearly identified [5] Fig 1 shows the several structural groups present in this glasses

At low R values $R \leq 0.25$ it was found [6] that the introduction in the lithium borate glasses of the copper oxide determine drastically changes in the glass structure. The rising of the CuO content determines the decrease of boroxol rings number and the increasing of the number of six membered borate rings [6]

The structure of the lithium borate glasses with gadolinium oxide content is pronouncedly influenced by the melting temperature of the sample [7]

The aim of this paper is to observe the structural changes of lithium borate glasses with large R value ($R = 0.5$) at different melting temperatures (1273, 1573 K) and different copper oxide concentration

Experimental. The glasses were obtained by melting of boric acid, lithium carbonate and copper oxide mixture in the desired proportion at the indicated temperatures. The parallelepiped shaped samples were obtained by pouring of melts in stainless steel forms. The Raman spectra have recorded on GDM 1000 monochromator instrument equipped with ILA-1 argon ion laser, the emission line at 488 nm was used with a incident power of about 0.5W

A 90° geometry and a spectral slit width of 3-4 cm^{-1} were used to collect the scattered light. The spectra were recorded without polarizer in the gathering optics. The measurements were carried out at room temperature

Results. The Raman spectra of lithium borate glasses with copper oxide content obtained at the melting temperatures 1273 and 1573 K are presented in fig. 2 and 3,

respectively

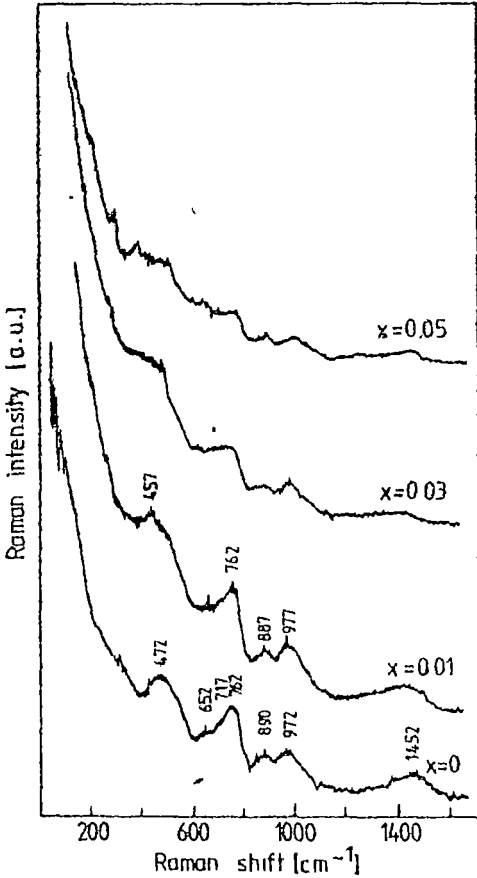


Fig 2

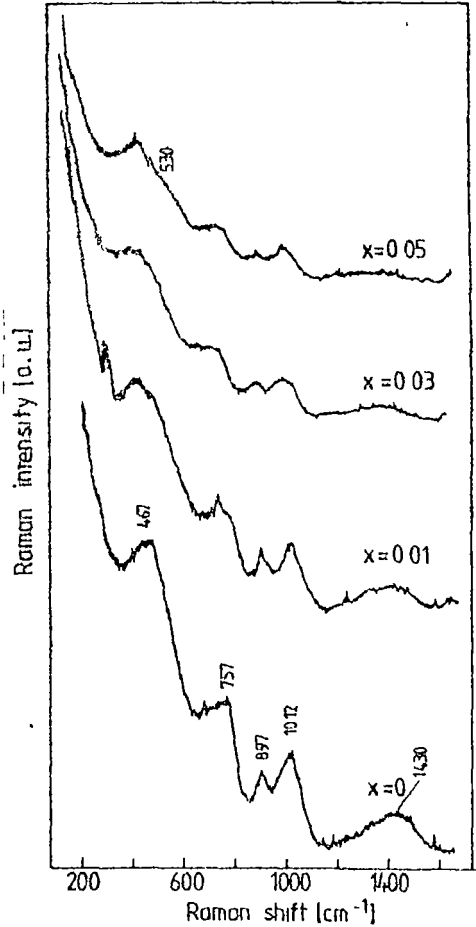


Fig 3

In the Raman spectra of the glass system $(1-x) [2B_2O_3, 1.1_2O] xCuO$ obtained at melting temperature 1273 K (fig 2) there are present intense bands at 472 and 762 cm^{-1} and weak

bands at 652, 890, 972 and 1452 cm^{-1} . The weak band at 652 cm^{-1} , which is present as a shoulder in low frequency side of the 762 cm^{-1} band for $x = 0$, increases in intensity at large copper oxide concentration. The same increasing is observed for 472 cm^{-1} band. For the other bands is not observed a significant change in intensity. Note that the position of the bands is not modified at different x values. From the glasses with $x > 0.05$ the Raman spectra are very difficult to be obtained. From these spectra we observe the absence of 805 cm^{-1} band which was present at low R values (0.25 - 0.33) [6]. In the Raman spectra of the glass system $(1-x)[2\text{B}_2\text{O}_3 \cdot \text{Li}_2\text{O}] \cdot x\text{CuO}$ obtained at melting 1573 K we see the intense band 467 cm^{-1} which changes its position to low frequency side at large x values and 757, 987, 1012 and 1430 cm^{-1} bands with unchanged position at different x values. At $x = 0.05$ a shoulder at 530 cm^{-1} is observed.

Discussion. From the absence of 807 cm^{-1} band in the Raman spectra of $(1-x)[2\text{B}_2\text{O}_3 \cdot \text{Li}_2\text{O}] \cdot x\text{CuO}$ glass system we conclude that boroxol rings are not present in our system for all x values and both melting temperatures. The Raman peak at 782 cm^{-1} which is present distinctly in the spectra of the sample obtained at 1273 K with $x = 0$, can be assigned to six membered borate rings with two BO_3 tetrahedra. For six membered borate rings with one BO_4 tetrahedron 780 cm^{-1} band and its constant position in the spectrum [4,6], is specific.

Based on the Raman spectra of crystalline $\text{Li}_2\text{O} \cdot \text{B}_2\text{O}_3$ which contains chain of metaborate ions, Konijnendijk and Stevels [8] associated the bands at ~ 720 and 1470 cm^{-1} with the presence of a shoulder at 717 cm^{-1} and of the very broad band centered at 1452 cm^{-1} is an indication that at $x = 0$ the chain type metaborate units are present in our system. From the spectra presented in fig. 2 we observe that chain type metaborate units are present at all

x values and their concentration are practically unchanged at different λ values. For pure B_2O_3 the band at 470 cm^{-1} was assigned to ring bending mode of the boroxol rings [9]. In our system the bending mode is probably due of a free BO_4 unit or one that is attached very weakly to a ring type structure. From the rising in intensity of this band at large x values (fig 2) we conclude about the break of the glass network with increasing copper oxide concentration.

On the basis of comparison with the spectra of crystalline analogs [10] the band at 972 cm^{-1} can be assigned to the stretch of orthoborate units. The bands at 890 and 652 cm^{-1} indicate the presence of pyroborate and metaborate units, respectively. The band at 762 cm^{-1} is asymmetrical in the low frequency side because of the presence of the bands at 717 and 652 cm^{-1} . This asymmetry became more pronounced with increasing copper oxide concentration. From the fact that the intensity of the band at 1452 cm^{-1} is not changed, we suppose that this asymmetry is determined by the increasing in intensity either of 652 cm^{-1} band or of the wing of 472 cm^{-1} band. This means the increasing either of metaborate unit number or of the free BO_4 unit number at large copper oxide concentration. By comparing the Raman spectra obtained from the samples prepared at 1573 K (fig 3) with those obtained from the samples prepared at 1273 K , we can observe a shift to the low frequency side of some bands, from 472 to 467 cm^{-1} , 762 to 755 cm^{-1} , 1452 to 1447 cm^{-1} and to high frequency side of the other bands, from 890 to 907 cm^{-1} and 972 to 1005 cm^{-1} . The band at 467 cm^{-1} is more intense than one 472 cm^{-1} band. This means that rising of the melting temperature of the glass determines the break of regular borate groups. The same situation was observed in the lithium borate glasses with gadolinium oxide content obtained at 1273 and 1473 K [7].

The shift of the band at 762 cm^{-1} to 755 cm^{-1} position confirms our supposition about

the presence of two BO_4 tetrahedra in the six membered borate rings

The shoulder at 530 cm^{-1} developed at $x = 0.03-0.05$ values can be associated with the presence of BO_4 tetrahedra in well defined, yet interconnected borate arrangement, confirming the idea that copper oxide acts as modifier in lithium borate glasses

Conclusions In the glass system $(1-x)[2\text{B}_2\text{O}_3, \text{Li}_2\text{O}] \cdot x\text{CuO}$ there are not drastical changes in the network structure as copper oxide is added. In this glass system there are present six membered borate rings, with two BO_4 tetrahedra, chain type metaborate groups, ortoborate, pyroborate, metaborate and BO_4 units. Rising of the melting temperature from 1275 to 1573 K determines a stronger break of network and the increase of free BO_4 units

REFERENCES

- 1 M Scaglioni, M Villa, G Gerodelli, J Non-Cryst Solids 93, 350 (1987)
- 2 E T Kamitsos, G D Chryssikos, J Molec Structure 247, 1 (1991)
- 3 J Lorosch, M Couzi, J Pelous, R Vacher, A Lavvseur, J Non-Cryst Solids 69, 1 (1984)
- 4 T W Brill, Philips Rep Suppl Nr 2, 117 (1967)
- 5 B N Mtera, A K Sood, N Chaudrabhas, J Ramakrishna, J Non-Cryst Solids 126, 224 (1990)
- 6 T Iliescu, S Simion, D Călugăr, J Molec Structure 267, 231 (1992)
- 7 T Iliescu, S Simion, D Manu, I Ardelean, J Molec Structure 294, 201 (1993)
- 8 W L Konignendijk, J M Stevels, J Non-Cryst Solids 18, 307 (1975)
- 9 A Bhargava, R L Snyder, R A Condrate, Mat Res Beril 22, 1603 (1987)
- 10 G D Chryssikos, E I Kamitsos, J Non-Cryst Solids 93, 155 (1987)

Figure caption

- Fig 1 Borate group and specific Raman peak observed in several borate compounds. Dotted line through the oxygen ions indicate that these are of the bridging type (from ref [3] and [5])
- Fig 2 Raman spectra of the glass system $(1-x)[2\text{B}_2\text{O}_3, \text{Li}_2\text{O}] \cdot x\text{CuO}$ Melting temperature 1273 K
- Fig 3 Raman spectra of the glass system $(1-x)[2\text{B}_2\text{O}_3, \text{Li}_2\text{O}] \cdot x\text{CuO}$ Melting temperature 1573 K



COMPARISON OF INTERACTION ENERGIES FOR METHANE USING BUCKINGHAM AND LENNARD-JONES POTENTIALS

G. V. DAMIAN*

Received 10 11 1993

ABSTRACT. One of the most important problem in molecular dynamics simulation is the choice the good force field parameters for intermolecular interaction. The Buckingham and Lennard-Jones interaction potentials sensibility, was compared using some C-C, C-H and H-H potential parameters for methane dimers. The new Buckingham potential parameters was obtained by fitting with quantum calculations in fourth-order Moller-Plesset perturbation method.

Introduction. The requirements on the interaction potential and its parameters (also known as the force field) depend on the area of application and the type of data one is interested in. When the focus of the simulation is on the low energy conformations only, a force field giving the proper potential minima will be considered reliable. The some force field considered highly unreliable when thermodynamic or dynamic data are being simulated. These types of data also require a correct shape of the potential well near its (local) minimum, thermodynamical data are determined by the phase space density function, dynamical data by the spatial derivative of the potential function.

For biomolecular applications the potential is in general divided into a part describing the interaction between covalently bonded atoms (atoms separated by up to 3 covalent bonds) and a part describing the remaining part of the interaction (nonbonded interaction, i.e. Van der Waals and Coulomb potential).

In the molecular dynamics (MD) simulation, the nonbonded atom-atom interactions

* "Babeș-Bolyai" University, Faculty of Physics, 3-400 Cluj-Napoca, Romania

of carbon and hydrogen are important to describe the time evolution of simulated molecular system. The atom-atom nonbonded interaction energy can be described as

$$E_t = E_r + E_d + E_c$$

where

E_t is the total atom-atom interaction energy

E_r is the repulsion term of interaction energy

E_d is the dispersion term of interaction energy

E_c is the coulombic term of interaction energy and wish for nonpolar molecules

The empirical representation of the intermolecular interaction energy of nonpolar molecules is a sum of pairwise additive atom-atom interaction energy terms with each term being the sum of several energy component

Two type of atom-atom interaction potential are frequently used to describe the total nonbonded interaction energy of nonpolar fluid, the Lennard-Jones and Buckingham interaction potential

Results and Discussion. Intermolecular interaction energies of nonpolar methane dimer were compared using Buckingham and Lennard-Jones nonbonded interaction potential. The initial configuration of molecules has been choice thus to correspond to the dimer configuration for which intermolecular interaction energies was calculated by the fourth-order Moller-Plesset perturbation method using the 6-311(2d,2p) basis set [1/

In order to investigate the sensitivity of the atom-atom interaction energy to respect the type of nonbonded interaction potential, were used three sets of parameters

The interaction energies using some type of potential and parameters are plotted in fig,

1 and fig 2

a. Lennard-jones interaction potential

The general form of Lennard-Jones interaction energy is

$$E_{i,j} = \sum_{i,j} E_{i,j} = \sum_{i,j} \left(\frac{C_{ij}^{12}}{r_{ij}^{12}} - \frac{C_{ij}^6}{r_{ij}^6} \right) \quad i,j = 1 \dots n \text{ atoms} \quad (1)$$

where r_{ij} is the atom-atom distance

The following sets of parameters were used

a1. Gromos parameters /2/

	$C^{12}(\text{kcal A}^{12})$	$C^6(\text{kcal A}^6)$
C-C	6250000	2121 52

a2. Proposed by H.J.C.Berendsen /3/

	$C^{12}(\text{kcal A}^{12})$	$C^6(\text{kcal A}^6)$
C-C	476746 21	440 689
C-H	57904 695	104 705
H-H	9902 173	26 076

a3. Q.S.Randall et al. /4/

	$C^{12}(\text{kcal A}^{12})$	$C^6(\text{kcal A}^6)$
C-C	3401262	2406 42
C-H	412242	571 18
H-H	70461	142 705

b. Buckingham interaction potential.

The Buckingham potential are given by

$$E_B = \sum_{i,j} E_{i,j} = \sum_{i,j} B_{ij} e^{-C_{ij} r_{ij}} - A_{ij} r_{ij}^{-6} \quad (2)$$

with r_{ij} the atom-atom distance

The parameters used are

b1. MM3 parameters /5/:

Fig.1 The shape of some potential interaction

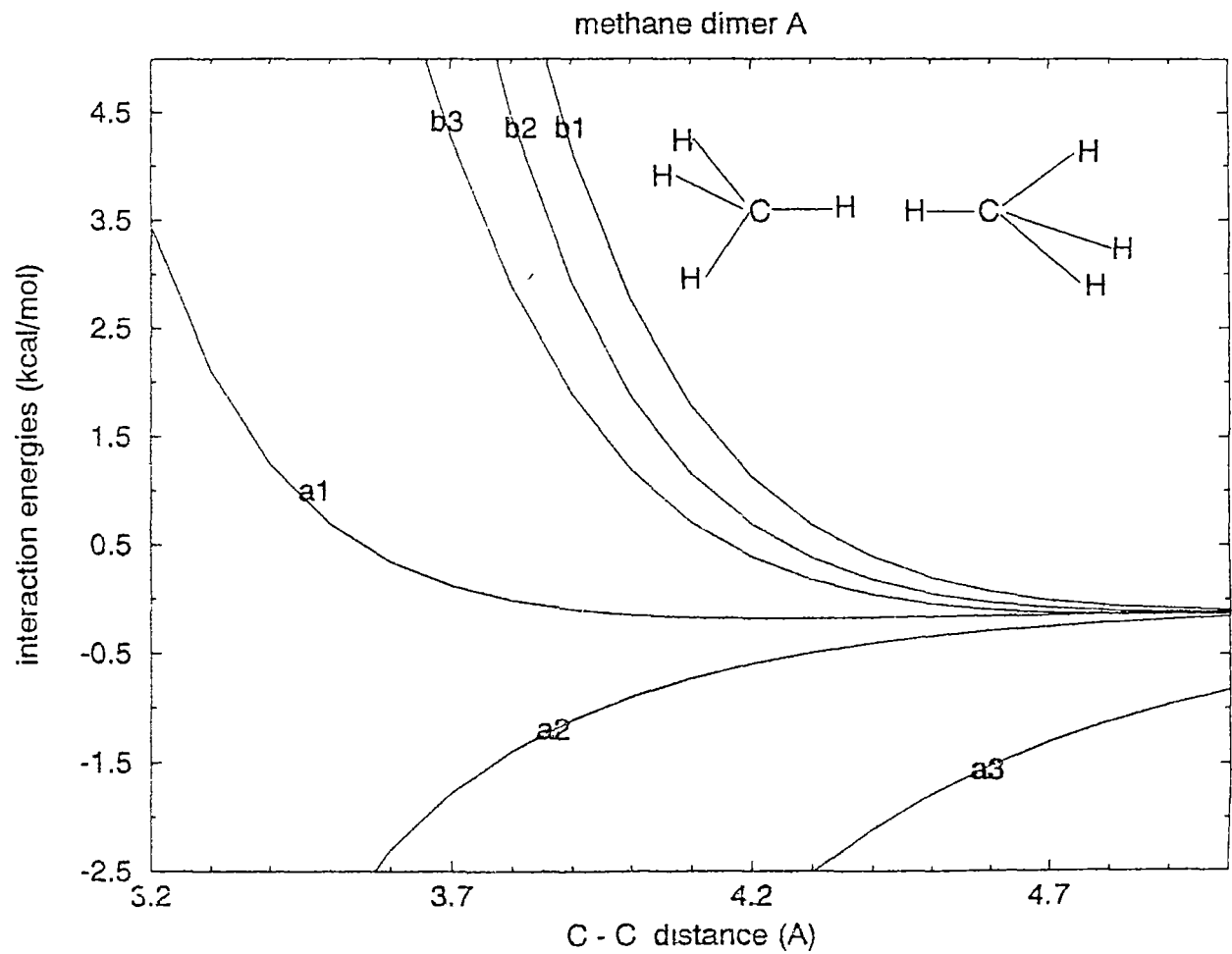
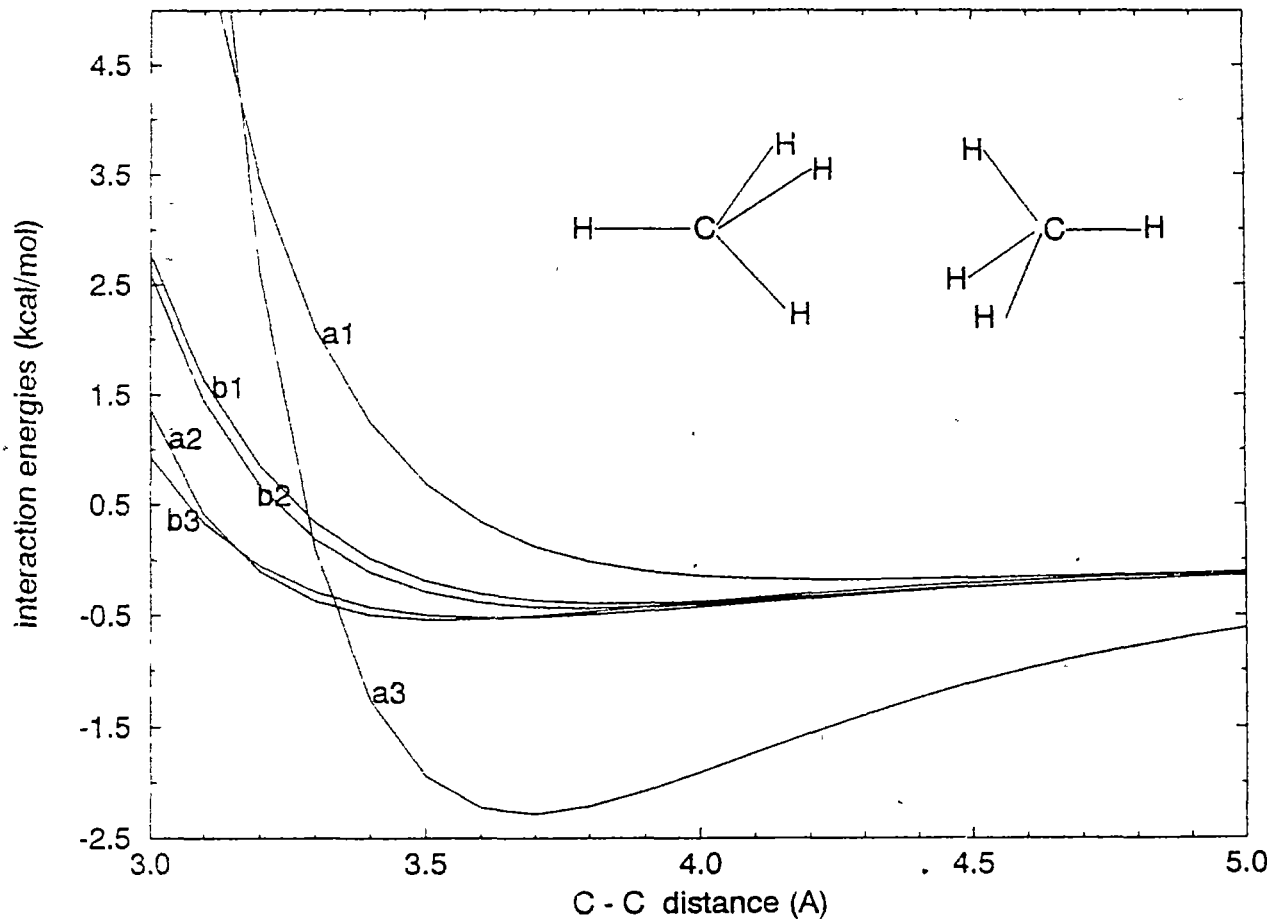


Fig. 2 The shape of some potential interaction

methane dimer B



	A(kcal)	B(kcal A ⁻¹)	C(kcal A ⁶)
C-C	4968	2.94	280.22
C-H	4232	3.37	105.34
H-H	3580	3.70	52.06

b2. Dauchez et al. /6/:

	A(kcal)	B(kcal A ⁻¹)	C(kcal A ⁶)
C-C	83630	3.60	568.0
C-H	8766	3.67	125.0
H-H	2654	3.74	27.3

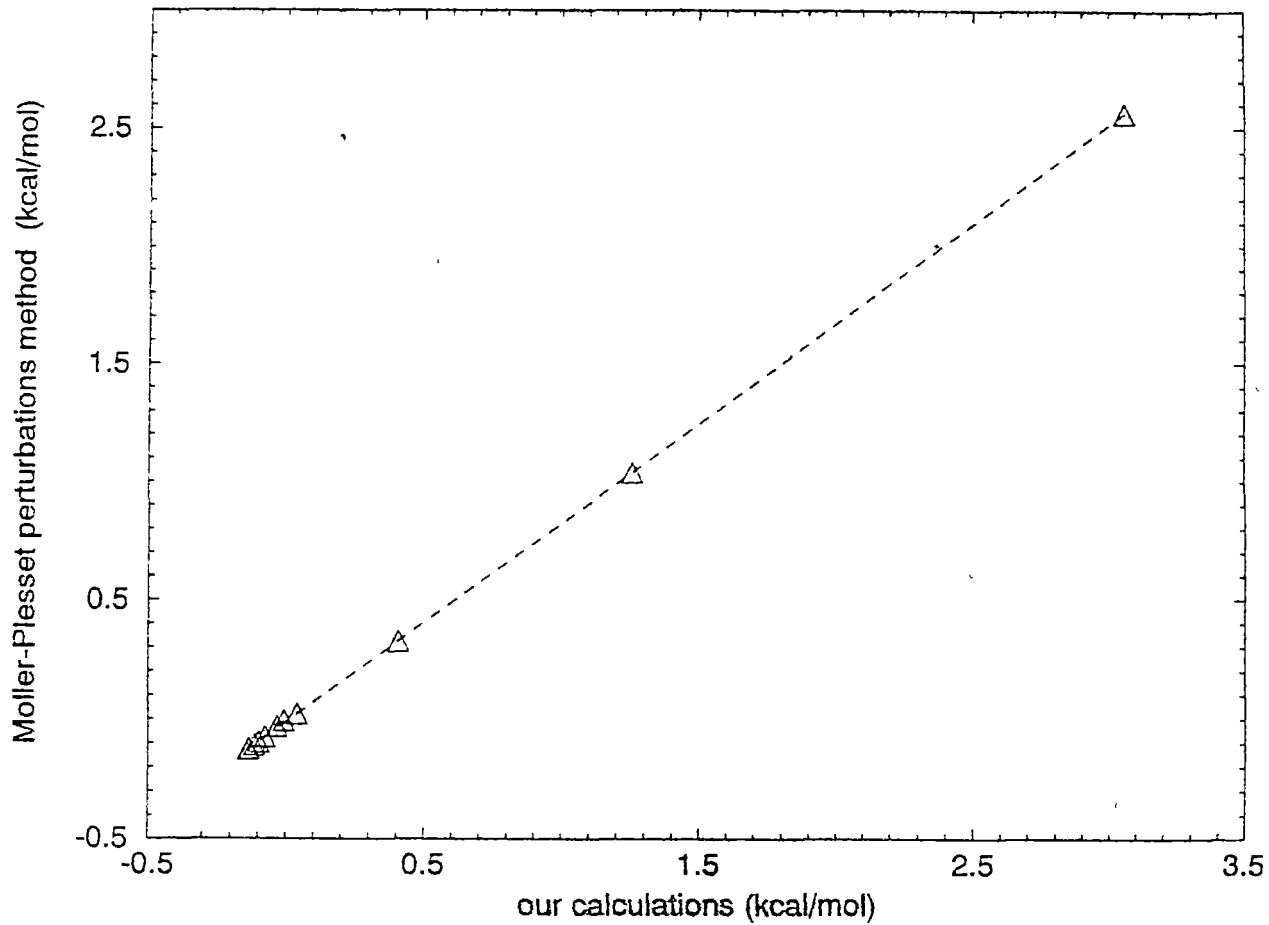
b3. Parameters obtained by fitting with MP4 /1/ calculation:

	A(kcal)	B(kcal A ⁻¹)	C(kcal A ⁶)
C-C	3148	2.84	280.225
C-H	2690	3.26	105.344
H-H	2332	3.70	52.057

Plotting the interaction energies to respect the C-C distances, for two configurations it can be seen that, the repulsive term of Lennard-Jones potential is strongly dependent by the spatial orientations of molecules having only two adjustable parameters to describe small changes in interaction process

Conclusions In this paper, the nonbonded interaction energy for two methane configuration molecules was calculated using Buckingham and Lennard-Jones potential functions with the parameters used in molecular dynamics simulations. The new Buckingham potential parameters were obtained by fitting with ab-initio quantum calculations. The correspondence between our calculations and Moller-Plesset perturbation method are presented in fig 3

Fig.3 Interaction energies calculation for methane



COMPARISON OF INTERACTION ENERGIES

Acknowledgement. The author is grateful to prof H J C Berendsen and MD Group from Department of Biophysical Chemistry, Groningen University, The Netherlands, for the possibility to perform this paper

R E F E R E N C E S

- 1 Tsuzuki,S , Tanabe,K , *Phys Chem.* 1991, 95, 2272
- 2 Van Gunsteren,F W , Berendsen,C J H , *Groningen Molecular Simulation (GROMOS) Library Manual*, Groningen 1987
- 3 H J C Berendsen, Private communication, Groningen University, 1993.
- 4 Randall,S Q , et al , *Mol Sim.*, 1991, vol 8, 73
- 5 Allinger,L N , et al , *J Am Chem Soc* , vol III, no 23, 1989, 8553
- 6 Dauchez et al , *Mol Sim* , 1990, vol 5, 128

A RF GENERATOR FOR CAPACITIVELY COUPLED PLASMA AT ATMOSPHERIC PRESSURE

S. D. ANGHEL*

Received 15.06.1993

ABSTRACT. - A radiofrequency generator for maintaining a capacitively coupled plasma is presented. The plasma can be operated at low radiofrequency powers (100 - 500 W), argon or a mixture of argon and air at atmospheric pressure being the plasma gas. Data referring to the oscillator structure, the theoretical treatment of the subject and the first experimental results are presented. This plasma can be used as spectral source for emission spectrometric determinations in liquid or solid samples.

1. Introduction. The realization of the spectral sources based on the radiofrequency (rf) plasmas is one of the most important progresses in the atomic spectrometry domain in the last twenty years. Among these sources a distinct class is represented by the rf plasmas at atmospheric pressure named inductively coupled plasma (ICP) and capacitively coupled plasma (CCP).

Although CCP was discovered in 1928 [1], the most attention has been accorded of ICP till four years ago because of its extremely good performances as spectral source. Its disadvantages (raised consumption of plasma gas and rf power, difficulty of solid samples analysis, great price) have determined the reappraisal of CCP as spectral source. After Bădărău et al [2], Cristescu and Gurgea [3] and Mavrodineanu and Hughes [4] who have tested the possibility to use as spectral source of CCP, Blades et al [5-7] and Sturgeon et al [8-10] have improved and developed them in various forms.

Because the informations about radiofrequency generators are summary and

* "Babeș-Bolyai" University, Faculty of Physics, 3400 Cluj-Napoca, Romania

incomplete, we have developed a research direction for study and achieve of generators for maintaining of rf plasmas at atmospheric pressure. The starting point of our works have been the informations of Boumans et al [12], the first results being related in the papers [13] and [14]

This paper presents the obtained results after the research work with a view to achieve a rf generator capable of striking and maintaining a CCP at atmospheric pressure. The discharge gas is argon or a mixture of argon and air. The plasma can be sustained at rf powers ranging from 100 to 500W and an oscillating frequency about 22MHz.

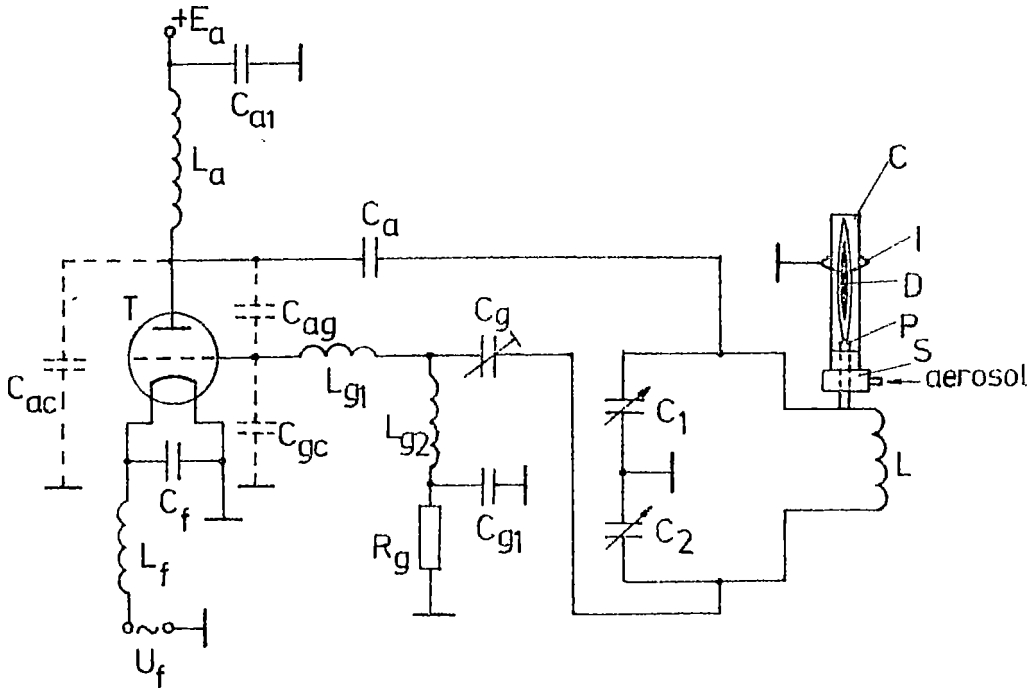


Fig 1 - The diagram of the oscillator T-oscillating triode $L_a C_{a1}$, $L_f C_f$, $L_{g2} C_{g1}$ - rf filter cells $R_g C_{g1}$ - automatic negative group C_a - coupling condenser L_{g1} - suppressing coil C_1, C_2 - condensers of the oscillating circuit L - coil of the oscillating circuit C_{a1}, C_{ag}, C_{gc} - parasitic capacitities of the oscillator tube P-sharp electrode I-annular counterelectrode C-quartz tube D-rf plasma (CCP) S-system for aerosol introduction

2. Execution of the rf generator. For obtaining a generator capable to maintain a rf CCP at atmospheric pressure in various gaseous media we have carried out a number of experimental assemblages using different diagrams of oscillators. Finally, a Colpitts oscillator type, the diagram of which is shown in Fig 1, has been chosen. This type of oscillator very easy enter in oscillation, hasn't the tendency to oscillate at high parasite frequencies, can be used until 150MHz and has a good transfer efficiency (50-60%) of the rf power towards the discharge.

This generator has some characteristics resulting from the purpose it has been accomplished for (using of the plasma as spectral source). The condensers of the oscillating circuit are variable and with air as dielectric, making possible to obtain a high radiofrequency voltage between the ends of the coil L and a good adjustment of the load impedance (the plasma) to that of the generator. The plasma is striking by a Tesla coil on the sharp platinum tip of a cylindrical brass piece (8mm o.d. and 60mm in length) connected at the high rf potential end of the coil L. It is placed into a quartz tube C (15mm i.d., 18mm o.d. and 100mm in length) sustained by the sample introduction system S, which is made of teflon (PTFE) and assures a laminar flow of the aerosol (the liquid sample pneumatic nebulized) through the tube. The carrier gas (Ar or Ar and air) which is the plasma support gas too, has a flow rate of 1,5 l/min. At a distance of 45mm from platinum tip, the quartz tube is surrounded by an annular counterelectrode I connected at the ground clamp. It represents the second electrode of the discharge but the plasma isn't touching it. It assures the symmetry of the electromagnetic field lines, therefore the symmetry of the discharge. Both the coil L and the piece P are water-cooled.

3. Calculation of the oscillator parameters. For the rf generator presented in Fig 1 we shall determine the electrical parameters of which depends its good function, namely the oscillation frequency, the condition of starting the oscillations and the negative resistance effect introduced through the active element (the electronic tube)

In the absence of the plasma the equivalent diagram of the circuit shown in Fig 1 is presented in Fig 2, in which μ and R_i are the amplification coefficient and the internal resistance of the triode, r is the loss

resistance of the coil L and C_3 is the capacity of the condenser formed by the sustaining electrode of the plasma and the annular counterelectrode. For the actual values of circuit elements the impedances of the capacitors C_a , C_{a1} and C_g are very small and $\omega L_a \gg 1/\omega C_1$ (ω is the angular frequency of the oscillator). Also $C_{13} \cong C_1$

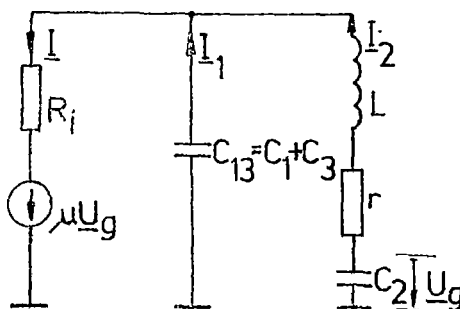


Fig 2 - The equivalent diagram of the oscillator

By means of Kirchhoff's theorems and employing complex values, we obtain

$$I = I_1 + I_2 \tag{1}$$

$$\mu U_g = IR_i + \frac{I_1}{j\omega C_1} \tag{2}$$

$$\frac{I_1}{j\omega C_1} - I_2 \left(r + j\omega L + \frac{1}{j\omega C_2} \right) = 0 \tag{3}$$

Solving the above system and taking into account that $U_g = -I_2 / j\omega C_2$, we obtain the equation

$$\omega C_2 \left(\omega L - \frac{1+\mu}{\omega C_2} + \omega C_1 R_1 r \right) - J \omega C_2 \left(R_1 + r + \frac{C_1 R_1}{C_2} - \omega^2 C_1 L R_1 \right) = 0 \quad (4)$$

From the condition that the real and the reactive parts of the equation (4) should be zero we obtain the equations

$$\omega L - \frac{1+\mu}{\omega C_2} + \omega C_1 R_1 r = 0 \quad (5)$$

$$R_1 + r + \frac{C_1 R_1}{C_2} - \omega^2 C_1 L R_1 = 0 \quad (6)$$

From the equation (6) we get the oscillation frequency

$$f = \frac{1}{2\pi \sqrt{L \frac{C_1 C_2}{C_1 + C_2}}} \cdot \sqrt{1 + \frac{r}{R_1} \frac{C_2}{C_1 + C_2}} \quad (7)$$

If the coil L of the oscillating circuit has a good quality, then $r \ll R_1$ and $r/R_1 \cdot C_2/(C_1 + C_2) \ll 1$ and the oscillation frequency can be calculated with the help of the following relationship

$$f_0 = \frac{1}{2\pi \sqrt{L \frac{C_1 C_2}{C_1 + C_2}}} \quad (8)$$

that represents just the proper oscillation frequency of the oscillating circuit of the oscillator

From the relation (5) and expression of the oscillation frequency (8), we obtain the condition of starting the oscillations

$$\mu = \frac{C_2}{C_1} + \frac{C_1 + C_2}{L} \cdot R_1 r \quad (9)$$

that, under conditions of small losses of the coil L, becomes

$$\mu \approx \frac{C_2}{C_1} \quad (10)$$

For calculation of the negative resistance effect introduced through the oscillating

triode, this is represented as an equivalent current generator. If the internal resistance of the triode is very great and the loss resistance of the coil is very small, we obtain the equivalent diagrams from Fig 3a and b, in which S is the slope of the triode and $\underline{\varepsilon}$ has the formula

$$\underline{\varepsilon} = S\underline{U}_g \left(j\omega L + \frac{1}{j\omega C_2} \right) \quad (11)$$

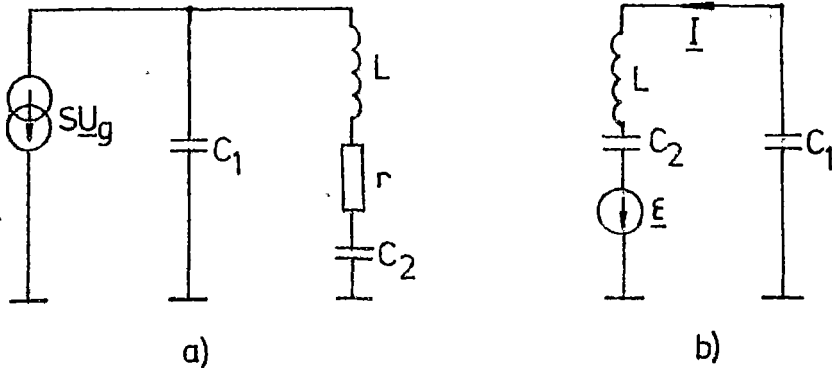


Fig 3 - The equivalent diagram for calculation of the negative resistance effect

Replacing the expression of $\underline{U}_g = -I_2/j\omega C_2$ in equation (11) we obtain

$$\underline{\varepsilon} = -S \left(\frac{L}{C_2} - \frac{1}{\omega^2 C_2^2} \right) I_2 \quad (12)$$

The equation (12) can be written $\underline{\varepsilon} = R_n I_2$, in which R_n represents the negative resistance effect introduced by the triode. Expressing the inductance L from equation (8) and replacing it in the equation (12) we obtain

$$R_n = -\frac{S}{\omega_0^2 C_1 C_2} \quad (13)$$

One can observe that the size of the negative resistance effect depends both of the parameters of the oscillating triode and the values of the circuit elements

4. Influence of the plasma on the oscillator parameters. In case on the sustaining electrode is striking a rf CCP the equivalent diagram from Fig 2 becomes that from Fig 4a

A RF GENERATOR FOR CAPACITIVELY COUPLED PLASMA

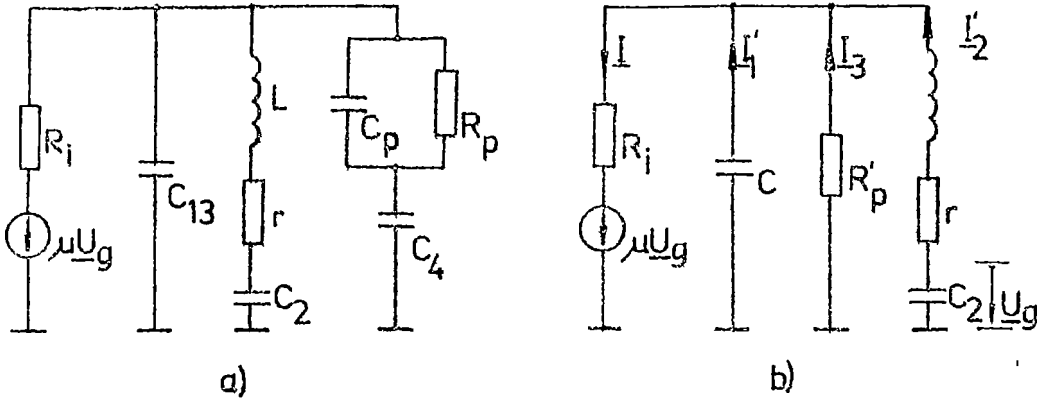


Fig 4 - The equivalent diagram of the oscillator and rf plasma

In this diagram R_p is the plasma resistance, C_p is the plasma capacity and C_4 is the capacity between the plasma and the annular counterelectrode. The presence of the condenser C_p in this equivalent diagram can be explained through the unhomogeneous distribution of the positive and negative electric charges inside the plasma. Because of less mobility of the positive ions it will exist a positive charge excess in the neighbourhood of the sustaining tip of the plasma and a negative charge excess in the upper part of the plasma. This represents a condenser whose capacity is C_p . Applying the theorem of the dipole transfiguration upon the diagram from Fig 4a we obtain the equivalent diagram from Fig 4b, in which

$$R'_p = R_p \left(1 + \frac{C_p}{C_4} \right)^2 \quad (14)$$

and

$$C = C_1 + C_3 + \frac{C_4 C_p}{C_4 + C_p} \quad (15)$$

Using the same calculation method as in the previous chapter we obtain the following formula for oscillation frequency

$$f = \frac{1}{2\pi \sqrt{L \frac{CC_2}{C+C_2}}} \cdot \sqrt{1 + r \frac{R'_p + R_i}{R'_p R_i} \frac{C_2}{C+C_2}} \quad (16)$$

For the actual values of the circuit elements we have $C_3 \ll C_1$ and $C_4 \gg C_p$ (the plasma is very near of the counterelectrode), therefore one can approximate that $C \approx C_1 + C_p$ and $R_p' \approx R_p$. Thus, the expression of oscillating frequency becomes

$$f \approx \frac{1}{2\pi \sqrt{L \frac{(C_1 + C_p) C_2}{C_1 + C_p + C_2}}} \cdot \sqrt{1 + r \frac{R_p + R_1}{R_p R_1} \cdot \frac{C_2}{C_1 + C_2 + C_p}} \quad (17)$$

Also, because $r \ll R_1$ and the capacities C_1 , C_2 and C_3 , and resistances R_1 and R_p have respectively the same order of magnitude, the expression of the oscillation frequency can be written

$$f \approx \frac{1}{2\pi \sqrt{L \frac{(C_1 + C_p) C_2}{C_1 + C_2 + C_p}}} \quad (18)$$

One can observe that in the absence of the plasma ($C_p = 0$) the expression of oscillation frequency is the same with that from expression (8), and the presence of the plasma must determine a diminution of the oscillation frequency

At this oscillation frequency we obtain the following expression for the condition of starting the oscillations

$$\mu = \frac{C_2}{C_1 + C_2} \cdot \left(1 + \frac{R_1}{R_p} \right) + \frac{C_1 + C_2 + C_p}{L} \cdot r R_1 \quad (19)$$

From this relationship one can observe that when we try to strike the plasma, if the amplification coefficient of the triode is too small then the oscillations tend to put out and the plasma isn't striken

The presence of the plasma determines a rise of the active resistance of the oscillating circuit of the oscillator which will determine a rise of the total power absorbed by the rf generator from the source of continuous voltage

In previous treating of our subject the contribution of the parasitic capacities of the

A RF GENERATOR FOR CAPACITIVELY COUPLED PLASMA

tube (10-50pF, interrupted lines in Fig 1) and of the grid capacity, C_g , on electrical parameters of the oscillator have been neglected Taking them into account, the equivalent diagram of the oscillator becomes that from Fig.5

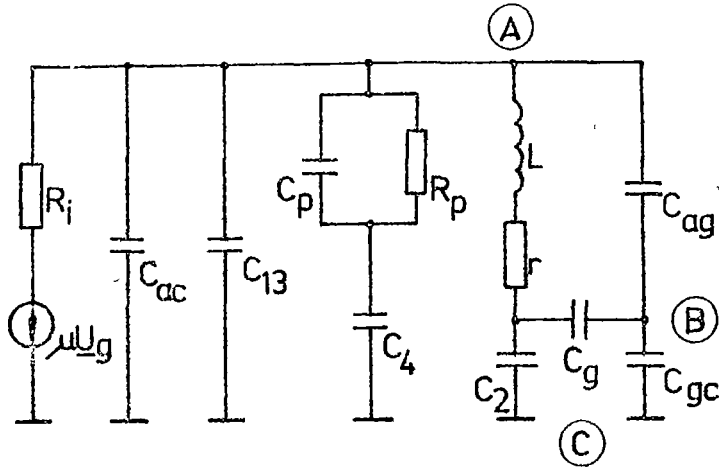


Fig.5 - The complete equivalent diagram of the oscillator

Applying the theorem of the dipole transfiguration and the star-triangle transformation

of the circuit between A,B and C points we obtain

the equivalent diagram shown in Fig 6

Such, the oscillation frequency of the

oscillator will be

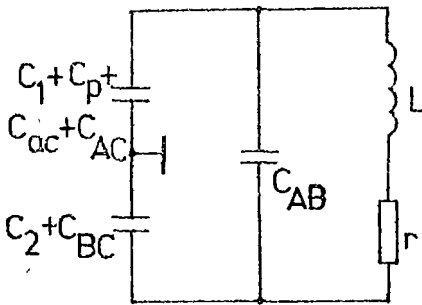


Fig 6 - The equivalent oscillating circuit

in which

$$C_{AB} = \frac{C_g C_{ag}}{C_g + C_{ag} + C_{gc}} \quad (21)$$

$$C_{BC} = \frac{C_g C_{gc}}{C_g + C_{ag} + C_{gc}} \quad (22)$$

$$f = \frac{1}{2\pi \sqrt{L \left[C_{AB} + \frac{(C_1 + C_p + C_{ac} + C_{AC})(C_2 + C_{BC})}{C_1 + C_2 + C_p + C_{ac} + C_{AC} + C_{BC}} \right]}} \quad (20)$$

$$C_{AC} = \frac{C_{ag} C_{gc}}{C_g + C_{ag} + C_{gc}} \quad (23)$$

5. Experimental results and conclusions. Using this generator we have succeeded in striking and maintaining a rf CCP at atmospheric pressure in argon or a mixture of argon and air. The results of the measurements and calculations are synthetically presented in Table 1

Table 1

E_a [V]	f [MHz]	f_p [MHz]	P_p [W]	C_p [pF]
1260	22 604	22 510	85	0 55
1416	22 606	22 497	135	0 65
1618	22 607	22 470	185	0 87
1888	22 609	22 436	275	1 14

Here E_a represents the anode supply voltage of the oscillator, f and f_p are respectively the oscillation frequencies in the absence of the plasma and in its presence, P_p is the rf absorbed power into the plasma and C_p is the electrical capacity of the plasma

The oscillation frequency was measured with an E-204 type digital frequency counter via a coil inductively coupled with the coil L of the oscillating circuit. The rf absorbed power into the plasma was calculated by making the difference between the power consumption of the generator in the presence of the plasma and the power consumption in its absence. This method can be used accepting an error of $\pm 10\%$. The capacity of the plasma was calculated from the relationship (20) in which C_p is the single unknown, all the other values being measurable or known (the parasitic capacities inclusively).

Analysing the data shown in Table 1 the few conclusions can be drawn. First, one can observe that in the absence of the plasma the oscillation frequency practically isn't influenced by the anode supply voltage. Secondly, the linear dependence of the power into the plasma

on the anode supply voltage (Fig 7) make possible to adjust it at desired magnitude. The diminution of the oscillating frequency when the power into the plasma rises can be correlated with the increase of the plasma capacity, C_p , thanks to the increase of the ionization degree of the plasma.

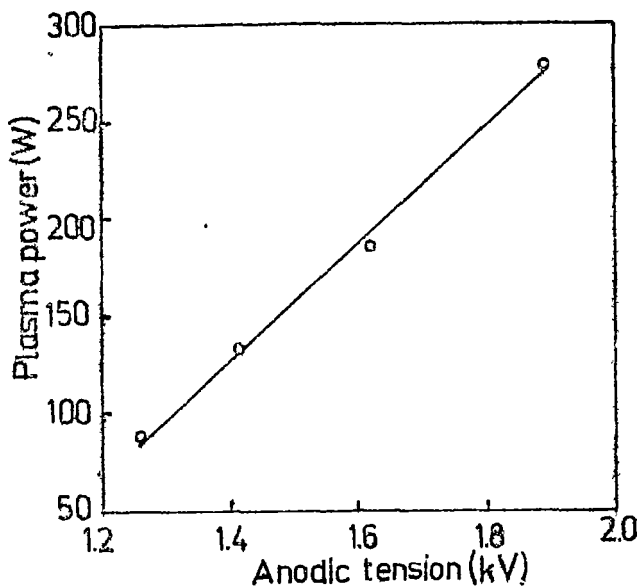


Fig 7 - Plasma power dependence upon the anodic tension.

If the plasma is used as

spectral source its stability is very important. It was appreciated through the relative standard deviation (RSD) calculated for argon emission line of 347.674nm (Fig 8) in accordance with the formula

$$RSD = \frac{\sigma}{\bar{x}} 100 [\%] \tag{23}$$

in which σ is the experimental standard deviation

$$\sigma = \pm \sqrt{\frac{\sum_{i=1}^n (x_i - \bar{x})^2}{n-1}} \tag{24}$$

and \bar{x} is the arithmetic average of the net intensities x_i , for a number of n determinations. In our case $n=9$ and $RSD = \pm 1.62\%$, what corresponds with the international standards ($RSD \leq 5\%$) for this kind of spectral sources.

This kind of discharge (rf CCP) can be used as spectral source in optical emission spectroscopy [6-11] and absorption emission spectroscopy [5], and as detector for gas chromatography

[15,16] At Research Center for Analytical Instrumentation from Cluj-Napoca is studied the possibility to use the above described rf CCP as spectral source for liquid and solid sample analysis

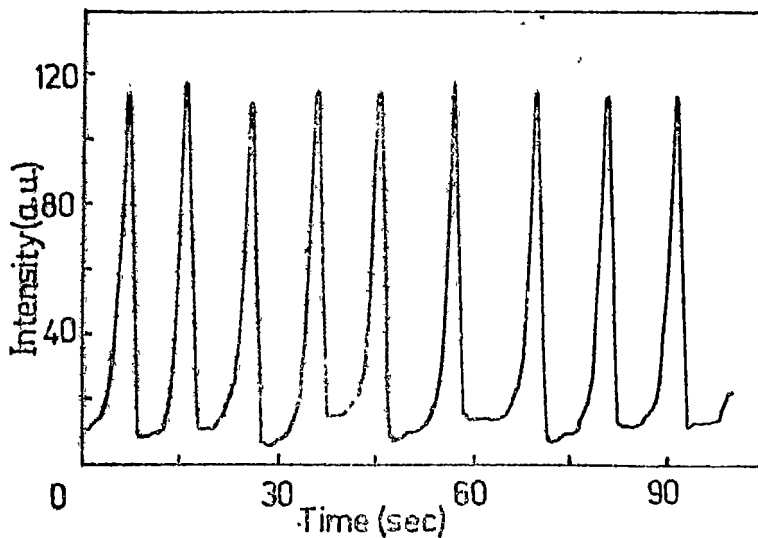


Fig 8 - The time stability of the emission of the plasma

Acknowledgement. The author acknowledge with thanks the help of Mr A Popescu from Research Center for Analytical Instrumentation, Cluj-Napoca

REFERENCES

- 1 K Baxter, Radio News 1204 (1928)
- 2 E Badarau, M Giurgea, G Giurgea, Ath Trutia, Colloquium Spectroscopicum Internationale VI, Amsterdam, Pergamon Press, London, 1956, p 441
- 3 G D Cristescu, M Giurgea, Opt Spectrosc 11,424(1961)
- 4 R Mavrodineanu, R C Hughes, Spectrochim Acta 19,1309(1963)
- 5 D C Liang, M W Blades, Anal Chem 66,27(1988)
- 6 D C Liang, M W Blades, Spectrochim Acta, 44B,1659(1989)

A RF GENERATOR FOR CAPACITIVELY COUPLED PLASMA

- 7 D L Smith, D C Liang, D Steel, M W Blades, *Spectrochim Acta* **45B**,493(1990)
- 8 R E Sturgeon, S N Willie, V T Luong, S S Berman, *J Anal At Spectrom.* **4**,669(1989)
- 9 R E Sturgeon, S N Willie, V T Luong, S S Berman, *Anal. Chem* **62**,2370(1990)
- 10 R E Sturgeon, S N Willie, V T Luong, *Spectrochim Acta* **46B**, 1021(1991)
11. R E Sturgeon, S N Willie, V T Luong, J G Dunn, *Appl. Spectrosc* **45**,1413(1991).
- 12 P W J M Boumans, F J de Boer, J W de Rueter, *Philips Techn Rev.* **33**,50(1972)
- 13 S D Anghel, A.Popescu, F Racz, E Tataru, E Cordos, *Rev. Chim* **40**,344(1989)
- 14 E Tataru, S D Anghel, I I popescu, *Rev Roum. Phys.* **36**,29(1991).
- 15 D.Huang, D C Liang, M W Blades, *J Anal At Spectrom.* **4**,789(1989)
- 16 D Huang, M W Blades, *J Anal At Spectrom.* **6**,215(1991)



APPLICATION OF THE SIMULATION METHOD
FOR A GYROTRON AMPLIFIER

Speranța COLDEA*

Received 1 06.1992

ABSTRACT. - The interaction between a beam of electrons gyrating in a cylindrical or circular wave guide and the oscillating electric field is studied by the small signal theory for this annular electron beam and by applying a numerical simulation method. The dispersion relation for the relativistic annular layer of electrons in a uniform magnetic field along the waveguide axis is done and some preliminary results of using a 1-dimensional electromagnetic relativistic program of simulation for the gyrotron amplifier are presented, being compared with the previous ones.

1. **Introduction.** In the case of the gyrotron (an electron cyclotron maser) electromagnetic radiation is produced as the result of gyrating of the electrons about a magnetic field. The magnetized beam of relativistic electrons propagates through a waveguide whose cut-off frequency is below than the electron-cyclotron frequency $\omega_{co} < \omega_c$. The electron beam has a high transverse energy. Coherent emission results from the orbital phase bunching due to the energy dependent relativistic electron-cyclotron frequency: an interaction between the oscillating electric field and the rotating electrons takes place and gives rise to a sinusoidal energy modulation due to the change in relativistic mass of electrons with energy. This determines an azimuthal modulation which forms a rotating bunch of charges which emits radiation at the relativistic electron-cyclotron frequency ω_c .

The gyrotron device amplifies radiation based on the phenomenon of cyclotron resonance instability. Since the free energy for this instability consists in the rotational motion

* "Babeș Bolyai" University, Faculty of Physics, 3400 Cluj-Napoca, Romania

of electrons the conversion of the electron streaming energy to a rotational energy can be considered as the classical analog of molecular pumping to produce an energy level population inversion (a laser).

We will investigate in this paper one of the mechanisms which transfer the kinetic energy of the relativistic beam to the field energy of an electromagnetic wave (the output radiation). The transverse dependence of the electromagnetic field is assumed to be similar to that of the *fundamental empty waveguide mode*.

Several theories of a small signal gyrotron device have been done [1]-[5]. Usually a thin rotating device has been considered, as we consider here. In the case when the axial wave number and beam are $k_z = 0$, $v_{0z} = 0$, the TM_0 and TE_0 modes are usually decoupled [5]. But if a finite axial wavelength is introduced the theory of gyrotron includes the generation of both TM and TE modes [1]-[2] and the coupling of these modes by magnetized beam in a waveguide has been demonstrated [6].

We will give a simple theoretical description of the gyrotron phenomenon in the second part of the paper and the results of applied particle simulation method for the gyrotron will be done in the last part of this paper with a short discussion of the results.

2. The Linear Theory for a Gyrotron Amplifier We recall here that the gyrotron amplifier is a device which generates an electromagnetic radiation through an interaction of a relativistic electron beam encircling an external magnetic field, usually in a cylindrical wave guide (of circular cross-section). The equations that describe the considered system and that must be integrated are the fluid equations and the Maxwell's equations

An annular layer of relativistic electrons is assumed, with a small but finite thickness ϵ , that rotates in a cylindrical waveguide. The beam is assumed to be monoenergetic having the unperturbed velocity $\vec{v}_0 = v_{0z} \cdot \hat{e}_z + v_{0\theta} \cdot \hat{e}_\theta$, where $v_{0\theta} = \rho \cdot \omega_c$ is the relativistic azimuthal velocity and $\omega_c = \frac{eB_0 g}{m_0}$ is the relativistic cyclotron frequency, g being the relativistic factor of the beam ($g = \frac{v_0^2}{c^2}$), $\frac{dy}{d\rho} = 0$ and $\frac{d\omega_c}{d\rho} = 0$, ρ being the radial position. The beam has a uniform density n_0 in a layer thickness ϵ at a radius $\rho = r$ around the axis.

The fluid equations are the relativistic Lorentz force equation and the continuity equation given by the following relations:

$$\frac{d}{dt} \left[\frac{m_0 \vec{v}}{\sqrt{1 - \frac{v^2}{c^2}}} \right] = -c \cdot E - \frac{e}{c} [\vec{v} \times B] \quad (1)$$

$$\frac{dn}{dt} + \nabla n \vec{v} = 0 \quad (2)$$

The Maxwell's equations that we use are the following

$$\nabla \times E = -\frac{1}{c} \cdot \frac{dB}{dt} \quad (3)$$

and

$$\nabla \times B = J + \frac{1}{c} \cdot \frac{dE}{dt} \quad (4)$$

where E , B are the perturbed electric and magnetic fields. The equations (1)-(2) will be linearized by the perturbation method $v = v_0 + \delta v$, $n = n_0 + \delta n$ and the perturbations will be of the form $\exp(ik_z \cdot z + i\theta - i\omega \cdot t)$, for a monoenergetic beam $v_{0\theta}^2 + v_{0z}^2 = v_0^2$.

The used form for our case of the Maxwell's equations is the following

$$\frac{\partial E_0}{\partial t} = ic k_x \cdot B_r + \omega_{c0} \cdot B_z - 4\pi J_0 \quad (5)$$

$$\frac{\partial B_r}{\partial t} = i c k_x \cdot E_0 \quad (6)$$

and

$$\frac{\partial B_z}{\partial t} = -\omega_{c0} \cdot E_0 \quad (7)$$

where ω_{c0} is the cut-off frequency of the waveguide

By integrating the Maxwell's equations on the surfaces $d\vec{K} = dA \cdot \vec{e}_z$ where $dA = \rho d\theta d\rho$, within the limits $\rho = r$ and $\rho + c$ as

$$\oint \vec{E} d\vec{r} = -\frac{i\omega}{c} \cdot \oint \vec{D}_z \cdot dA \quad (8)$$

some boundary conditions for the fields are obtained

After linearising the eq (1)-(2) the relations for the perturbed velocities δv_p , δv_θ and δv_z and for the current density \vec{J} are obtained after some algebraical calculations The current \vec{J} is of the form

$$\vec{J} = -en_0 \delta \vec{v} - e \cdot \delta n \cdot \vec{v}_0 = -e \left(1 - \frac{i v_0}{\omega} \cdot \nabla \right) n_0 \delta \vec{v}_\perp - en_0 \left[\vec{e}_z + \frac{k_x}{\omega} (v_{0z} \vec{e}_x + v_{00} \vec{e}_\theta) \right] \cdot \delta v_z \quad (9)$$

The assumption of a small beam density is made in the first approximation and it was considered that the electromagnetic field given by the current \vec{J} can be given by the vacuum waveguide EM-field [1]

After some standard algebra that is based on the equations (1)-(6) the dispersion relation for the resonance case $\omega \sim +\omega_c$, k_x , $v_{0,0} \neq 0$, $\frac{\partial v_{0z}}{\partial \rho} \neq 0$, is obtained under the form

$$J_z = (k_\perp \cdot R) \cdot J'_z(k \cdot R) \frac{2}{\pi r} - \frac{\omega}{c} C_1 \cdot \left(\frac{v_{0z}}{c} + \frac{v_{00}}{c} \cdot \frac{1}{r} \cdot \frac{k_x}{k_\perp^2} \right) \cdot J'_z(k_\perp \cdot R) [J_1(k_\perp \cdot r) \cdot Y_1(k_\perp \cdot R) - J_1(k_\perp \cdot R) \cdot Y_1(k_\perp \cdot r)] + \quad (10)$$

$$+ k_\perp \cdot C_2 \frac{v_{00}}{c} \cdot J_1(k_\perp \cdot R) \cdot J'_z(k_\perp \cdot r) \cdot Y'_1(k_\perp \cdot R) - J'_z(k_\perp \cdot R) \cdot Y'_1(k_\perp \cdot r) = 0$$

where

$$C_1 = + \frac{4\pi e^2 N}{m_0} \cdot g \cdot \frac{2k_z}{(\omega^2 - \omega_c^2)^2} \frac{\partial v_{0z}}{\partial \rho} \quad (11)$$

$$\left[\omega \cdot \frac{N_z}{k_z} \cdot k_{\perp} \cdot J_1'(k_{\perp} \cdot r) \left(\frac{v_{0z}}{c} - \frac{N_z}{N_z^2 - 1} + \omega_c \cdot J_1(k_{\perp} \cdot r) \frac{1}{r} \frac{N_z}{k_z} \cdot \left(\frac{N_z}{N_z^2 - 1} - \frac{v_{0z}}{c} \right) \right) \right]$$

and

$$C_2 = \frac{4\pi e^2 N g}{m_0} \cdot \frac{2k_z}{(\omega^2 - \omega_c^2)^2} \cdot \frac{\partial v_{0z}}{\partial \rho} \quad (12)$$

$$\left[-\omega \cdot J_1(k_z \cdot r) \left(\frac{v_{0z}}{c} - \frac{1}{r} \cdot \frac{k_0}{k_z^2} \frac{\omega - k_z \cdot v_{0x}}{\omega} \right) - \omega_c \cdot \frac{k_0}{k_{\perp}} \frac{\omega - k_z \cdot v_{0z}}{\omega} \cdot J_1'(k \cdot r) \right]$$

When the beam is not present $N = 0$ and in the presence of the beam $n = 0$, if $\delta\omega$ is the shift of the resonant frequency ω_0 , some expansions of the factors J_1 and J_1' are made and the expression for $\delta\omega$ can be given. For $N = 0$ the eq. (7) has the simplified form $J_1(k_{\perp} \cdot R) \cdot J_1'(k_{\perp} \cdot R) = 0$ that is the dispersion relation for the TE and TM modes. The eq. (7) indicates that the beam couples the TE and TM modes (that is a weak-coupling for J_1 or J_1').

In the considered case of a circular waveguide the reduced dispersion relation has the following form:

$$\omega^2 - c^2 \cdot k_x^2 - \omega_{c0}^2 \left[1 - \frac{\delta}{k_0} (I-1) \right] \cdot (\omega - k_x \cdot v - \omega_{ce}) = -\Gamma \cdot I \quad (13)$$

where δ is the thickness of the waveguide wall, I is the total current and the coupling constant Γ is defined as follows

$$\Gamma = 3.3 \cdot 10^{-5} \cdot v_{\perp}^2 \omega_{c0}^4 [J_1'(v_{\perp} \cdot \omega_{c0}/c \cdot \omega_{ce})] / v_{\perp} \cdot c \quad (14)$$

With the aim to make a numerical analysis of the gyrotron mechanism and to compare with the theory and experiment the particle simulation is used for the following model a

magnetized relativistic electron beam, of low density, with a high transverse energy, that flows by a waveguide with a cut-frequency ω_{co} smaller than the electron-cyclotronic frequency ($\omega_{co} < +\omega_{ce}$).

A relativistic electromagnetic 1-dimensional simulation code, with three components velocity is used, considering the gyrotron in the laboratory frame. An electron beam with the energy $E = 70 \text{ keV}$, $\frac{v_{\perp}}{v_{\parallel}} = 1.5$ and the current $I = 1 \text{ A}$, coupled to a TE_{01} mode of the waveguide of radius $r_0 = 0.5 \text{ cm}$ is taken into account for comparison with some previous results. The length of the gyrotron is taken as being of 10 cm and a wall-loss is considered for the cut-off frequency that may be varied.

3. Results and conclusions. By this simulation of a gyrotron instability diagnostics as spatial evolution of the transverse momentum, the electron positions in the normalized momenta space, the time evolution of the system and the relation between the input power and the output power by the Poynting-flux calculations can be given.

An adapted 1-dimensional electromagnetic code with three velocities (in the cylindrical coordinates and the laboratory frame) is used to simulate the considered gyrotron amplifier process. The simplest TE_{01} mode of the waveguide is considered and wall-losses could be or not to be taken into account for a cut-off frequency that could be varied. The simulation code is adapted in the sense that the transverse dependence of the electromagnetic fields is assumed to be that of the fundamental empty waveguide mode and the transverse position of the electrons is taken in the point where we have the maximum coupling of the electrons and fields. The electrons are injected at the input of the interaction region (the waveguide) and

are removed at the exit. An oscillating external charge in front of the beam input gives a RF input field. The electron beam is coupled to the TE_{01} mode of the circular waveguide of radius $R = 0.54\text{cm}$. The dispersion relation given by eq (13) is taken into account.

The frequency selective losses at the waveguide wall could be simulated by a resistive term that is defined in Fourier space. From calculations of the coupling factor Γ the losses at the guide wall could be eliminated.

We have seen earlier that the linear dispersion relation of the simulated gyrotron instability reduces at the approximation given by eq (13). As one increases the wall-loss the gain maxima above the cut-off frequency can be eliminated.

The results are illustrated

by the diagnostics of the stimulation, given by some selected graphics. The spatial evolution (along the beam) of the transverse momentum is given in Fig 1 (the particle positions in the normalized transverse momenta space). The diagnostic presents the illustration of electron

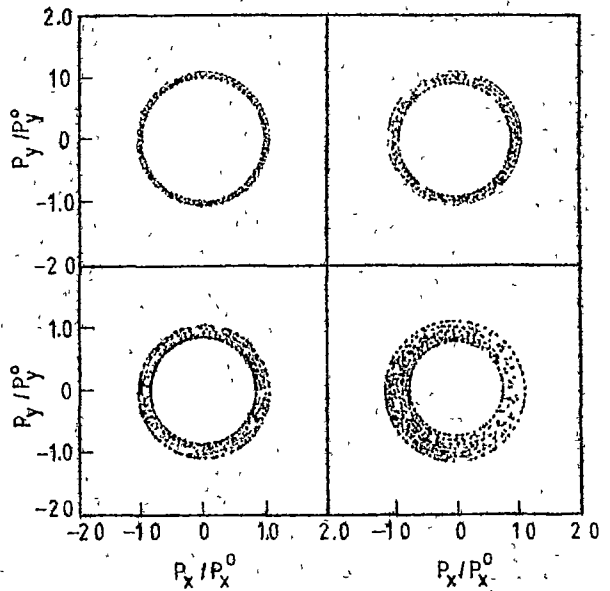


Fig 1

bouncing in the gyrotron by

the discussed saturation mechanism of this device, that is the phase trapping of electrons in

the unstable mode potential

The Fig. 2 gives the time evolution of the input and output powers (by calculating the Poynting flux time evolution) It can be seen that the simulated power is lower

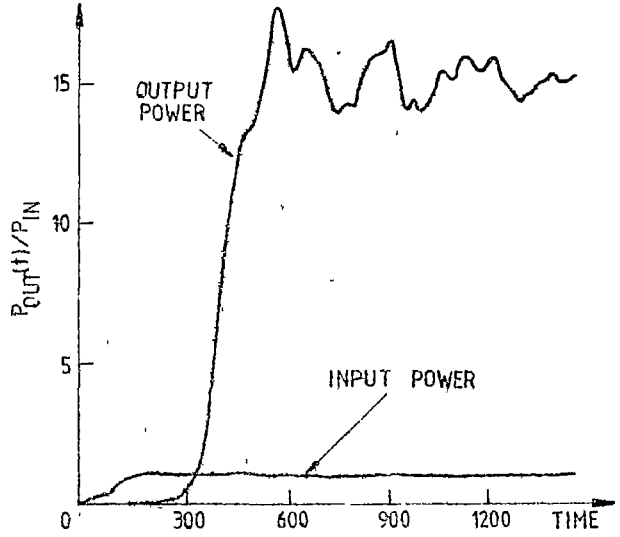


Fig.2

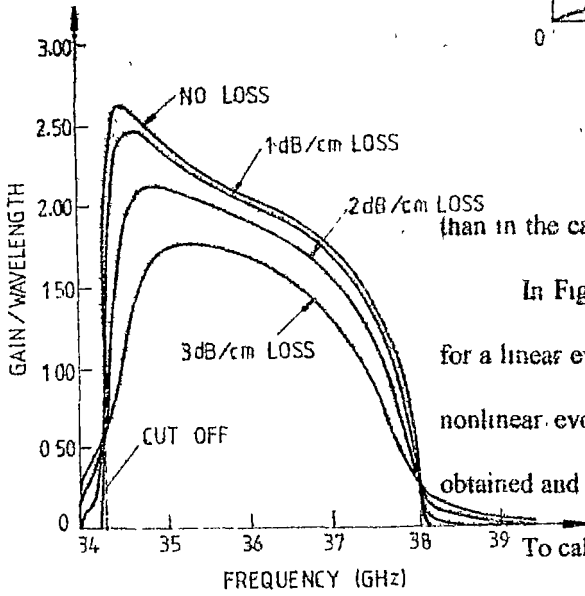


Fig 3

than in the case of the theoretical linear gain

In Fig. 3 the gain as function of frequency is given, for a linear evolution and also for the nonlinear case, for the nonlinear evolution a maximum linear gain of 12 dB was obtained and a corresponding maximum efficiency of ~ 10%

To calculate the growth rate of the gyrotron instability the linear and nonlinear bandwidth can be simulated with the

aim to be compared In Fig 4 the gain to the wavelength ratio is given as function of the frequency and the bandwidth can be observed If the bandwidth is 3 dB at an input power of 80 W the linear growth was calculated to be 4,5%, compared with the nonlinear value that is 7% at an input power of 500 W

APPLICATION OF THE SIMULATION METHOD

We can observe that the simulated gain and efficiency are slightly higher than the experimental results [8] but they are in agreement with the classical simulation results [9]-[10]

By taking a more sophisticated approximation (or model) of the gyrotron instability and also a more

stretched simulation code some other characteristics of the gyrotron devices could be further obtained and some new phenomena of this gyrotron interaction could be evidenced

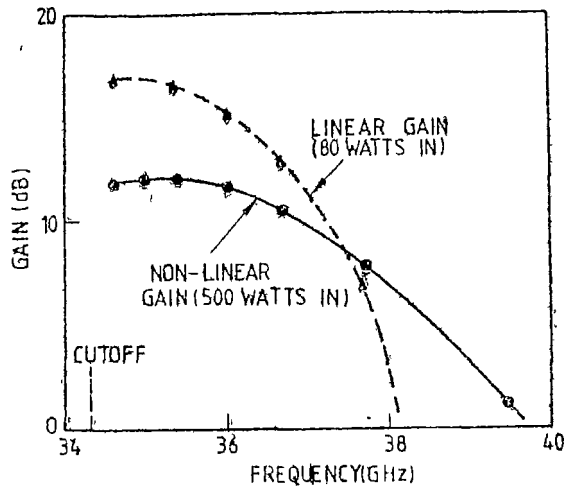


Fig 4

REFERENCES

- 1 Y Y Lau, IEEE Trans Electron Devices 29, 320 (1982) Phys Fluids 27, 2319 (1984)
- 2 G Dohler, Int J Electron 56, 481 (1984)
- 3 P Sprangle, J. Appl Phys, 47, 2935 (1976), Phys Rev Lett 43 1932 (1978)
- 4 W W Desler, R Kulkarni, C D Striffler, J Appl Phys 54, 4152 (1983)
- 5 M Shonker, A B Kitsenko, Plasma Phys 10, 699 (1968), Phys. Fluids 26 2271 (1983)
- 6 A Sommerfeld, Mechanics of Deformable Bodies, Chapt III Ed Academic Press New York (1950)
- 7 Ch.K Birdsall, A B Langdon, Plasma Physics Via Computer Simulation, Ed McGraw-Hill, New York (1985)
- 8 R S Symons, H R Jory, Cyclotron Resonance Devices, in Advances in Electronics and Electron Physics, C Marton Ed, Academic Press, New York, vol 55 (1981)
- 9 M Caplan, Gyrotron Simulations, Ed UCLA (1982)
- 10 J.M Dawson, Particle Simulation of Plasmas, Rev of Modern Phys 55, 403 (1983)

•



•

THE BRST-BV SYMMETRY IN CLASSICAL MECHANICS

D. JALOBEANU* and L. TĂTĂRU*

Received 25 05 1993

ABSTRACT. - In this note we develop a path-integral formulation of classical mechanics using BV-version of the BRST-symmetry. This is achieved by starting with a special quantum version of BV-action and by taking the classical limit $\hbar \rightarrow 0$.

1. Since its formulation, the path integral formulation of quantum mechanics has turned out of be one of the most powerful tools for the study of quantum mechanics. The quantization of many systems as YM theory, topological quantum field theory or superstring theory can hardly be formulated and understood in all canonical formulations of QFT except the path integral. However just a few attempts [1, 2] have been made to give an analogous path-integral formulation of *classical mechanics*. In these formulations it was suggested to use a Dirac δ function $\delta(\phi - \phi_{cl})$ for the measure which gives weight "one" to the classical paths ϕ_{cl} and weight "zero" to all the other paths. In this way the measure can be rewritten in the standard form as the exponent of an action \tilde{S} , which involves a set of anticommuting ghosts and which possesses a BRST-symmetry.

Nevertheless, it would be interesting to see if the classical mechanics can be obtained as the limit $\hbar \rightarrow 0$ of the quantum mechanics path integral formulation. In this note we shall try to formulate the path integral quantum field theory in such a way that the classical limit $\hbar \rightarrow 0$ could be easily achieved.

* "Babeș-Bolyai" University, Faculty of Physics, 3400 Cluj-Napoca, Romania

2. Let $S_0 = S_0(\phi)$ be the initial action for an arbitrary classical system, which is supposed to be without *any* gauge symmetry. Furthermore, we do not specify the formalism (Hamiltonian or Lagrangian) since we intend to be as general as possible. The fields $\phi = \phi'$ can be of any nature but for sake of simplicity we consider a system only with bosons (even variables).

While the quantum generating functional has the form

$$Z_{QM}(J) = N \int D\phi \exp \frac{i}{\hbar} [S_0(\phi) + J \cdot \phi] \quad (1)$$

and gives weight $\exp \left[\frac{i}{\hbar} S_0(\phi) \right]$ to each path, the classical one could be built as giving weight "one" to the classical paths and weight "zero" to all the others. It is given by

$$Z_{CM}(J) = N \int D\phi \delta(\phi - \phi_{cl}) \exp \frac{i}{\hbar} [J \cdot \phi] \quad (2)$$

where ϕ_{cl} is a solution of the classical equation of motion

$$\delta S / \delta \phi' = 0 \quad (3)$$

and N is a normalisation constant.

Since ϕ_{cl} is a solution of the equation of motion (3), it is possible to rewrite Z_{CL} as

$$Z_{CM} = N \int D\phi \delta(\delta S / \delta \phi') \cdot \det [\delta^2 S / \delta \phi' \delta \phi^k] \cdot \exp \left[\frac{i}{\hbar} J \cdot \phi \right]. \quad (4)$$

The delta function in (4) can be represented as

$$\delta(\delta S / \delta \phi') = \int D\lambda \exp \left[iN \cdot \frac{\delta S}{\delta \phi'} \right] \quad (5)$$

and the determinant could be conveniently reexpressed as a functional integral over two Grassmann variables $c^j(x)$ and $\bar{c}^j(x)$

$$\det(\delta^2 S_0 / \delta \phi' \delta \phi^k) = \int Dc D\bar{c} \exp [\bar{c}^j \cdot S_{0,jk} \cdot c^k], \quad (6)$$

with $S_{0,jk} = \delta^2 S_0 / \delta \phi' \delta \phi^k$. Inserting (5) and (6) in (4), we can obtain the classical generating functional in a form identical to the quantum generating functional (1) i.e.

$$Z_{CM} = \int D\phi D\lambda Dc D\bar{c} \exp\{i(\tilde{S} + J \cdot \phi)\} \quad (7)$$

where the action \tilde{S} is given by

$$\tilde{S} = \lambda^j \frac{\delta S_0}{\delta \phi^j} - i\bar{c}^j S_{0,jk} \cdot c^k \quad (8)$$

From its construction it is clear that the path integral with weight \tilde{S} is completely equivalent to the classical mechanics and there are no quantum fluctuations driving the classical system away from its own classical paths. A remarkable point of the action (8) is the existence of an *unexpected* BRST symmetry [1, 2]. This fact cannot be a mere formal coincidence but it indicates that something *profound* is behind. There should be a kind of "covariance" between the classical and the quantum regime i.e. we could rotate $S_0(\phi)$ into $\tilde{S}(\phi, \lambda, c, \bar{c})$.

In this note we shall try to obtain the action (8) by using the *standard* antibracket-antifield method of quantization developed by Batalin and Vilkovisky [3], called BV-method of quantization (see also [6, 7]). In order to implement the BV method for a system without any gauge symmetry, we shall use a trick due to Alfaro and Damgard [4, 5] and we shall duplicate all fields ϕ^j and introduce the "collective fields φ^j ". The initial action is taken to be

$$S_0 = S(\phi^j + \varphi^j) \quad (9)$$

and this new action is invariant under the *gauge transformation*

$$\delta\phi^j = \varepsilon^j \quad \delta\varphi^j = -\varepsilon^j, \quad (10)$$

where ε^j are a set of infinitesimal arbitrary functions

If we want to quantize the theory by using BV-method, we must introduce

- a set of antifields ϕ_j^* and φ_j^* ,

- a set of ghosts c^j corresponding to e^j ,
 - a set of conjugate ghosts \bar{c}^j and a set of Lagrange multipliers B^j which form together the non-minimal sector of the theory and
 - a set of antifields corresponding to all ghosts and Lagrange multipliers ($c_j^*, \bar{c}_j^*, B_j^*$)
- The quantum action for our theory S must satisfy the master equation introduced by Batalin and Vilkovisky [3].

$$(S, S) = 0 \tag{11}$$

where $(..)$ is the anti-bracket for our theory [3, 6, 7].

Due to the lack of any local symmetry for our system the solution of the master equation has a very simple form

$$S = S_0(\phi + \varphi) + (\phi_j^* - \varphi_j^*) \cdot c^j + \bar{c}^j \cdot B^j \tag{12}$$

The action S is the generator, through the anti-brackets, of the BRST symmetry

The final task in BV construction is the gauge fixing process. In our case this process should be a little bit nonstandard. We shall regard in the sequel φ_j^* as a field and φ , as a field that can be obtained via a canonical transformation [7]. The next step is to apply the standard procedure to fix the gauge [3, 6, 7]. The gauge fixed action is given by

$$S_\psi = S(\phi^j, c^j, \bar{c}^j, B^j, \varphi_j^*, \phi_j^*, \varphi_j^* = \delta\psi/\delta\phi^j, c_j^* = \delta\psi/\delta c^j, \bar{c}_j^* = \delta\psi/\delta\bar{c}^j, B_j^* = \delta\psi/\delta B^j, \varphi^j = \delta\psi/\delta\varphi_j^*) \tag{13}$$

For a system without any symmetry we could choose the fermion function $\psi = 0$ and the gauge fixed action coincide with the initial classical action S . However if we want to obtain the classical limit $\hbar \rightarrow 0$ we could choose

$$\psi = \hbar \bar{c}^j \cdot S_{\omega_j}(\phi) \tag{14}$$

In this way the generating functional Z_{QM} can be written as

$$Z_{QM} = Z_{CM} \int [D\varphi] \exp \frac{i}{\hbar} s_0(\varphi) \quad (15)$$

In the classical limit the last integral becomes a normalisation constant and the quantum generating functional coincide with the classical one

REFERENCES

1. E. Gozzi, M. Reuter and W.D. Thacker, *Phys. Rev.* **D40**(10) (1989) 3363
2. E. Gozzi, M. Reuter and W.D. Thacker, *Phys. Rev.* **D45**(2) (1992) 757.
3. I.A. Batalin and G.A. Vilkovisky, *Phys. Rev.* **D28**(1983) 2567; *Nucl. Phys.* **B234**(1984) 106, *J. Math. Phys.* **26**(1985) 172
4. J. Alfaro and P.H. Damgaard, *Ann. Phys. (NY)* **202** (1990) 388
5. J. Alfaro and P.H. Damgaard, preprint CERN-TH-6788/93, hep-th 9301103
6. M. Henneaux, "Lecture on the antifield-antibracket-BRST formalism for gauge theories" Proc. of the XXI GIFM Meeting (1989)
7. M. Henneaux and C. Teitelboim, *Quantization of gauge systems*, Princeton University Press, Princeton, New Jersey (1993)



THERMODYNAMIC THEORY OF CROSS-POLARIZATION IN A NMR-MOIST EXPERIMENT

I. ARDELEAN*

Received: 1 03, 1993

ABSTRACT. - A modified spin thermodynamic theory of an experiment which provide an efficient cross-polarization even for mismatch Hartman-Hahn condition is developed for $S I_N$ spin-systems S spin polarization for a given mismatch is obtained.

1. Introduction. The introduction of the cross-polarization technique made is possible to overcome the low sensitivity of dilute spins, and provided a means of observing the NMR signals of those nuclei in solids [1] A simple experimental scheme for cross-polarization between spin species I and S involving simultaneous spin locking (SL) of two species has been firstly proposed by Hartmann and Hahn [2] The maximum of cross-polarization transfer is obtained for Hartmann-Hahn match condition

A new cross-polarization experiment has been suggested by Levitt et al. [3] which provides an efficient cross-polarization even for mismatched Hartmann-Hahn condition They used a double irradiation scheme for "mismatch optimized IS transfer" (MOIST) experiment. This resembles to a normal Hartmann-Hahn cross-polarization excepting the synchronous (π) phase reversal of the two spin locking r.f. fields (Fig 1.)

The phases of the two r.f. irradiation fields are reversed every 1 ms so that a quasi-equilibrium is attained after each phase shift. As a result of the each CP-process is obtained a larger S spin polarization.

* Technical University, Physics Department, 3-400 Cluj-Napoca, Romania

In order to design an efficient cross-polarization transfer the understanding of the spin thermodynamic and obtaining a CP-spectrum is essential. In the following a modified spin thermodynamic theory is developed whose main

Fig 1 Pulse sequence for CP-MOIST experiment. X and X represent the phases of the rf spin locking fields

features are the important role of the dipolar energy for the quasi-equilibrium state and the existence of constants of motion others than total energy [4]

2. The Hamiltonian We will describe in the following a SI_N spin-system, where N abundant I spins (strongly coupled among themselves) are coupled to a single S spin. The coupling to further S spins is neglected. The sample is placed in a large static magnetic field which is assumed to be along the Z axis. We discuss only the situation in which we may neglect the relative motions of the spins, and all the spin - lattice relaxation times of both spin species are taken to be infinitely long.

For the spin system described above in "doubly rotating" interaction frame after " m " phase alternating of the rf field and to resonance ($\Delta\omega_I = \Delta\omega_S = 0$) the Hamiltonian becomes [3]

$$H = H_I + H_S + H_{IS} + H_{II} \quad (1)$$

Here the Hamiltonian $H_I + H_S$ describes the Zeeman interaction of the spins-system and it is

given by

$$H_I + H_S = \omega_{II} \sum_k I_{kx} (-1)^m + \omega_{IS} S_x (-1)^m \quad (2)$$

where $\omega_{II} = \gamma_I B_{II}$ and $\omega_{IS} = \gamma_S B_{IS}$ with B_{II}, B_{IS} - rf magnetic field amplitudes and γ_I, γ_S - the gyromagnetic ratios. The Hamiltonian H_{IS} represents heteronuclear-dipolar interaction Hamiltonian between I and S spins,

$$H_{IS} = \sum_k b_k (2I_{kz} S_z) \quad (3)$$

and H_{II} is homonuclear-dipolar interaction Hamiltonian

$$H_{II} = \sum_{jk} d_{jk} \left[2I_{jz} I_{kz} - \frac{1}{2} (I_j^+ I_k^- + I_j^- I_k^+) \right] \quad (4)$$

where

$$b_k = -\frac{\mu_0 \gamma_I \gamma_S \hbar^2}{4\pi r_k^3} \frac{1}{2} (3 \cos^2 \theta_k - 1)$$

and

$$d_{jk} = -\frac{\mu_0 \gamma_I^2 \hbar^2}{4\pi r_{jk}^3} \frac{1}{2} (3 \cos^2 \theta_{jk} - 1)$$

are heteronuclear and homonuclear coupling constants, with r_k, r_{jk} - the internuclear distance, θ_k, θ_{jk} - the angles between internuclear vectors and the static magnetic field. All constants are in angular frequencies units.

For a strong irradiation on both channels ($\omega_{II} d_{jk}, \omega_{IS} b_k$) it is convenient to write the Hamiltonian (1) in a tilted frame rotated about the "Y" axis defined by

$$A' = \exp \left[i \frac{\pi}{2} \left(\sum_k I_{ky} + S_y \right) \right] A \exp \left[-i \frac{\pi}{2} \left(\sum_k I_{ky} + S_y \right) \right] \quad (5)$$

giving

$$H'^I = \omega_{II} \sum_k I_{kx} (-1)^m + \omega_{IS} S_x (-1)^m + \sum_k b_k (2I_{kz} S_x) + H_{II}' \quad (6)$$

where

$$H_{II}' = -\frac{1}{2} \sum_k d_{jk} \left[2I_{jz} I_{kz} - \frac{1}{2} (I_j^+ I_k^- + I_j^- I_k^+) \right] \quad (7)$$

the secular part of the homonuclear-dipolar interaction Hamiltonian, because the nonsecular part has been neglected for strong I spins r f field (ω_{0l}, d'_{lk})

3. The spin thermodynamic theory We assume in the following that the initial spin density operator σ is prepared by an initial ($\pi/2$), pulse on the I spins, applied to a system in thermal equilibrium at the high lattice temperature T_1 in the static field B_0 . The initial spin-density operator in rotating frame becomes

$$\sigma(0) = \left(1 - \frac{\hbar\omega_{0l}}{kT_L} \sum_k I_{kz} \right) / Tr(1) \quad (8)$$

Defining

$$\alpha_{0l} = - \frac{\hbar\omega_{0l}}{kT_L Tr(1)}$$

and neglecting the unity operator term, the initial density operator in the titled rotating frame is

$$\sigma(0) = \alpha_{0l} \sum_k I_{kz} \quad (9)$$

In accordance with modified thermodynamic theory proposed by Levitt et al [4] after a sufficiently long time (about 1 ms) the system evolves to a state of quasi-equilibrium in which the observables such as magnetization and dipolar order do not change anymore. Analyzing the nature of quasi-equilibrium state we obtained that, after "m"-phase alternating r f field (π -shifts), the quasi-equilibrium density operator can be represented as the projection of the vector $\sigma(0)$ onto a two-dimensional plane defined by two orthogonal quasi-invariants $\{Q_1^{(n)}, Q_2^{(n)}\}$

They are

$$Q_1^{(m)} = q_1 \left[\sum_k I_{kz} (-1)^m + S_2 (-1)^m \right] \quad (10a)$$

and

$$\mathcal{Q}_2^{(m)} = q_2 \left[NS_z(-1)^m - \sum_k I_{kz}(-1)^m \right] + H_{II}' \quad (10b)$$

where

$$q_1 = \frac{N\omega_{1I} + \omega_{1S}}{N+1}$$

and

$$q_2 = \frac{\Delta\omega}{N+1}, \quad \Delta\omega = \omega_{1S} - \omega_{1I}$$

are the normalization factors. Then the quasi-equilibrium density operator becomes

$$\sigma^{(m)} = \alpha_{0I} \sum_{q=1}^2 a_q^{(m)} \mathcal{Q}_q^{(m)} \quad (11)$$

where the coefficients $a_q^{(m)}$ are given by recursion relation

$$a_q^{(m+1)} = a_q^{(m)} \frac{\left(\mathcal{Q}_q^{(m)} | \mathcal{Q}_q^{(m+1)} \right)}{\left(\mathcal{Q}_q^{(m+1)} | \mathcal{Q}_q^{(m+1)} \right)} \quad (12)$$

with $(A | B) = \text{Tr}\{A B\}$. Substituting (10) and (11) in (13) we obtain

$$a_1^{(m+1)} = -a_1^{(m)} \quad (13a)$$

$$a_2^{(m+1)} = -a_2^{(m)} \cos(2\theta^\lambda) \quad (13b)$$

here $\text{tg}(\theta^\lambda) = \lambda/\Delta\omega (N+1)/N$ with cross-polarization width λ given by

$$\lambda^2 = \frac{\left(H_{II}' | H_{II}' \right)}{\left(I_{kz} | I_{kz} \right)} = \frac{1}{4} N M_2'$$

where M_2' is the second moment of the I spin resonance line [4]

For $m = 0$ the coefficients $a_q^{(0)}$, $q = 1, 2$ are

$$a_1^{(0)} = \frac{N}{N\omega_{1I} + \omega_{1S}} \quad (14a)$$

$$a_2^{(0)} = -\frac{1}{\Delta\omega} \cos^2(\theta^\lambda) \quad (14b)$$

Using Eq (14) in Eq (13) we obtain

$$a_1^{(m)} = (-1)^m \frac{N}{N\omega_{1I} + \omega_{1S}} \quad (15a)$$

$$a_2^{(m)} = (-1)^m \left(-\frac{1}{\Delta\omega} \right) \cos^2(\theta^\lambda) \cdot \cos^m(2\theta^\lambda) \quad (15b)$$

Taking into account these coefficients in Eqs (11) for density operator, after "m"

phase alternating r f field the density operator becomes

$$\begin{aligned} \sigma^{(m)} = & \alpha_{0I} \frac{N}{N+1} \left[1 - \cos^2(\theta^\lambda) \cos^m(2\theta^\lambda) \right] S_z + \\ & + \alpha_{0I} \frac{N}{N+1} \left[1 + \frac{\cos^2(\theta^\lambda) \cos^m(2\theta^\lambda)}{N} \right] \sum_k I_{kz} + \\ & + (-1)^m \frac{\alpha_{0I}}{\Delta\omega} \cos^2(\theta^\lambda) \cos^m(2\theta^\lambda) H_{II}^{T'} \end{aligned} \quad (16)$$

The expected value for S spin polarization (CP-spectrum) after CP-MOIST experiment for SI_N spin-systems is given by

$$(S_z)^{(m)} = Tr(\sigma^I S_z) = - \frac{\hbar\omega_{0I}}{4KT_L} \frac{N}{N+1} \left[1 - \cos^2(\theta^\lambda) \cos^m(2\theta^\lambda) \right] \quad (17)$$

From Eq (17) we observe that, for a given mismatch ($\Delta\omega \neq 0$) we obtain the increase of polarization amount with number of phase shifts "m". Also for $m = 0$ in Eq (17) we find the result (22) from Ref [5]

4. Conclusions The modified spin thermodynamic theory whose main features are the important role of dipolar energy for the quasi-equilibrium state and the existence of the motion others than the total energy has been applied to a CP-MOIST experiment for a SI_N system. The S spin polarization has been derived for "m" phase shifts and a given mismatch $\Delta\omega$. A qualitative agreement with experimental results [4] has been obtained.

REFERENCES

- 1 A. Pines, M N Gibby, and J S Waugh, J Chem Phys, 59, 569 (1973)
- 2 S R Hartmann and E L Hahn, Phys Rev 128, 2024 (1962)
- 3 M H Levitt, D Suter and R R Ernst J Chem. Phys., 84, 4243 (1986)
- 4 A Abragam, The Principles of Nuclear Magnetism (Clarendon, Oxford 1961)
- 5 B H Meier, Chem Phys Lett, 188, 201 (1992)

THE RECONSTRUCTION OF THE STATE SPACE FROM CHAOTIC TIME SERIES

Steliana CODREANU*

Received 1 03 1993

ABSTRACT. - There are various observational evidences that in variable stars the temporal behavior is often an irregular one. A new insight on this domain can be obtained with the methods of nonlinear dynamics. The purpose of the paper is to describe the method of the reconstruction of the state space from time series and then to apply this method to the variable star Wolf-Rayet 16.

1. Introduction. Chaos is the irregular behavior of simple deterministic equations, and irregular fluctuations are present in both natural and man-made systems. Chaos is a new paradigm for the understanding of complex dynamics and irregular structures, in an enormous range of quite different systems [1] [2]. For a physicist confronted with a dynamical system that exhibits aperiodic fluctuations, this is an appealing notion, because it implies that these fluctuations might be explained in terms of only a few equations of motion. If it is possible to model these complicated variations with simple deterministic equations, then it becomes possible to predict future variations, at least in the short term.

The mathematical properties of nonlinear equations have been studied since the time of Poincaré [3], but the physical implications of chaos have been not widely appreciated until the numerical work of Lorenz [4], which provided researchers with a simple and specific example of chaos.

Until recently, the notion of determinism and randomness were seen as opposites and

* "Babeș-Bolyai" University, Faculty of Physics, 3400 Cluj-Napoca, Romania

were studied as separate subjects with little or no overlap. Complicated phenomena so only simple phenomena were assumed to result from complicated physics among many degrees of freedom, and thus they were analyzed as random processes. Simple dynamical systems were assumed to produce simple phenomena were modeled deterministically.

Chaos provides a link between deterministic systems and random processes. In a deterministic system, chaotic dynamics can amplify small differences, which in the long run produces unpredictable behavior. But, on the other hand, chaos implies that not all random-looking behavior is the product of complicated physics. Under the influence of nonlinearity, only few degrees of freedom are necessary to generate chaotic motion [5]. In this case, it is possible to model the behavior deterministically, and to make short term predictions, that are far better than those that would be obtained from a linear stochastic model. So, chaos implies that even approximate long-term predictions may be impossible, but that very accurate short-term predictions may be possible.

In this paper we consider the situations in which one tries to find a model directly from the experimental data. We are interested in time series which arise from observations of a supposed deterministic dynamical system. Of course, the dynamics are never strictly deterministic due to dynamical noise which perturbs the states of the system or due to observational noise. We will consider those situations where the dynamical and observational noise are reasonably small and where much of the apparent randomness is caused by low dimensional chaotic behavior.

An important notion in nonlinear dynamics is the dimension of the dynamics, which indicates the number of irreducible degrees of freedom. We have considered that complex aperiodic behavior can result from deterministic physical systems with only a few degrees of

freedom. But it is also the case that a dissipative dynamical system which has many degrees of freedom (such as a fluid), may settle down, after an initial transient, to motion in which only a few degrees of freedom are active. The dimension counts the number of degrees of freedom necessary to describe this motion, and thus quantifies the difficulty with which the system's behavior can be modeled.

Usually one observes a time series with fewer variables than are needed to fully describe the dynamical system. Indeed, the time series in many cases consists only of a sequence of scalar values. Building a dynamical model directly from the data involves two steps: the state space reconstruction and the nonlinear function approximation. In this paper we will consider only the first step of the problem, with an interesting application to the variable stars.

2. State space reconstruction. A state $s(t)$ is a parameters set, typically a real vector, which fully describes the system at a fixed instant in time t . If it is known with complete accuracy and if the system is strictly deterministic, then the state contains sufficient information to determine the future of the system. The goal of state space reconstruction is to use the immediate past behavior of the time series to reconstruct the current state of the system (at least to a level of accuracy permitted by noise). The *dynamics* is a function f which maps the current state $s(t)$ to a future state $s(t + T)$. In the case of chaotic behavior the functional form of f must be nonlinear.

There are many situations in which a time series $\{x(t_i)\}$, $i = 1, 2, \dots, N$ is believed to be at least approximately described by a smooth dynamical system f on a d -dimensional manifold M (for simplicity it is often assumed that $M = \mathbb{R}^d$). We can represent the dynamical system

by the map f^t which relates the initial state $s(0)$ to a state $s(t)$:

$$s(t) = f^t[s(0)] \quad (1)$$

The time variable t can be either continuous or discrete, and f^t is some times called the time - t map of dynamical system.

In the absence of noise, the time series is related to the dynamical system by

$$x(t) = h[s(t)] \quad (2)$$

where h is called the measurement function

In the presence of noise, the time series can be generated by a dynamical system

$$s(t) = f^t[s(0)] + \eta(t)$$

$$x(t) = h[s(t)] + \xi(t)$$

where ξ denotes the observational noise, η denotes the dynamical noise, and because the only observable is $\{x(t)\}$ then s , f^t , η , h , and ξ must be obtained from the time series.

For simplicity we will consider the case in the absence of noise (1), (2). The time series $x(t)$ is D -dimensional, so that $h: M \rightarrow \mathbb{R}^D$ where $D < d$. The measurement function h is often a scalar one and it is implicitly assumed $D = 1$.

The state space reconstruction problem is that of recreating states when the only information available is contained in time series, and this problem is necessarily the first step that must be taken to analyze a time series in terms of dynamical system's theory

Typically f and h are both unknown, so that we can not hope to reconstruct states in their original form, but we may be able to construct a space that is in some sense equivalent to the original. This state space can be used for qualitative analysis, such as phase portraits, or for quantitative statistical characterizations

The state space reconstruction was introduced into dynamical systems theory

independently by Packard et al [6] and Takens [7] by the demonstration that it is possible to preserve geometrical invariants, such as the eigenvalues of a fixed point, the fractal dimension of an attractor, or the Lyapunov exponents of a trajectory, and can in principle be estimated from the time series

The basic idea behind state space reconstruction is that the past and future of time series contain information about unobserved state variables that can be used to define a state at the present time. The past and future information contained in the time series can be described by the delay vector defined by

$$\underline{x}(t) = [x(t+\tau m_p), \dots, x(t), \dots, x(t-\tau m_f)]^T \quad (3)$$

where for convenience the sampling time τ is assumed uniform. Here "+" denotes the transpose and by convention all states are taken to be column vectors

The dimension of the delay vector is $m = 1 + m_p + m_f$, where m_p is the number of samples taken from the past and m_f the number from the future. If $m_f = 0$ then the reconstruction is predictive (otherwise is mixed). In this case

$$\underline{x}(t) = [x(t), \dots, x(t-(m-1)\tau)]^T \quad (4)$$

and m is called the *embedding dimension*.

Takens studied the global properties of the map that takes the original states(t) to the delay $\underline{x}(t)$, and proved that in absence of noise, if $m \geq 2d + 1$, then this map generically forms an *embedding*. An embedding is a smooth one-to-one coordinate transformation with a smooth inverse. So that the reconstructed state space is diffeomorphic to the original state space

Delay vectors are currently the most widely used choice for state space reconstruction, but in order to use them it is necessary to choose the delay parameter τ . Although Takens

theorem indicates that this choice is not important, in practice, because of noise, is very important to choose a good value for τ . Now there are many theoretical approaches to choose an optimal τ and m [8], [9]

Another method of state space reconstruction is the principal components technique. This is a standard procedure in signal processing, and was first applied to chaotic dynamical systems by Broomhead and King [10]. The procedure is to compute a covariant matrix

$$C_{ij} = \langle x(t-i\tau) \times (t-j\tau) \rangle, \quad (5)$$

where $|i - j| < m$, and $\langle \rangle_t$ denotes a time average, and then compute its eigenvalues. The eigenvectors of C_{ij} define a new coordinate system, which is a rotation of the original delay coordinate system. The eigenvalues are the average root mean-square projection of the m -dimensional delay coordinate time series onto the eigenvectors. Ordering them according to size, the first eigenvector has the maximum possible projection, the second has the largest possible projection for any fixed vector orthogonal to the first, and so on.

Filtering is another procedure that is often used in state space reconstruction and can be used in combination with any reconstruction technique [11]. Results of Badii et al [12] show that some type of filtering can increase the dimension of a time series, but recently Mitschke [13] has shown numerically that this effect can be corrected if acausal filters are used.

It is clear that the method of reconstruction can make a difference in the quality of resulting coordinates, but at this moment it is not clear which method is the best [14].

3.Dimension estimation The development of algorithms for estimating the dimension of an attractor directly from a time series has been an active field of research over

the last decade. The objective of these algorithms is to estimate the fractal dimension of a hypothesized chaotic attractor in a reconstructed state space. If the time series is deterministic and of finite dimension, the estimated dimension of the reconstructed attractor should converge to the chaotic attractor, as the embedding dimension is increased. If the time series is random, the estimated dimension should be equal to the embedding one.

Historically, the first numerical algorithm was based on a "box-counting" principle [15], but this was found impractical in many situations [16]. The most used way to compute dimension is the method developed by Grassberger and Procaccia [17]. The method defines a correlation integral $C(m, N, l)$, which is an average of the pointwise mass functions $B(\underline{x}, m, N, l)$ at each point \underline{x} in the reconstructed state space. Here m is the dimension of the embedding space, N is the number of points, $B(\underline{x}, m, N, l)$ is the fraction of points within a distance l of the point \underline{x} . The asymptotic scaling of $C(m, N, l) \sim l^d$ for small l defines the *correlation dimension* d .

There are also other approaches for estimating dimension [18] and even recently was proposed an electronic instrument for measuring the pointwise correlation dimension from time series, called "dimensimeter" [19].

4. Applications A variety of time series have been analyzed with nonlinear methods, exposed briefly by us, in a wide class of domains such as fluid flows [20], sunspots [22], mechanical vibrations [21], ice ages [23], measles epidemics [24], electrodynamical convection [25], white dwarf star [26], magnetoencephalograms from human brain [27], etc. We also have investigated the time series from the variable star Wolf-Rayet 16 (WR16) with the same methods [28]. The complexity of the Fourier spectrum (Fig 1) obtained in this case

could indicate a nonlinear dynamics

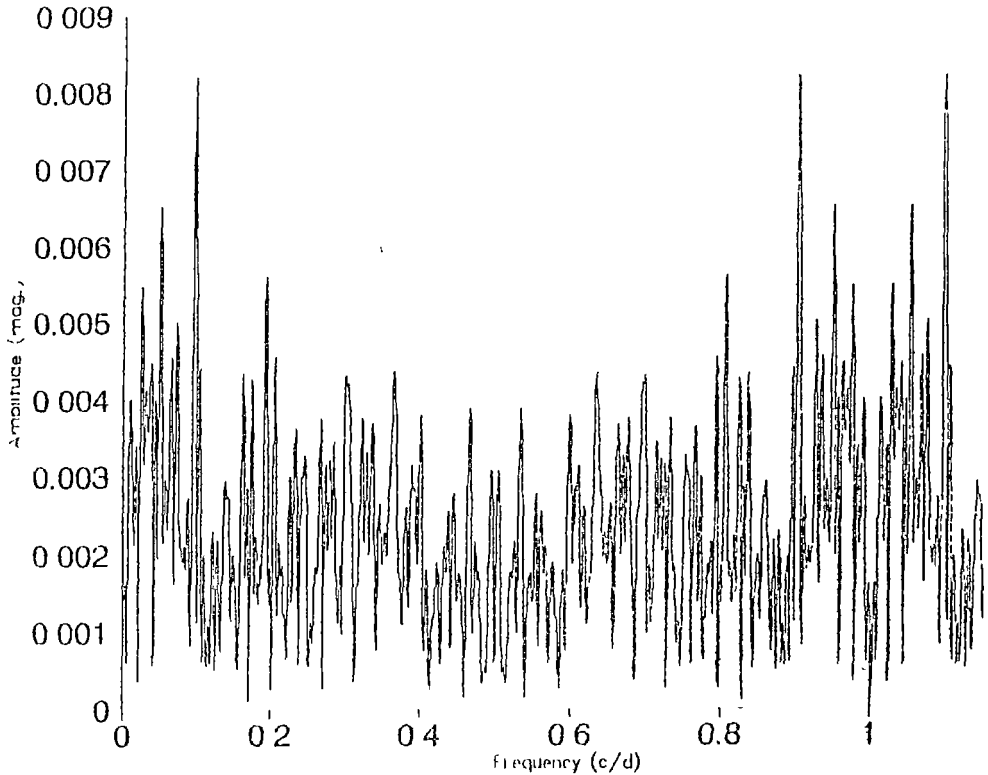


Fig 1 Fourier spectrum

The basic consideration is that the stars with irregular light curves and variables frequencies might be associated with nonlinear dissipative systems. A variable star, as a dissipative oscillator, can have a rich dynamics exhibiting quasiperiodic or even chaotic behaviors. It is known that a dissipative system do not remember their initial conditions. It has a great sensitivity to the initial conditions and an intrinsic unpredictability in the long term. By using a statistical description of the states of the system, the trajectories in the phase space (the state space), as the time evolves, will converge and remain in a given region of this

space. This invariant subset of the phase space is the attractor of the system. Its dimension is a very useful tool to obtain informations on the dynamics of the system. For instance, if the dimension d is $d = 1$, the system exhibits self-sustained periodic oscillations, if $d = 2$ the oscillations of the system are quasiperiodic with two incommensurate frequencies, and if d is non-integer the system exhibits a chaotic oscillation. It is also very important to know the minimal dimension of the state within which the attractor is embedded, because this defines the minimum number of variables that must be considered in the description of the system's dynamics.

In the case of variable star that we have investigated the dynamical system is known only through a single observable $x(t)$, its magnitude, and the series is actually the light curve [29], indicated in Fig 2.

For the phase space reconstruction we have used the time delay method (the embedding theorem [30]) a m dimensional portrait of the system, topologically equivalent to the one constructed from the physical variables is given by the set

$$A = \{ X \in \mathbb{R}^m = [x_1(t), x_2(t+\tau), x_3(t+2\tau), \dots, x_m(t+(m-1)\tau)] \}$$

where τ is the delay time.

This allowed us to draw the projection of the phase portrait of the system to a low-dimensional subspace of the full phase space. In Fig 3 a two dimensional projection of the reconstructed phase space is plotted. The dimension of the attractor - the fractal dimension d - was calculated by using the integral correlation function [17]. This correlation function $C(l)$, defined by

$$C(l) = \lim_{N \rightarrow \infty} \frac{1}{N^2} \sum_{\substack{i, j=1 \\ (i \neq j)}}^N \theta(|x_i - x_j| - l) \tag{6}$$

where θ is the Heaviside step function, has the property

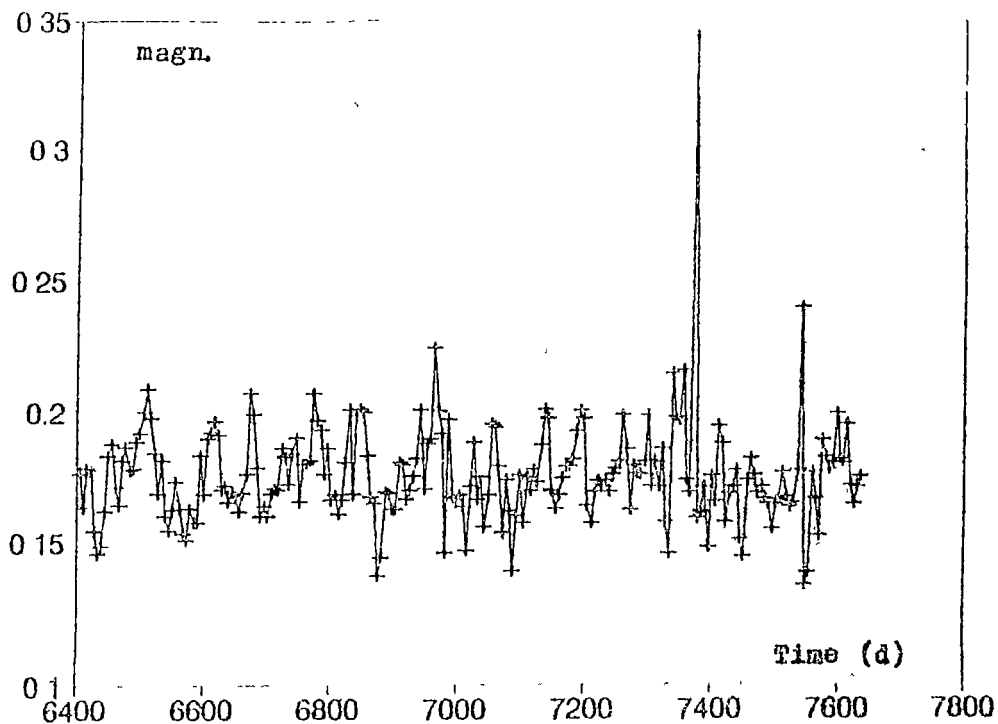


Fig 2 Light-curve of WR 16

$$C(1) \sim 1^d \quad (7)$$

and for small values of 1 , d can be considered as a fractal dimension. We have calculated the correlation function (6) for different values of m . To visualise the fractal dimension it is convenient according to (7) to plot $\ln C(1)$ as a function of $\ln 1$. The general slope of the curves indicates the values of d . In Fig 4 the correlation function is shown for different values of m .

5. The limitations of the method and conclusions. The discontinuities in the data sets due to day-night alternance and to the variable seeing conditions do not allow one to treat these data sets like those obtained in a laboratory experiment when no real limitation on the

THE RECONSTRUCTION OF THE STATE SPACE

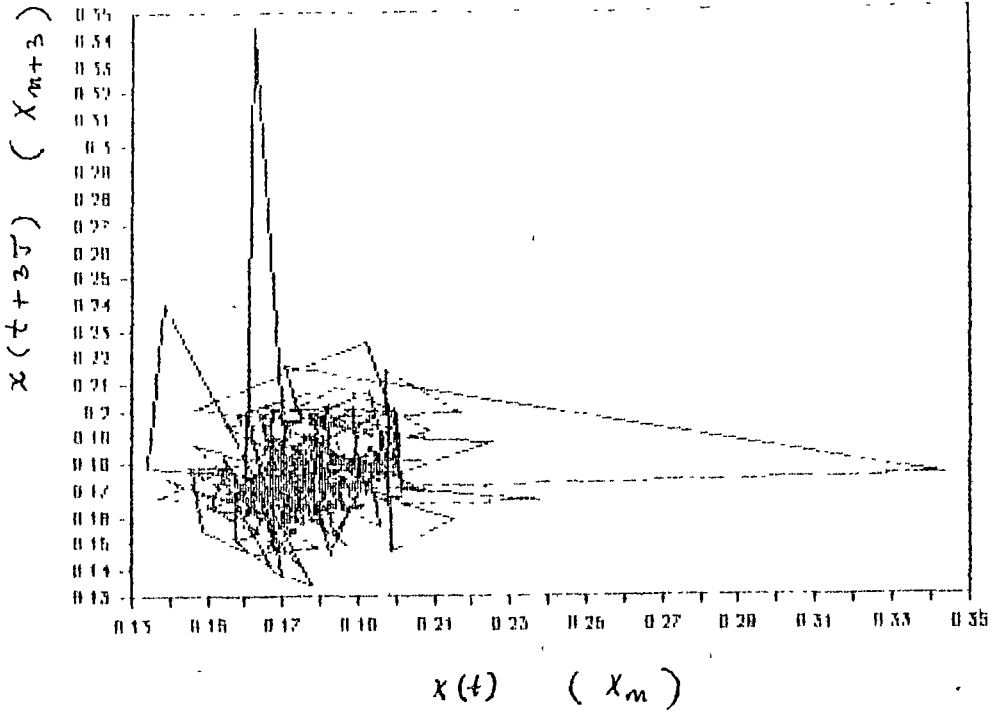


Fig 3 Two dimensional projection of the reconstructed phase-space

length of set of data exists. From this point of view a very precise description of the attractor of the stellar oscillations is not possible. So the method used by us does not aim to obtain a precise value of the fractal dimension on such sets observational data, but to evaluate the number of independent parameters responsible for dynamics of the system. From Fig 4, as m increases, the correlation function varies, but for $m \geq 4$ the slope can be considered as constant in a given range of 1. This indicates that the number of differential equations necessary to describe the light variations for WR 16 must be at least four.

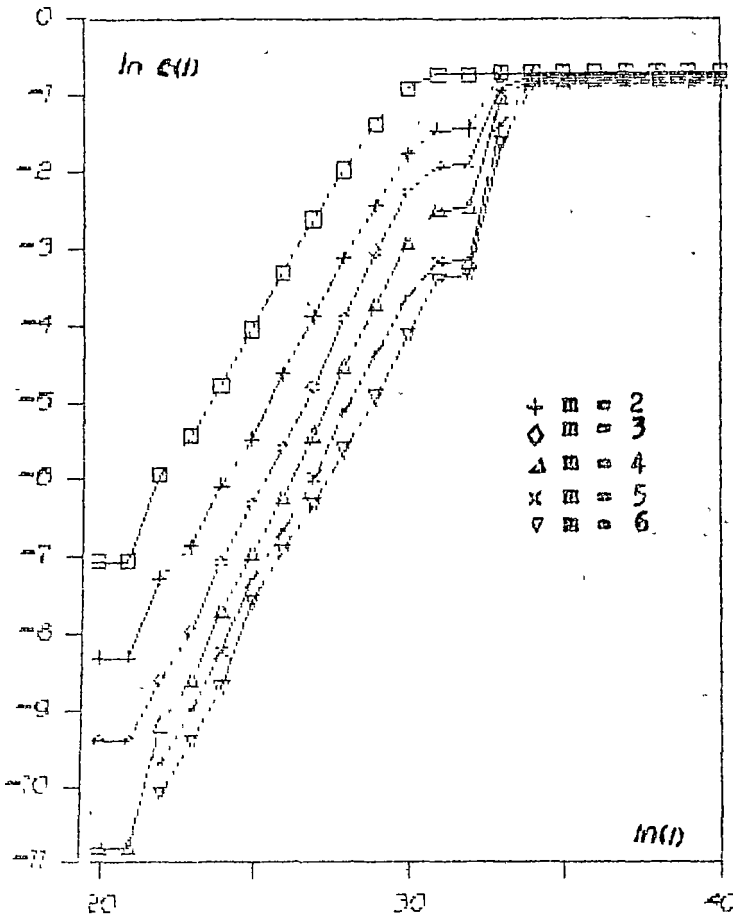


Fig 4 Correlation function of WR 16 for different values of m .

REFERENCES

- 1 Evolution of Order and Chaos in Physics, Chemistry and Biology- ed by H Haken, Springer Series in Synergetics, Vol 17, Springer 1982
- 2 H G Schuster - Deterministic Chaos, Physik Verlag, Weinheim, 1984
- 3 H Poincaré - Science et Methode, Bibl Scientifique, 1908
- 4 E N Lorenz- Journal of Atmospheric Science, 20, 130, 1963
- 5 G L Baker, J P Gollub- Chaotic dynamics- an introduction, Cambridge Univ. Press, 1992
- 6 N H Packard, J P Crutchfield, J D Farmer, R S Shaw- Phys Rev Lett, 45, 712, 1980
- 7 F Takens- Dynamical Systems and Turbulence, Berlin, Springer-Verlag, 1981
- 8 W Liebert, H G Schuster - Phys Lett A, 142, 107, 1988
- 9 A Cenys, K Pyragas, - Phys Lett A, 129, 227, 1988
- 10 D S Broomhead, G P King- Physica D, 20, 217, 1987

THE RECONSTRUCTION OF THE STATE SPACE

- 11 A Chennaoui, K Pawelzik, W Liebert, H G Schuster, G Pfister - Phys Rev A, 41, 4151, 1990
- 12 R Badin, G Boggi, B Derighetti, M Ravagni, S Ciliberto, A Politu, M A Rubio - Phys Rev Lett, 60, 979, 1988
- 13 F Mitsche - Phys Rev A, 41, 1169, 1990
- 14 M Casdagli, D Des Jardins, S Eubank, J D Farmer, J Gibson, N Hunter, J Theiler Preprint LA-UR-91-1637, 1991
- 15 D.A Russell, J D Hanson E Ott-Phys Rev Lett, 45, 1175, 1980
- 16 H S Greenside, A Wolf, J Swift, T Pignataro - Phys Rev A, 25, 3453, 1982
- 17 P Grassberger I Procaccia - Phys Rev Lett 50, 346, 1983, Physica D, 9, 189, 1983
- 18 Dimensions and Entropies in Chaotic System - Proc of International Workshop New Mexico, sept , 11-16 1985, Editor G Mayer-Kress, springer Verlag Berlin, 1986
- 19 A.Namajunas A Tamasevicius-Physica D, 58, 482, 1992
- 20 J.D Farmer, J J Sidorowich - Phys Rev. Lett , 59, 845, 1987
- 21 F Moon-Perspectives in Nonlinear Dynamics, Editors-M F Shlesinger, R Cawley, A W Saez, W Zachary, World Scientific, 1986
- 22 J Kurthas, A A Ruzmaikin-Solar Phys , 126, 407, 1990
- 23 G Nicolis-Report on Progress in Physics, 49, 873, 1986
- 24 G Sugihara, R.May-Nature, 344, 734, 1990
- 25 J G Caputo-Advances in Nonlinear Dynamics, World Scientific, 1985
- 26 M Auvergne, A Baglin-Astron Astrophys , 168, 118, 1986
- 27 H R Blank et al. - Dimension and entropy analysis of MEG time series from human α - rhythm - Zeitschrift fur Physik B, (to appear)
- 28 S Codreanu, Z Toroczkat, A Pentek, Al.V Pop - The 18th IUPAN Internat Conf on Statistical Physics, Berlin 2-8 Aug 1992. 401, 1992
- 29 E Gosset, J M.Vreux, J Manfroid, M Remy, C.Sterken - ESO Sci Preprint Nr 703, 1990
- 30 F Takens - Phys Rev Lett , 51, 14, 1265, 1980



THE BEHAVIOUR OF THE NUCLEON SPIN
IN A PERIODIC PHASE OF THE NUCLEAR MATTER

Attila MIHÁLY

Received 20.06.1993

ABSTRACT. - A phase transition of nuclear matter into a periodic phase has been found. Studying the third component of nucleon spin in this phase, we have found that the $\exp(-mkz)$ type modulations of the plane wave states are not present in the expectation value of this component.

Recently a periodic structure in nuclear matter has been found [1] in the framework of quantumhydrodynamics using mean-field approximation. In this letter we summarise the main features of this periodic phase and calculate the third component of nucleon spin expectation values.

In the last few years the possibility of a periodic structure in nuclear matter was investigated extensively [2,3,4]. In these works the periodic behaviour of the matter density is studied. In a recent work [1] a periodic structure in the current density at constant matter density has been found.

In the framework of the quantumhydrodynamics the nucleons (ψ), the scalar mesons (σ), and the vector mesons (ω^μ) are described by the following field equations

$$[\gamma_\mu (i\partial^\mu - g_\omega \omega^\mu(x)) + g_\sigma \sigma - m] \psi(x) = 0 \quad (1)$$

$$\square \sigma + m_\sigma^2 \sigma = g_\sigma \bar{\psi} \psi \quad (2)$$

$$\square \omega_\mu + m_\omega^2 \omega_\mu = g_\omega \bar{\psi} \gamma^\mu \psi \quad (3)$$

The coupling constants g_ω , g_σ and the masses m , m_σ , m_ω are given in [1] In the mean field approximation the meson fields operators are replaced by their expectation values, which are assumed to have the following forms

$$\begin{aligned} \langle \sigma(x) \rangle &= \bar{\sigma}, \quad \langle \omega^0(x) \rangle = \bar{\omega}^0, \\ \langle \omega^1(x) \rangle &= \bar{\omega} \cos kz, \quad \langle \omega^2(x) \rangle = -\bar{\omega} \sin kz, \quad \langle \omega^3(x) \rangle = 0 \end{aligned} \quad (4)$$

According to this Ansatz the ω -field has a static, periodic variation along the z axis, defined by the wave vector k This periodicity induces a similar periodic behaviour of the nuclear vector current, i.e. the matter density $(\bar{\psi} \gamma^0 \psi)$ is constant and the current densities $(\bar{\psi} \gamma^1 \psi)$ and $(\bar{\psi} \gamma^2 \psi)$ are periodic

In this approximation the single particle nucleon states can be considered as independent quasiparticle states described by Bloch waves

$$\psi_i(p, x) = e^{-ipx} \sum_{n=-N}^N u_i(\vec{p}, n) e^{-inkx} \quad (5)$$

Here the bispinors $u_i(\vec{p}, n)$ are the solutions of the following equation

$$\sum_{n'=-N}^n H_{nn'} U_i(\vec{p}, n') = E_i u_i(\vec{p}, n), \quad (6)$$

where

$$\begin{aligned} H_{nn'} &= \gamma^0 [\vec{\gamma} \vec{p} + \gamma^3 nk + m^* + \gamma^0 g_\omega \bar{\omega}^0] \delta_{nn'} - \\ &- \frac{1}{2} g_\omega \bar{\omega} \gamma^0 (\gamma^{1-} \delta_{n+1, n'} + \gamma^{1+} \delta_{n-1, n'}) \end{aligned} \quad (7)$$

and

$$\gamma^{1\pm} = (\gamma^1 \pm i \gamma^2) \quad (8)$$

The source terms $\bar{\psi} \Gamma \psi$ are also replaced by their expectation values $\langle \bar{\psi} \Gamma \psi \rangle$, which are defined by the help of the Fermi-Dirac distribution

$$\theta(T, \mu, E_i(\vec{p})) = (1 + e^{(E_i(\vec{p}) - \mu)/T})^{-1} \quad (9)$$

where $E_i(\vec{p})$ are the energy eigenvalues from Eq (6) The temperature and the baryon chemical potential are denoted by T and μ respectively (The chemical potential of the antibaryons is $-\mu$) The field equations lead to a set of selfconsistent equations At fixed values of the parameters T, μ and k these selfconsistent equations can be solved numerically for $\bar{\sigma}, \bar{\omega}^0$, and $\bar{\omega}$

The

$$\begin{aligned} (\bar{\psi} \sum_K \psi) &= \sum_i \sum_{n=-N}^N \sum_{n'=-N}^N e^{i(n'-n)kz} \\ &\int_{-\infty}^{\infty} dp_1 \int_{-\infty}^{\infty} dp_2 \int_{-k/2}^{k/2} dp_3 \theta(T, \mu, E_i(\vec{p})) u_i(\vec{p}, n') \sum_K u_i(\vec{p}, n) \end{aligned} \quad (10)$$

where

$$\sum_K = \begin{pmatrix} \sigma_K & 0 \\ 0 & \sigma_K \end{pmatrix} \quad (11)$$

In (11), σ_K ($K = 1, 2, 3$) are the Pauli matrices

We have found by direct calculation that the coefficients of $\exp[-i(n-n')kz]$ in (10) at $K = 3$ were more than four orders of magnitude smaller in the case $n' \neq n$ than those with $n' = n$ This means that the $\exp(-inkz)$ ($n = 1, 2, \dots, N$) type modulations of the plane wave states are not present in the third component of nucleon spin

For the sake of physical interpretation of this result, we calculate the selfconsistent "magnetic" field due to the periodicity of the ω -field

The field tensor defined as

$$F^{\mu\nu} = \partial^\nu \omega^\mu - \partial^\mu \omega^\nu \quad (12)$$

has only two non-vanishing elements

$$\begin{aligned} F^{13} &= \bar{\omega} k \sin kz \approx H^2, \\ F^{23} &= \bar{\omega} k \cos kz \approx -H^1 \end{aligned}$$

This means that this "magnetic" field is perpendicular to the z axis

Therefore, the parallel component of the "magnetic" field is null and it cannot influence the projection of the nucleon spin on this direction. In other words, the z component of the nucleon spin can "choose" any orientation, and our numerical results are quite natural.

However, we must notice that the situation is quite different for the other directions, where the periodic components of the "magnetic" field do act. Thus the next step in our study is going to be the study of the perpendicular components of the nucleon spin, which, by using the same line of thought, should have periodic expectation values along the z axis.

Acknowledgement. The author is very much indebted to I. Lovas and L. Tătaru for the illuminating discussions.

REFERENCES

- 1 I. Lovas, L. Molnár, K. Sailer and W. Greiner, Phys. Rev. **C45** (1992) 1693
- 2 Yu. B. Ivanov, Nucl. Phys. **A474** (1987) 669
- 3 B. L. Friman and P. Henning, Phys. Lett. **B206** (1988) 579
- 4 C. E. Price, J. R. Shepard and J. A. McNeil, Phys. Rev. **C41** (1990) 1234

STUDIA

UNIVERSITATIS BABEŞ-BOLYAI

PHYSICA

38(2)

1993

CLUJ-NAPOCA

REDACTOR ȘEF: Prof. A. MARGA

**REDACTORI ȘEFI ADJUNCȚI: Prof. N. COMAN, Prof. A. MAGYARI, Prof. I. A. RUS,
Prof. C. TULAI**

**COMITETUL DE REDACȚIE AL SERIEI FIZICĂ: Prof. E. BURZO (redactor
coordonator), Prof. I. ARDELEAN, Prof. O. COZAR, Prof. S. SIMON, Prof. E.
TĂTARU, Conf. A. NEDA, Cercet. și. II S. COLDEA (secretar de redacție)**

În cel de al XXXVIII-lea an (1993) *Studia Universitatis Babeş-Bolyai* apare în următoarele serii:

matematică (trimestrial)
fizică (semestrial)
chimie (semestrial)
geologie (semestrial)
geografie (semestrial)
biologie (semestrial)
filosofie (semestrial)
sociologie-politologie (semestrial)
psihologie-pedagogie (semestrial)
ştiinţe economice (semestrial)
ştiinţe juridice (semestrial)
istorie (semestrial)
filologie (trimestrial)
teologie ortodoxă (semestrial)
educaţie fizică (semestrial)

In the XXXVIII-th year of its publication (1993) *Studia Universitatis Babeş-Bolyai* is issued in the following series:

mathematics (quarterly)
physics (semesterly)
chemistry (semesterly)
geology (semesterly)
geography (semesterly)
biology (semesterly)
philosophy (semesterly)
sociology-politology (semesterly)
psychology-pedagogy (semesterly)
economic sciences (semesterly)
juridical sciences (semesterly)
history (semesterly)
philology (quarterly)
orthodox theology (semesterly)
physical training (semesterly)

Dans sa XXXVIII-e année (1993) *Studia Universitatis Babeş-Bolyai* paraît dans les séries suivantes:

mathématiques (trimestriellement)
physique (semestriellement)
chimie (semestriellement)
géologie (semestriellement)
géographie (semestriellement)
biologie (semestriellement)
philosophie (semestriellement)
sociologie-politologie (semestriellement)
psychologie-pédagogie (semestriellement)
sciences économiques (semestriellement)
sciences juridiques (semestriellement)
histoire (semestriellement)
philologie (trimestriellement)
théologie orthodoxe (semestriellement)
éducation physique (semestriellement)

CONTENTS

Theoretical Physics

- S. CODREANU, T. COLOȘI, M. DANCA: A Study of a Simple **Nonlinear** Mechanical System 3
- D. ȚAȚOMIR, D. RADU, O. MIHALACHE: Massive Vector, Tensor and Spin-3/2 Particles Gravitationally Scattered on Schwarzschild Background 31
- T. A. BEU: Fourth Order Torsion L-Tensor Formulas For Anharmonic Force Constant Transformation 43

Plasma Physics

- J. KARÁCSONYI, Z. KISS: Excitation of Lower Hybrid Waves in a Warm Plasma by a Warm Relativistic Electron Beam 53
- S. COLDEA: Analysis of the Physical Characteristics of a Dusty Plasma I. The Grain Charges and Their Effects 61
- S. COLDEA : Analysis of a Physical Characteristics of a Dusty Plasma II. The Collective Effects for the Drag on a Moving Dust Grain 71

Optics, Spectrometry and Nuclear Physics

- T. ILIESCU, A. SIKE: Vibrational and Rotational Relaxation in Pyrrole Pure **Liquid** and Solutions Studied by Raman Spectroscopy 77
- L. DĂRĂBAN, T. FIAT, E. VARI-NAGY: Total Cross Section Determination by Fast Neutrons Spectrometry on an Isotopically Enriched ^{15}N Target Using an ^{241}Am - ^{9}Be Neutron Source 89
- E. CULEA, I. MILEA: Spectroscopic Investigation of the Influence of Melting Temperature on the Redox Equilibrium of Uranium Ions in $0.95\text{Na}_2\text{B}_4\text{O}_7$ - $0.05\text{Al}_2\text{O}_3$ - 0.02UO_3 Glasses 105

S T U D I A

UNIVERSITATIS BABEŞ-BOLYAI

PHYSICA

2

Redacția 3400 CLUJ-NAPOCA str. M. Kogălniceanu nr. 1 ▶ Telefon: 116101

S U M A R - C O N T E N T S - S O M M A I R E

Theoretical Physics

- S CODREANU, T COLOȘI, M DANCA A Study of a Simple Nonlinear Mechanical System 3
 D ȚĂTOMIR, D RADU, O MIHALACHE Massive Vector, Tensor and Spin-3/2 Particles Gravitationally Scattered on Schwarzschild Background 31
 T A BEU Fourth Order Torsion L-Tensor Formulas For Anharmonic Force Constant Transformation 43

Plasma Physics

- J KARÁCSONYI, Z KISS Excitation of Lower Hybrid Waves in a Warm Plasma by a Warm Relativistic Electron Beam 53
 S COLDEA Analysis of the Physical Characteristics of a Dusty Plasma I The Grain Charges and their Effects 61
 S COLDEA Analysis of a Physical Characteristics of a Dusty Plasma II The Collective Effects for the Drag on a Moving Dust Grain 71

Optics, Spectrometry and Nuclear Physics

- T. ILIESCU, A. SIKE Vibrational and Rotational Relaxation in Pyrrole Pure Liquid and Solutions Studied by Raman Spectroscopy 77
 L. DĂRĂBAN, T. FIAT, E. VARI-NAGY. Total Cross Section Determination by Fast Neutrons Spectrometry on an Isotopically Enriched ^{15}N Target Using an ^{241}Am - ^9Be Neutron Source 89
 E. CULEA, I. MILEA. Spectroscopic Investigation of the Influence of Melting Temperature on the Redox Equilibrium of Uranium Ions in $0.95\text{Na}_2\text{B}_4\text{O}_7-0.05\text{Al}_2\text{O}_3-0.02\text{UO}_3$ Glasses 105



A STUDY OF A SIMPLE NONLINEAR MECHANICAL SYSTEM

S. CODREANU*, Tb. COLOȘI**, M. DANCA**

Received 30 05 1994

ABSTRACT. - The aim of a paper is an analytical and numerical investigation of a nonlinear mechanical system. This system is a parametrically forced mechanical oscillator, with cubic nonlinearity. We demonstrate that the system exhibits a very complicated dynamics, including equilibrium points, limit cycles and complicated chaotic attractors. For the numerical simulation we have used an original method.

Introduction. The irregular and unpredictable time evolution of many nonlinear systems has been called chaos or deterministic chaos. It occurs in many and different domains of the science like physics, chemistry, astronomy, biology, economy etc. [1], [2]. For example it can be observed in mechanical oscillators such as forced pendula or vibrating object [3], [4], but also in rotating or heated fluids [5], [6], in nonlinear circuits [7], in laser cavities [8], in nonlinear optical devices [9], [10], in Josephson junction [11]-[13], in plasmas [14], in some chemical reactions [15]-[17], in biological and ecological models [18], [19] or in stimulated heart cells [20] and in Electroencephalogram data [21].

The central characteristic of the systems which exhibit a chaotic dynamics is that the systems do not repeat their past behavior although they follow deterministic equations. For chaotic systems the slightly different initial conditions lead to an error in prediction that grows exponentially in time. This characteristic, which occurs only when the governing equations are nonlinear, is known as sensitivity to initial conditions. The first who recognized

* "Babeș-Bolyai" University, Faculty of Physics, 3400 Cluj-Napoca, Romania

** Technical University, 3400 Cluj-Napoca, Romania

this phenomenon was Henri Poincaré (1913). Although a chaotic system can resemble a stochastic one, (i.e. a system subject to a random external force), the source of the irregularity is quite different. For chaos the irregularity is part of the intrinsic dynamics of the system, not unpredictable outside influences. If the dynamical system is described by a set of first order differential equations the necessary conditions for chaotic motion are that the system has at least three independent dynamical variables and the equations of motion contain a nonlinear term.

The equations can often be expressed in the form

$$\frac{dx_i}{dt} = F_i(x_1, x_2, \dots, x_n)$$

where $i = 1, 2, \dots, n$ ($n \geq 3$) and with F for example of the form

$$F = ax_1 + bx_2 + cx_1x_2 + \dots + f\lambda_n$$

where a, b, c, f are constants. For some choice of the constants, such systems are often chaotic.

From a historical point of view the development of the study of chaotic systems is a recent one, despite the fact that chaotic systems are deterministic and are described by many of the well known equations. This is due to the fact that, with the exception of some first order equations, nonlinear differential equations are either difficult or impossible to solve analytically. So, the solution of nonlinear differential equations generally requires numerical methods. The first who detected chaos in a nonlinear dynamical system by a numerical study was E. Lorenz [22].

One of the simplest physical systems with a rich and complex behavior, which has been intensively analyzed, is the damped driven pendulum [23], [24]. This is a based nonlinear model system for different more complicated physical problems (nonlinear oscillators) like

the forced motions of a particle in a two-well potential (such an electron in a plasma) [25], [26], the magnetic pendulum [27], or the radio-frequency driven Josephson junctions [11], [28]

In the same class of nonlinear dynamical systems is also the motion of a shallow arch subjected to horizontal and vertical pulsating loads proposed by Szemplinska-Stupnicka [29] and recently explored by Lamarque and Malasoma [30]. The aim of our paper is an analytical study of the steady states of this system and then a numerical integration of differential equation which models the system by using an original method proposed by one of the authors [31].

The model and its fixed points. The equation of motion for a particular shallow arch subjected to horizontal and vertical pulsating loads is:

$$\ddot{x} + ax - 0,5(1 - 2f\cos\omega t - x^2)x = f\cos\omega t \quad (1)$$

where a is the damping coefficient, f and ω are the amplitude and the circular frequency of parametric excitation.

To analyze the behavior of the system we consider the following system of autonomous equations, which is equivalent to the differential equation (1).

$$\begin{aligned} \dot{x} &= y \\ \dot{y} &= -ay + 0,5(1 - 2f\cos z)x - 0,5x^3 + f\cos z \\ \dot{z} &= \omega \end{aligned} \quad (2)$$

We can see that this set of equations (or this flow) describes a dissipative system for any $a > 0$. A system is dissipative if an arbitrary volume V , enclosed by some surface S in

the phase space of the variables of the system, contracts. The surface S evolves by having each point on it follow an orbit generated by (2). If the system (2) has the general form

$$\dot{\vec{x}} = F(\vec{x}), \quad \vec{x} = (x_1 = x, x_2 = y, x_3 = z) \quad (3)$$

The statement of divergence theorem is

$$\frac{dV}{dt} = \int \left(\sum_{i=1}^d \frac{\partial F_i}{\partial x_i} \right) d_x^d$$

and the dissipative system is defined by $\frac{dV}{dt} < 0$

In the case of the flow defined by (2)

$$\frac{dV}{dt} = -aV \quad \text{or} \quad V(t) = V(0)e^{-at} \quad (4)$$

the volume element contracts exponentially in time for $a > 0$

If the parametric excitation is switched off ($f = 0$), the system (2) becomes

$$\begin{aligned} \dot{x} &= y \\ \dot{y} &= -ay + 0,5x - 0,5x^3 \end{aligned} \quad (5)$$

and from $F(\vec{x}) = 0$, we find the following fixed points of the system (5)

$$\vec{x}_1(0, 0), \quad \vec{x}_2(-1, 0), \quad \vec{x}_3(1, 0) \quad (6)$$

If $f \neq 0$, from (2) one finds the fixed points (the steady states)

$$\vec{x}_1(1, 0, 0), \quad \vec{x}_2\left(-\frac{1}{2} + \frac{1}{2}\sqrt{1-8f}, 0, 0\right), \quad \vec{x}_3\left(-\frac{1}{2} - \frac{1}{2}\sqrt{1-8f}, 0, 0\right) \quad (7)$$

with the obvious condition of reality of them $f \leq \frac{1}{8}$

The stability of the steady states. First we investigate the stability of the fixed points

(6) For $\vec{x}_1(0, 0)$, the matrix of stability is

$$\begin{vmatrix} 0 & 1 \\ 0,5 & -a \end{vmatrix}$$

and the characteristic equation

A STUDY OF A SIMPLE NONLINEAR MECHANICAL SYSTEM

$$\begin{vmatrix} -\lambda & 1 \\ -0,5 & -a-\lambda \end{vmatrix} = 0 \quad (8)$$

The eigenvalues of (8) are

$$\lambda_{1,2} = \frac{1}{2} \left(-a \pm \sqrt{a^2 + 2} \right) \quad (9)$$

and we have $\lambda_1 > 0$ and $\lambda_2 < 0$ for any $a > 0$. Thus the origin ($x = 0$) is a saddle fixed point

For the fixed points $\bar{x}_2(-1, 0)$ and $\bar{x}_3(1, 0)$, the characteristic equation is

$$\begin{vmatrix} -\lambda & 1 \\ -1 & -a-\lambda \end{vmatrix} = 0$$

with the eigenvalues:

$$\lambda_{1,2} = \frac{1}{2} \left(-a \pm \sqrt{a^2 - 4} \right) \quad (10)$$

In this case $\lambda_1 < 0$ and $\lambda_2 < 0$ for any $a \geq 2$. If $\lambda_{1,2}$ has the form $\lambda_{1,2} = \lambda' \pm i\lambda''$ we observe that $\lambda' < 0$ for any $a > 0$. Thus $x = -1$ and $x = 1$ are stable fixed points, or stable equilibrium

The stability of the fixed points (7) is investigated by the same method. One finds for $x = 1$, the characteristic equation

$$\begin{vmatrix} -\lambda & 1 & 0 \\ -1-f & -a-\lambda & 0 \\ 0 & 0 & -\lambda \end{vmatrix} = 0$$

with the eigenvalues

$$\lambda_1 = 0, \lambda_{2,3} = \frac{1}{2} \left(-a \pm \sqrt{a^2 - 4(1+f)} \right)$$

If $-1 \leq f \leq \frac{1}{8}$, λ_2 is real and negative, also if $f < \frac{a^2}{4} - 1$, λ_3 is real and negative. If $\frac{a^2}{4} - 1 < f \leq \frac{1}{8}$, $\lambda_{2,3} = \lambda \pm i\Lambda$ with $\lambda < 0$ for $a > 0$. Thus $x = 1$ remains a stable fixed point in the presence of the parametric excitation ($f \neq 0$)

For the fixed points $x = \frac{1}{2}(-1 + \sqrt{1-8f})$ and $x = \frac{1}{2}(-1 - \sqrt{1-8f})$, the eigenvalues of the characteristic equations are

$$\lambda_1 = 0$$

$$\lambda_{2,3} = \frac{1}{2} \left[-a \pm \left(a^2 + 8f - 1 \pm 3\sqrt{1-8f} \right)^{1/2} \right]$$

with $\lambda_2 > 0$ and $\lambda_3 < 0$, respectively $\lambda_2 < 0$ and $\lambda_3 > 0$. We conclude that for $0 < f < \frac{1}{8}$ these fixed points are unstables

But the system has, beside the steady states, also the other important behaviors like limit cycles with different periods, which form a cascade of period doubling cumulating in chaos, as the amplitude of parametric excitation is used as a control parameter. We observed this behavior by numerical investigation of (2) for different values of f , ω and a being constants

The numerical study. We have performed a numerical investigation of equation (1), or of equivalent set of equations (2), by using a new method of integration based on local linearization iterative (LLI). This method realises, with remarkable performances, the numerical approximation of the solutions through the segments of straight, considered in the neighbourhood of a pivot moment. With this method the relative errors cumulated was smaller than 0,1%, for sufficient large characteristic time intervals. Also, in the same domain of errors, the computing time is smaller than those spent with usual fourth order Runge-Kutta method

By fixing the parameters at the following values $a = 1,5$, $\omega = 8$, except the amplitude of parametric excitation f , which was used as a control parameter, we have constructed the projections of the trajectories in the phase space for a wide range of the control parameter. Thus, for $f = 0$, when the parametric excitation is awiched off, we found the stable

equilibrium $x = -1$ and $x = 1$. Because the trajectory goes to one or another fixed point, for different initial conditions, we drew the basins of attraction of these coexisting stable solutions. Figure 1 shows the basins of attraction in the phase space region defined by $-20 \leq x \leq 20$, and $-20 \leq y \leq 20$. The basin of equilibrium point $x = -1$ is colored in white, while that of $x = 1$ is in black. In Figure 2 we present two projections in XOY and XOZ planes of the trajectory in this case.

With parametric excitation ($f \neq 0$), the focus $x=1$ remains a solution of equation (1). This point is numerically found to be a stable equilibrium state until the amplitude f is $f \approx 29,28$, when a limit cycle is created. The projections in XOY plane of the trajectories with $f=5$ and $f=20$ are shown in Figures 3 and 4. Figure 5 shows two

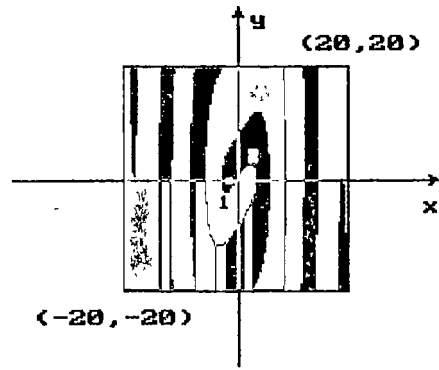
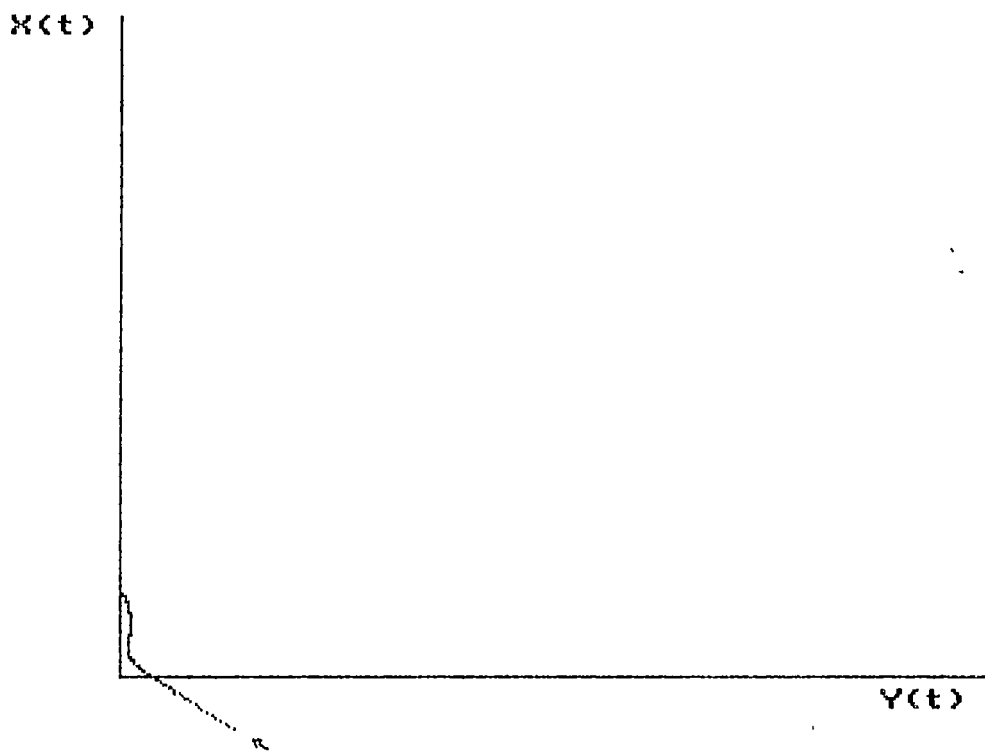


Fig 1

projections in XOY and YOZ planes of the trajectory when $f = 29,28$. When $f = 29,29713$ we can see, from Figure 6, that a cycle limit is created. In Figure 7 a and b we present the cycle limit for $f = 32$ in two projections on XOY and ZOZ planes. This period-1 limit cycle is also stable until amplitude f is $f \approx 45,5$ when a period-2 motion is created (see Figure 8). At $f = 47,5$ we can see, from Figure 9, that a period-4 motion is generated. As f increases further, a period doubling cascade followed by chaos is clearly visible. We present this in Figures 10-12 for $f = 47,7$, $f = 48$ and $f = 55$. At $f = 65$ a new period-1 limit cycle is created (see Figure 13), and the same scenario of period doubling cascade followed by chaos is visible. We have carried out extensive numerical simulation and we found the same behavior for

different values of f Figures 14-16 show some particular trajectories

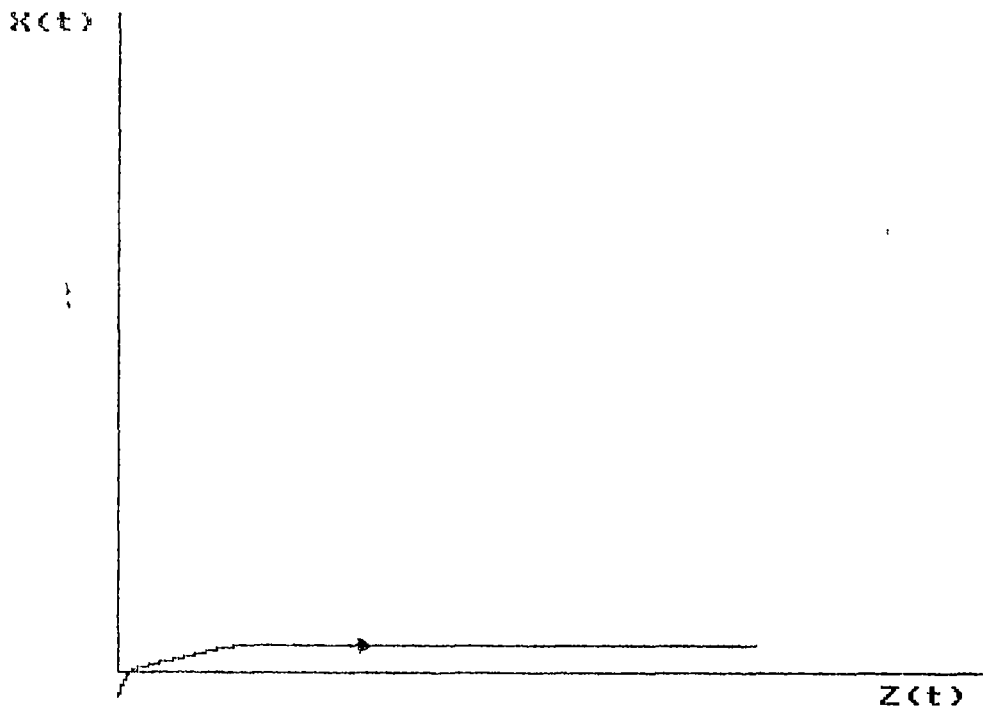


Damp. coef. = 1.5000000000E+00
Amplitude = 0.0000000000E+00
Circ. freq. = 6.0000000000E+00

X init = -1.0000000000E+00
Y init = 0.0000000000E+00
U init = 0.0000000000E+00
H scale = 3.0000000000E+01
V scale = 3.0000000000E+01

Fig 2

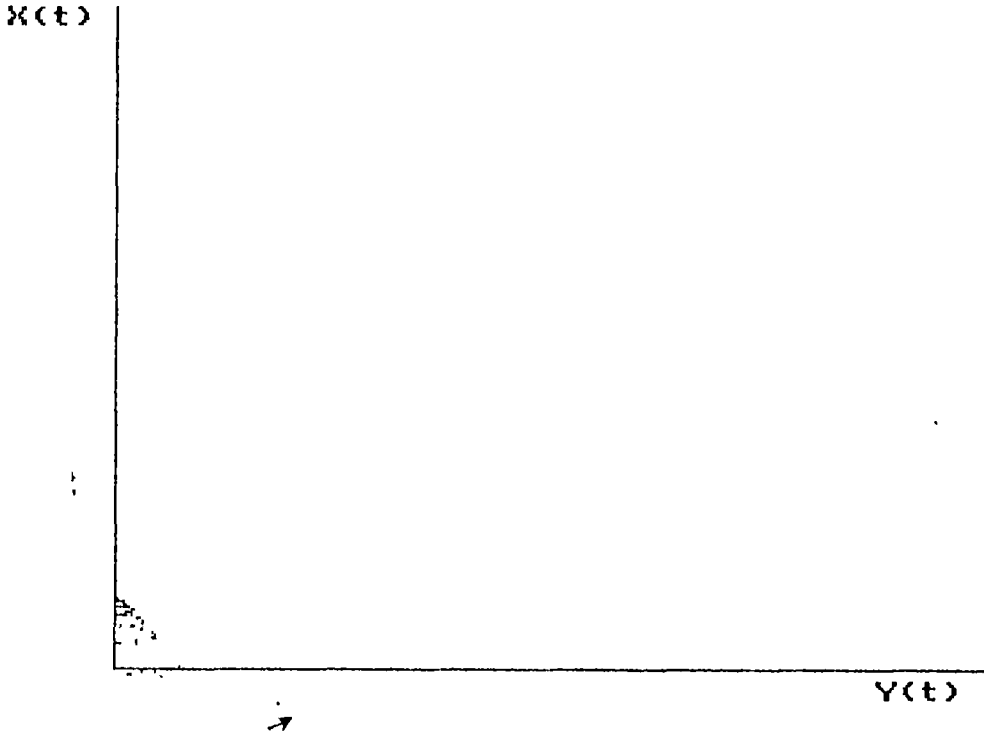
A STUDY OF A SIMPLE NONLINEAR MECHANICAL SYSTEM



Damp. coef. = 1.5000000000E+00
Amplitude = 0.0000000000E+00
Circ. freq. = 8.0000000000E+00

X init = -1.0000000000E+00
Y init = 2.0000000000E+00
Z init = 0.0000000000E+00
U Scale = 1.0000000000E+01
H Scale = 5.0000000000E-01

Fig.3

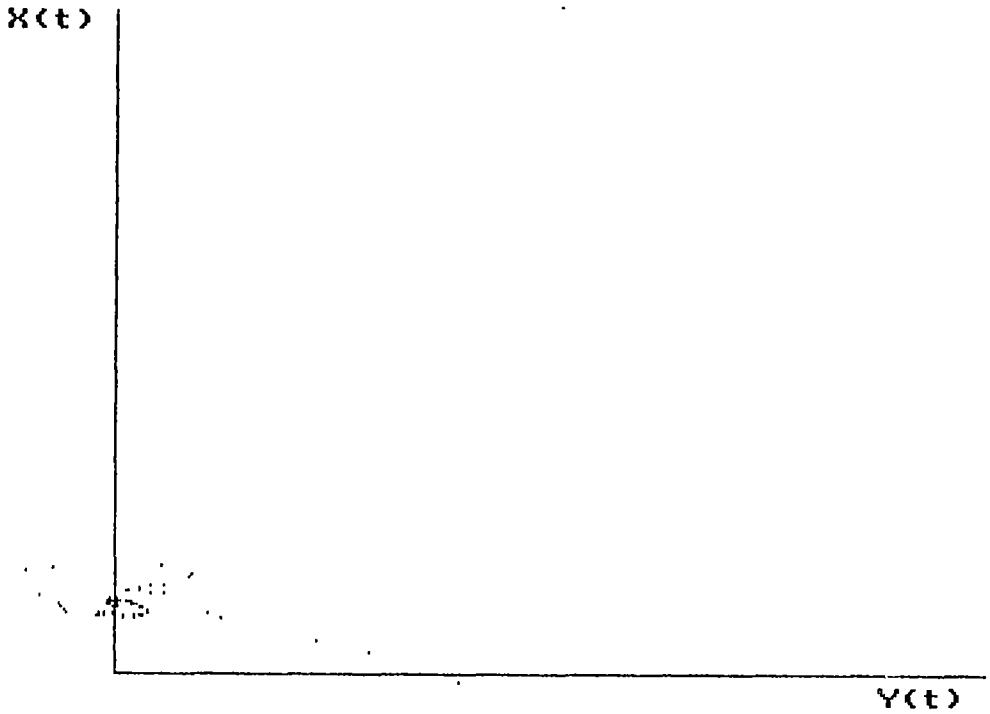


Damp. coef. = 1.5000000000E+00
Amplitude = 5.0000000000E+00
Circ. freq. = 8.0000000000E+00

X init = -1.0000000000E+00
Y init = 2.0000000000E+00
Z init = 0.0000000000E+00
U scale = 2.5000000000E+01
H scale = 2.5000000000E+01

Fig 4

A STUDY OF A SIMPLE NONLINEAR MECHANICAL SYSTEM



Damp. coef. = 1.5000000000E+00
Amplitude = 2.0000000000E+01
Circ. freq. = 8.0000000000E+00

X init = -1.0000000000E+00
Y init = 2.0000000000E+00
Z init = 0.0000000000E+00
U scale = 2.5000000000E+01
H scale = 2.5000000000E+01

Fig.5

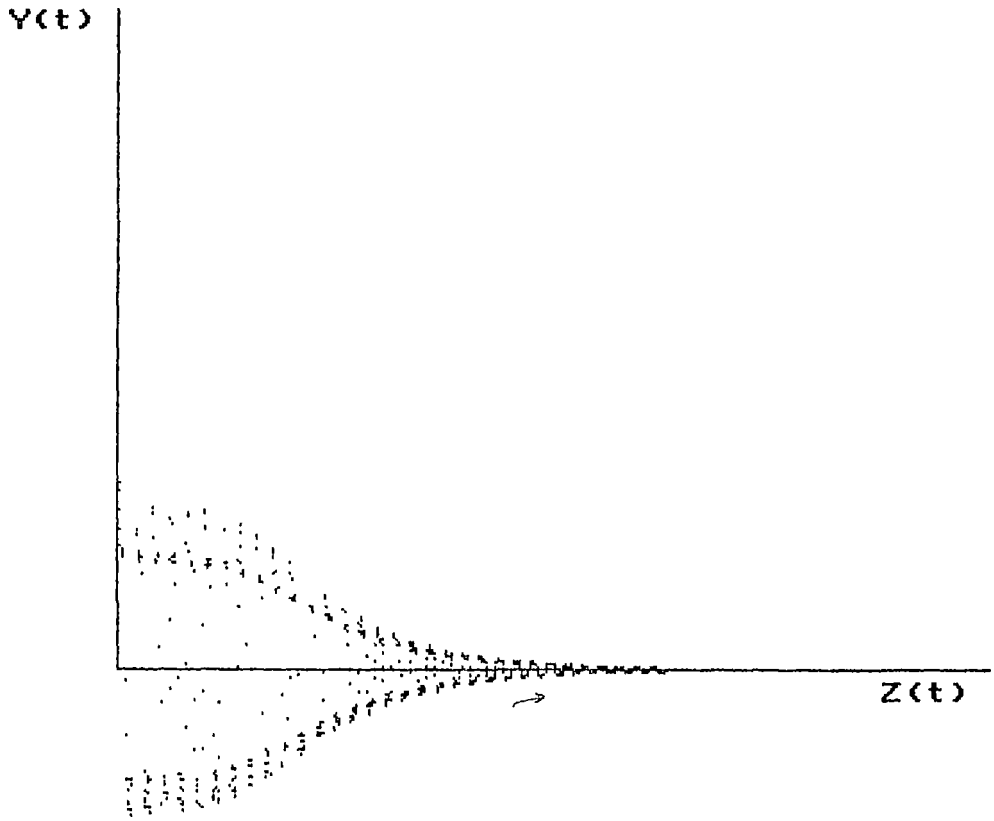


Damp. coef. = 1.5000000000E+00
Amplitude = 2.9280000000E+01
Circ. freq. = 8.0000000000E+00

X init = -1.0000000000E+00
Y init = 2.0000000000E+00
Z init = 0.0000000000E+00
U scale = 1.0000000000E+01
H scale = 1.0000000000E+01

Fig 6

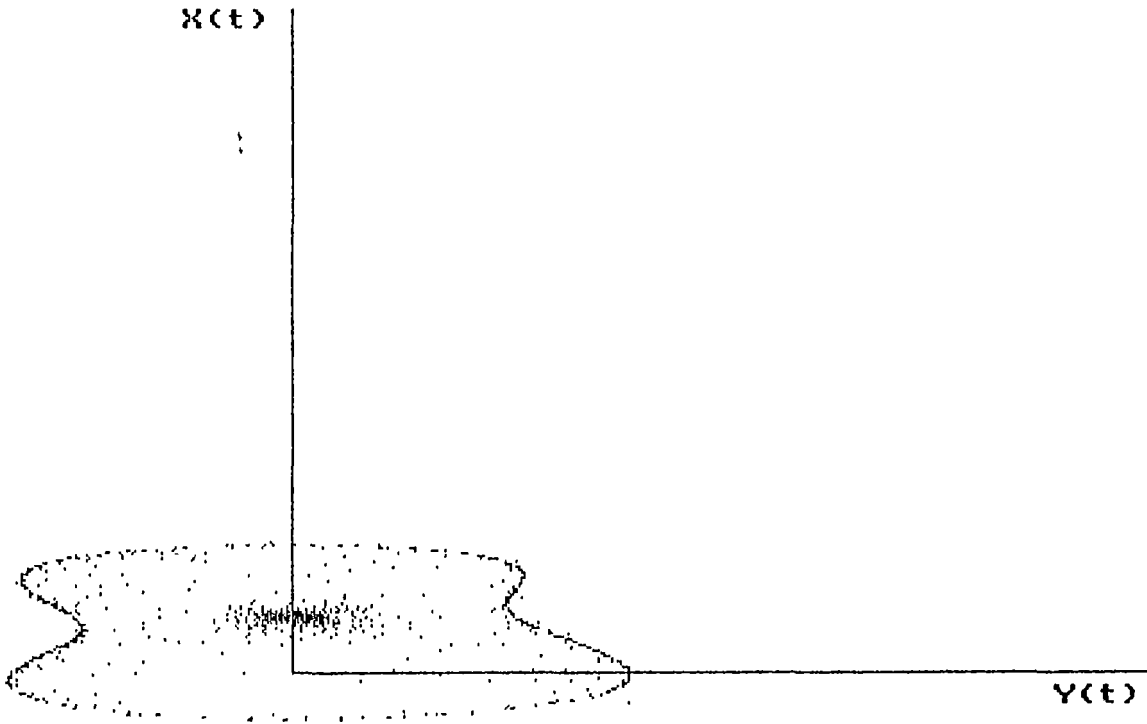
A STUDY OF A SIMPLE NONLINEAR MECHANICAL SYSTEM



Damp. coef. = 1.5000000000E+00
Amplitude = 2.9280000000E+01
Circ. freq. = 8.0000000000E+00

X init = -1.0000000000E+00
Y init = 2.0000000000E+00
Z init = 0.0000000000E+00
U Scale = 1.0000000000E+01
H Scale = 5.0000000000E-01

Fig 7



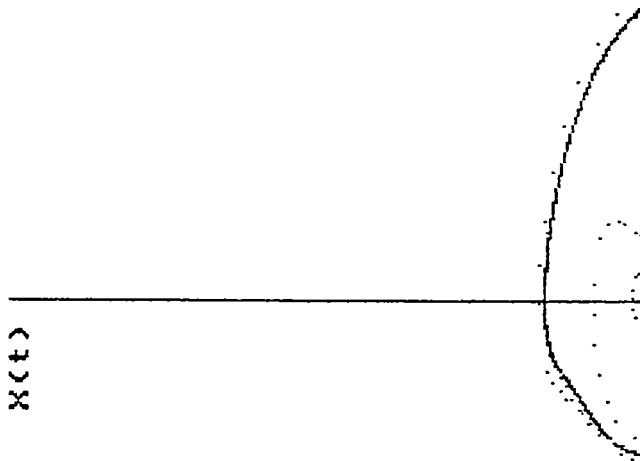
Damp. coef. = 1.5000000000E+00
Amplitude = 2.9287130000E+01
Circ. freq. = 8.0000000000E+00

X init = -1.0000000000E+00
Y init = 2.0000000000E+00
Z init = 0.0000000000E+00
U Scale = 2.0000000000E+01
H Scale = 2.0000000000E+01

Fig.8

A STUDY OF A SIMPLE NONLINEAR MECHANICAL SYSTEM

$x(t)$





```

Damp: coef = 1.50000000000E+00
Amplitude = 3.20000000000E+01
Circ: freq. = 8.00000000000E+00
X Y N D H
init = -1.00000000000E+00
init = 3.00000000000E+00
init = 0.00000000000E+00
scale = 5.00000000000E+00
scale = 2.00000000000E+00

```

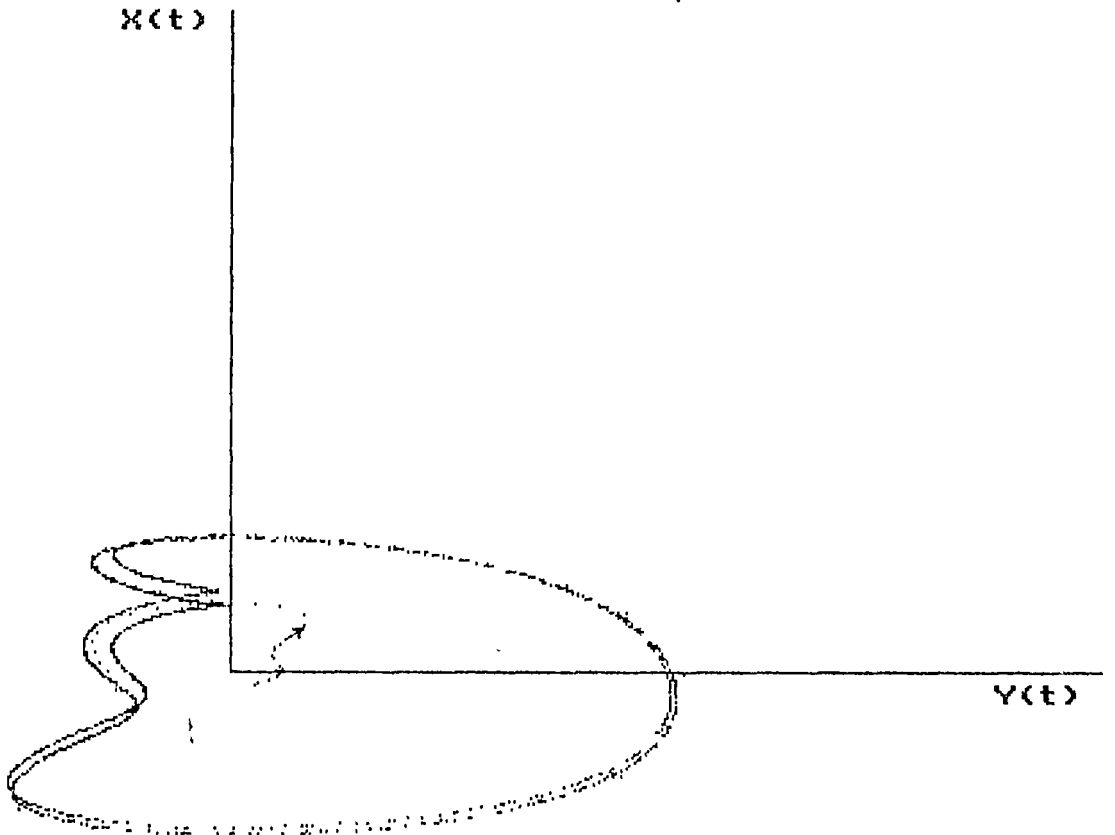
Fig 9

Z(N)

```
Damp. coef. = 1.500000000000E+00  
Amplitude = 3.200000000000E+01  
Circ. freq. = 8.000000000000E+00  
X)  init = 1.000000000000E+00  
N)  init = 2.000000000000E+00  
D)  init = 0.000000000000E+00  
H)  scale = 5.000000000000E+00  
      scale = 1.000000000000E+00
```

Fig 10

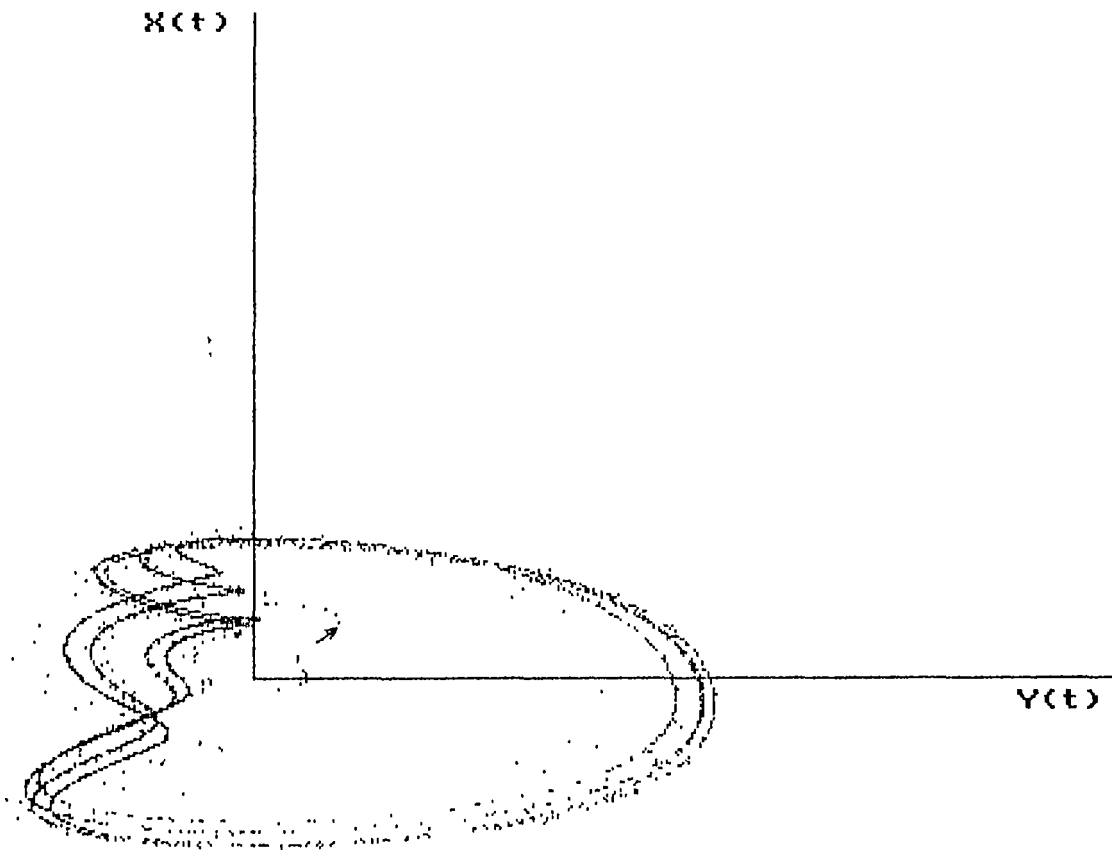
A STUDY OF A SIMPLE NONLINEAR MECHANICAL SYSTEM



Damp. coef. = 1.5000000000E+00
Amplitude = 4.5500000000E+01
Circ. freq. = 8.0000000000E+00

X init = -1.0000000000E+00
Y init = 2.0000000000E+00
U init = 0.0000000000E+00
N scale = 5.0000000000E+00
H scale = 2.0000000000E+00

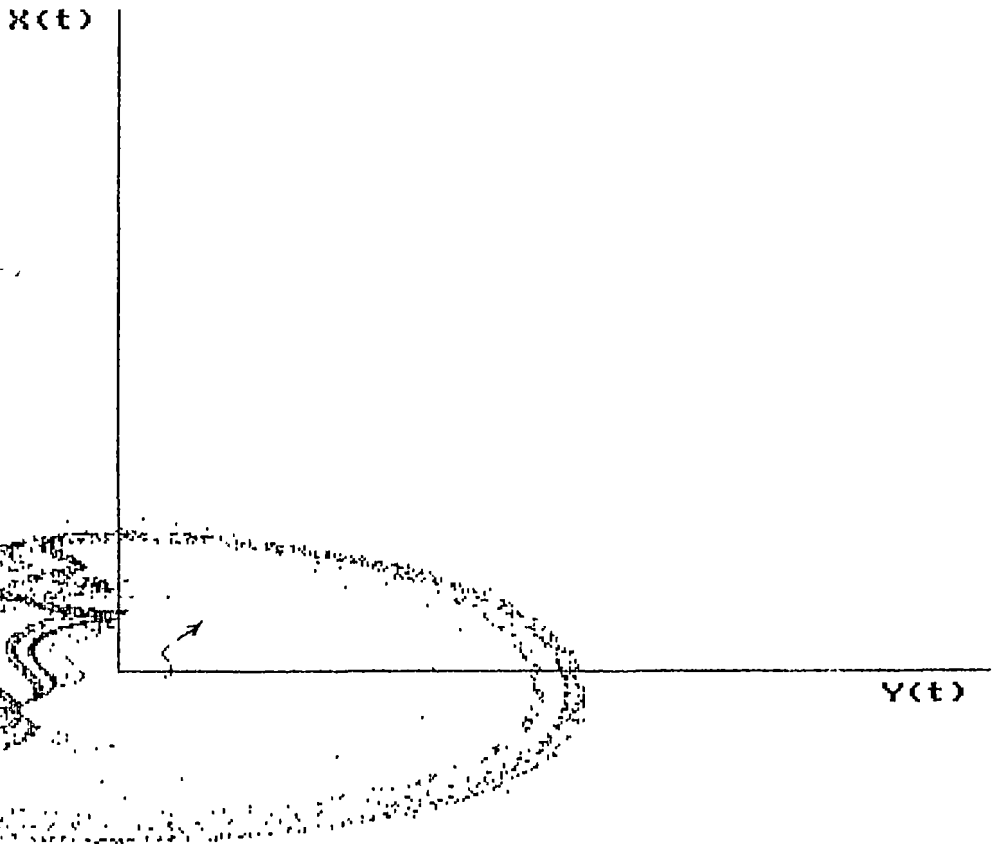
Fig 11



```
Damp. coef. = 1.5000000000E+00  
Amplitude = 4.7500000000E+01  
Circ. freq. = 8.0000000000E+00  
  
X init = -1.0000000000E+00  
Y init = 2.0000000000E+00  
Z init = 0.0000000000E+00  
U Scale = 5.0000000000E+00  
H Scale = 2.0000000000E+00
```

Fig 12

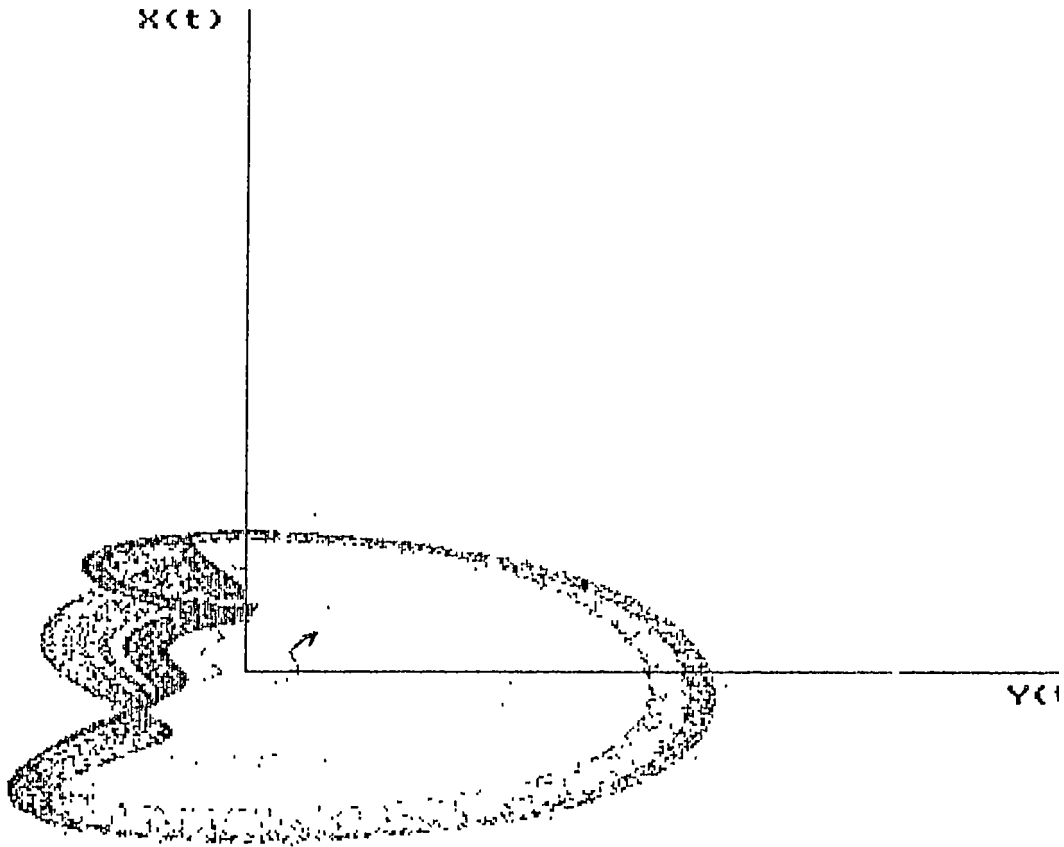
A STUDY OF A SIMPLE NONLINEAR MECHANICAL SYSTEM



Damp. coef. = 1.5000000000E+00
Amplitude = 4.7700000000E+01
Circ. freq. = 8.0000000000E+00

X init = -1.0000000000E+00
Y init = 2.0000000000E+00
Z init = 0.0000000000E+00
U scale = 5.0000000000E+00
H scale = 2.0000000000E+00

Fig 13

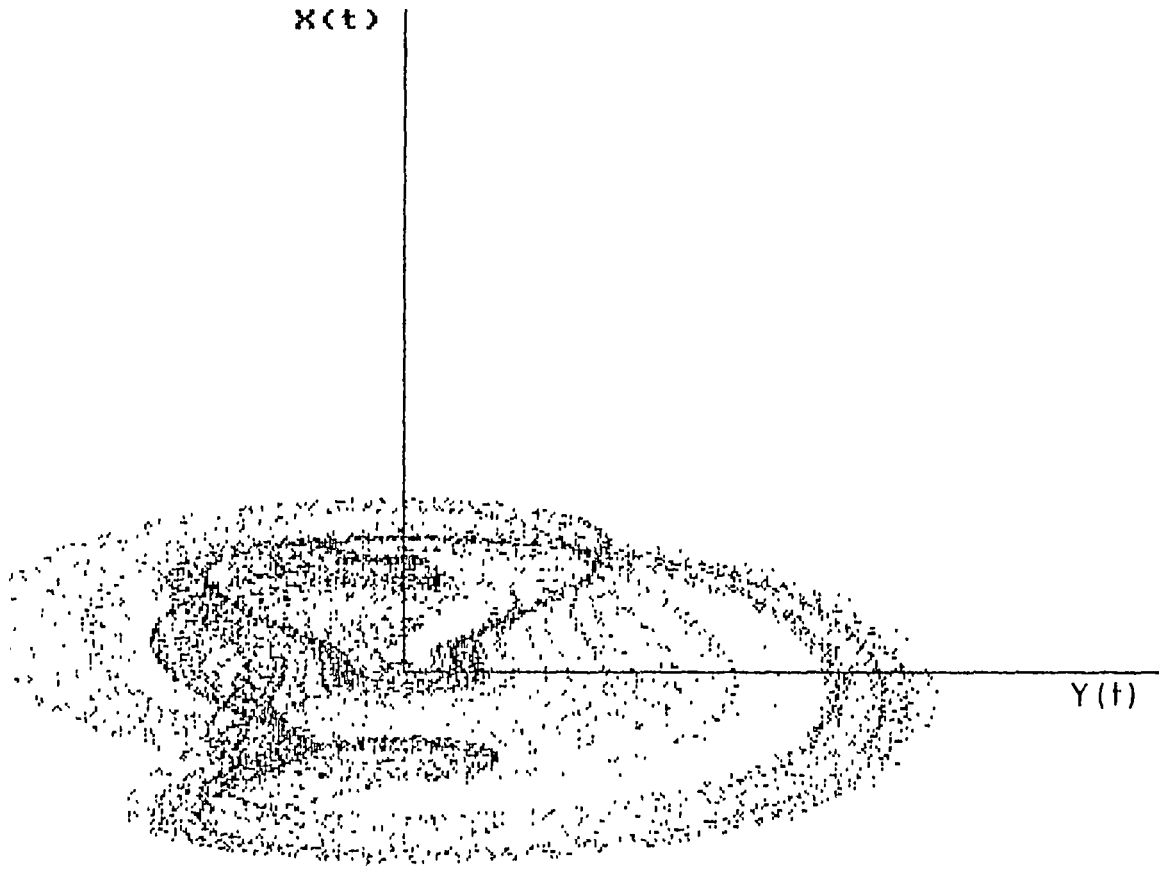


Damp. coef. = 1.5000000000E+00
Amplitude = 4.8000000000E+01
Circ. freq. = 8.0000000000E+00

X init = -1.0000000000E+00
Y init = 2.0000000000E+00
Z init = 0.0000000000E+00
U scale = 5.0000000000E+00
H scale = 2.0000000000E+00

Fig.14

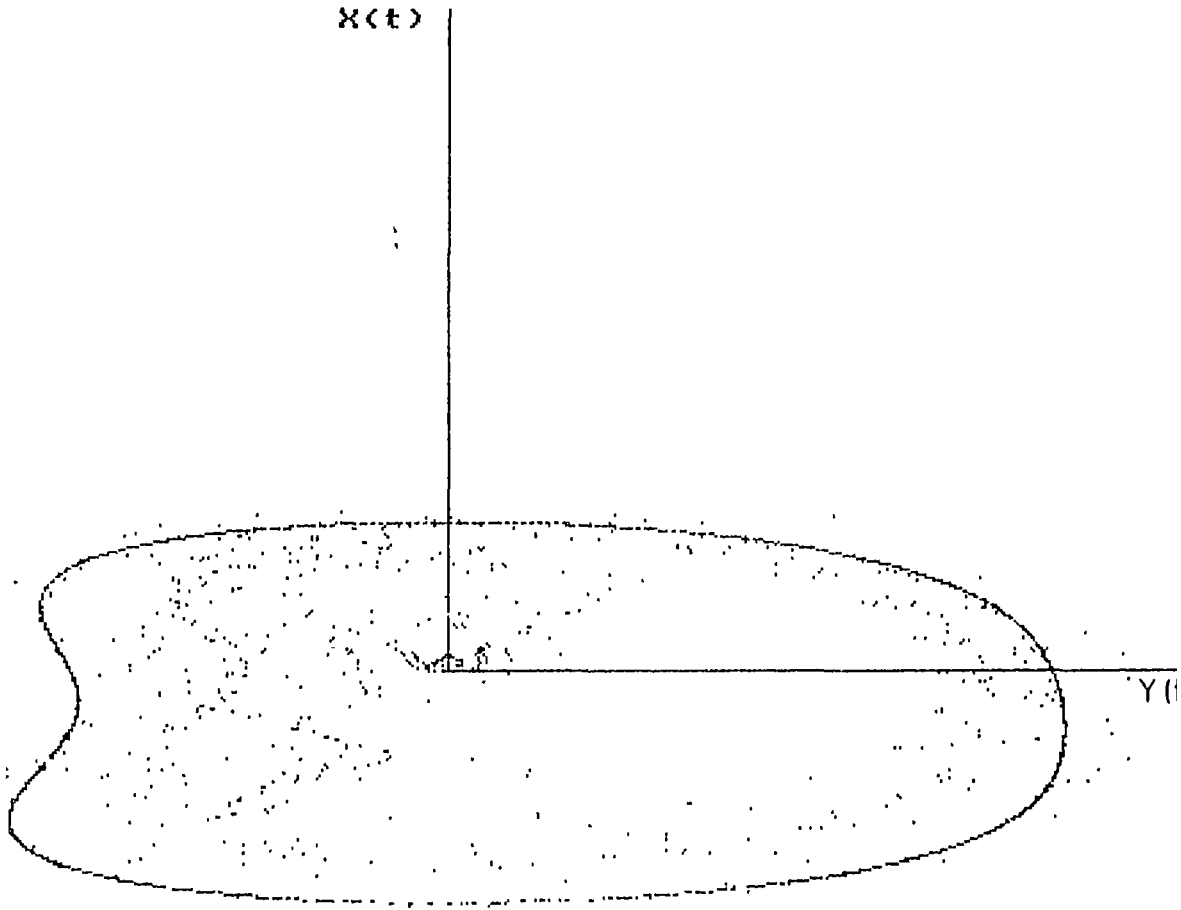
A STUDY OF A SIMPLE NONLINEAR MECHANICAL SYSTEM



Damp. coef. = 1.5000000000E+00
Amplitude = 5.5000000000E+01
Circ. freq. = 8.0000000000E+00

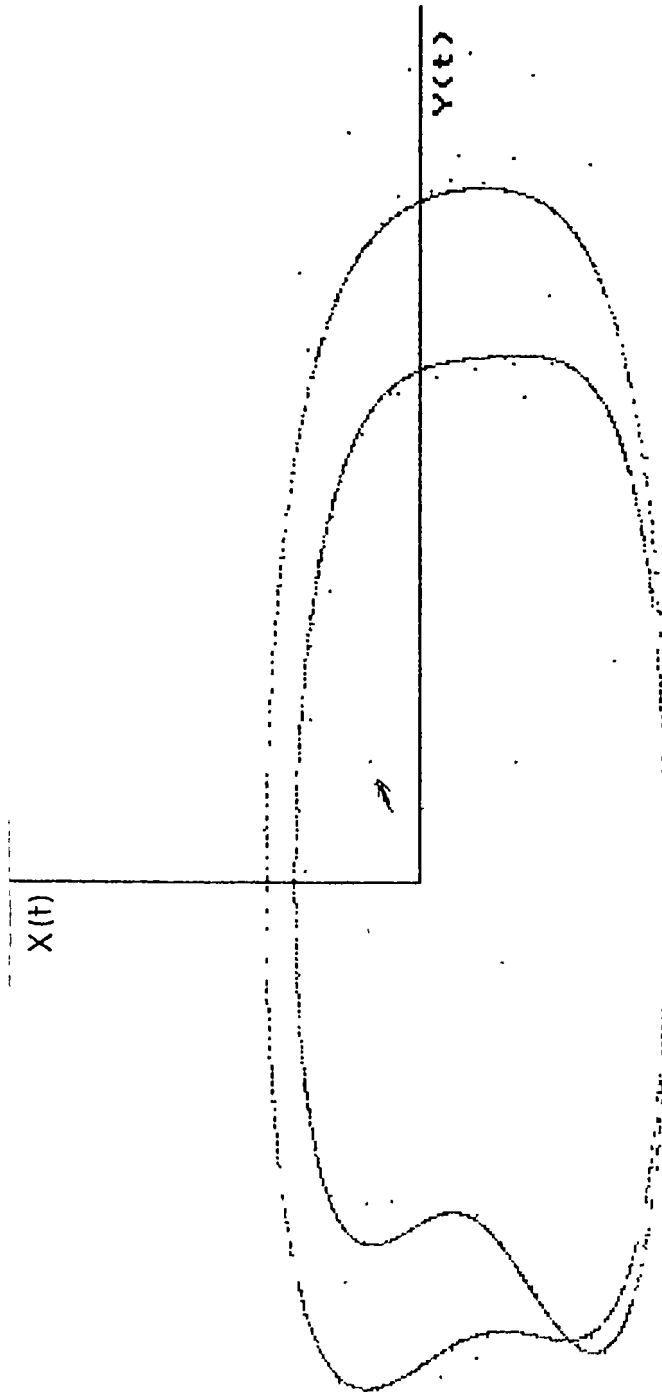
X init = -1.0000000000E+00
Y init = 2.0000000000E+00
Z init = 0.0000000000E+00
U Scale = 5.0000000000E+00
H Scale = 2.0000000000E+00

Fig. 15



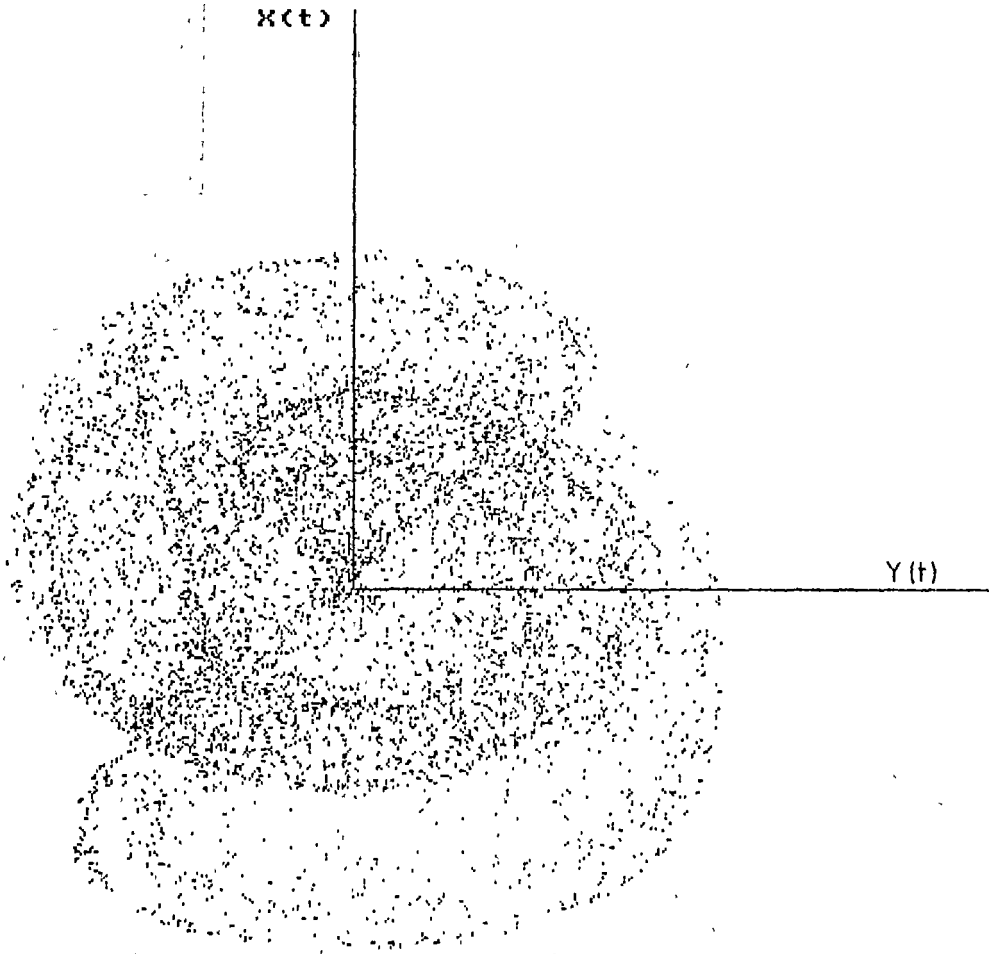
```
Damp. coef. = 1.5000000000E+00  
Amplitude = 6.5000000000E+01  
Circ. freq. = 8.0000000000E+00  
  
X init = -1.0000000000E+00  
Y init = 2.0000000000E+00  
Z init = 0.0000000000E+00  
U scale = 5.0000000000E+00  
H scale = 2.0000000000E+00
```

Fig.16



```
Damp: coef. = 1.5000000000E+00  
Amplitude = 8.5000000000E+01  
Circ. freq. = 8.0000000000E+00  
X init = -1.0000000000E+00  
Y init = 2.0000000000E+00  
Z init = 0.0000000000E+00  
N scale = 5.0000000000E+00  
H scale = 2.0000000000E+00
```

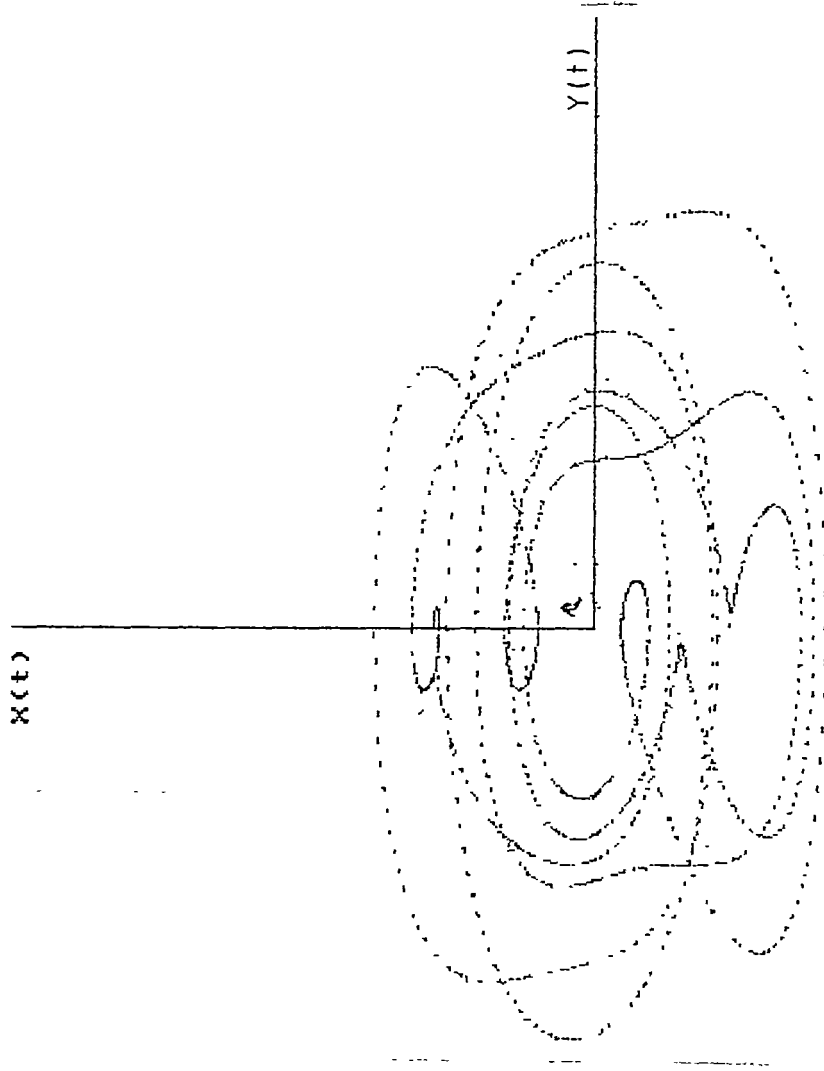
Fig 17



Damp. coef. = 1.5000000000E+00
Amplitude = 2.2000000000E+02
Circ. freq. = 8.0000000000E+00

X init = -1.0000000000E+00
Y init = 2.0000000000E+00
Z init = 0.0000000000E+00
W scale = 5.0000000000E+00
H scale = 5.0000000000E-01

A STUDY OF A SIMPLE NONLINEAR MECHANICAL SYSTEM



```
Damp: coef = 1.500000000000E+00  
Amplitude = 2.900000000000E+02  
Circ. freq. = 8.000000000000E+00  
X init = 1.000000000000E+00  
Y init = 2.000000000000E+00  
Z init = 0.000000000000E+00  
H scale = 3.000000000000E+00  
H scale = 3.000000000000E-01
```

Fig. 19

Conclusions. This work investigated the nonlinear dynamics of a mechanical system with cubic nonlinearity and parametric excitation, by using the LLI technique. We have constructed different trajectories in the phase space as the amplitude of parametric excitation was used as a control parameter and shown that the system exhibits different chaotic behaviors. The route to chaos is shown to be via period-doubling bifurcations.

REFERENCES

- 1 H C Schuster - Deterministic chaos, Physik-Verlag, 1984
- 2 Hao Bai-Lin - Chaos II, World Scientific, 1990
- 3 D D'Humières, MR Beasley, B A Hunberman, A Libchaber-Phys Rev 26A, 3483, 1982
- 4 F Moon- vol "Perspectives in Nonlinear Dynamics" World Sci , 230, 1985
- 5 H I. Swinney, J.P Gollub-Hydrodynamic Instabilities and the Transition to Turbulence, Springer Berlin 1981
- 6 A Libchaber-Proc Roy Soc London, A413, 633, 1987
- 7 B V Buskirk, C Jeffries-Phys Rev A31, 3332, 1985
- 8 C O Weiss, J Brock-Phys Rev Lett , 57, 2804, 1986
- 9 P A Hopf, D L Kaplan, H M. Gibbs, R L Shoemaker-Phys Rev A25, 2172, 1982
- 10 R G. Harrison, D J Biswas-Nature, 321, 394, 1986.
- 11 M Cirillo, N F Pedersen-Phys., 90A, 150, 1982
- 12 E C Gwinn, R M Westervell-Phys Rev Lett Vol 54, Nr 15, 1613, 1985
- 13 G Cicogna-Phys Lett 131A, 98, 1988
- 14 C A Held, C D Jeffries-vol "Dimensions and Entropies in Chaotic Systems" editor G Mayer-Krieger Springer-Verlag Berlin, p 158, 1986
- 15 O E Rössler-Z Naturforsch 319, 1168, 1976
- 16 J C Roux, A Rossi, S Bachelart, C Vidal-Phys Lett 77A, 391, 1980
- 17 MR Bassett, J L Hudson-Physica 35D, 289, 1989.
- 18 L F Olsen, H Degh-Quarterly Rev Biophys 18, 165, 1985
- 19 W M Schaffer-Ecology 66, 93, 1985
- 20 A L Goldberger, B J West-Ann NY Acad Sci , 504, 195, 1987
- 21 S P Layne, G Mayer-Kress, J Holzfuss-vol "Dimensions and Entropies in Chaotic Systems" editor G Mayer-Krieger Springer-Verlag Berlin, p 246, 1986
- 22 E N Lorenz-J Atmos Sci 20, 130, 1963
- 23 G I Baker, J.P Gollub-Chaotic Dynamica, Cambridge University Press, 1990
- 24 P Holmes-Phy 1 trans Roy Soc A292, 419, 1976
- 25 F C Moon-Phys Rev Lett, vol 53, Nr 14, 1439, 1985
26. F C Moon-Phys Rev Lett, vol 53 Nr 10, 967 1984
- 27 F C Moon-Chaotic Vibrations (transl in russ) Ed Mir 1984

A STUDY OF A SIMPLE NONLINEAR MECHANICAL SYSTEM

- 28 M Iansiti, Qing Hu, R M Westervelt-Phys Rev Lett, vol 55, Nr 7, 1985.
- 29 W Szemplinska-Stupnicka, R H Plant, J C Hsieh-A S M E J Appl Mech, 56, 947, 1989
- 30 C H Lamarque, J M Malasoma-Eur J. Mech. A/Solids, 11, Nr 6, 781, 1992
- 31 T. Colosi-Regelungstechnik und Prozessdatenverarbeitung München, Nr 4, S138, 1978



MASSIVE VECTOR, TENSOR AND SPIN-3/2 PARTICLES GRAVITATIONALLY SCATTERED ON SCHWARZSCHILD BACKGROUND

D. ȚĂȚOMIR, D. RADU, O. MIHALACHE*

Received 15 10 1993

ABSTRACT. - Using the S -matrix formalism and Feynman's diagram-technique, the gravitational scattering of the minimally coupled vector, tensor and spin-3/2 (Rarita-Schwinger) particles on Schwarzschild background is studied for any value of the scattering angle

We mention that accordingly to our knowledge the previous works in this branch dealt only with the small angle cases. As it has been shown, in the small angle approximation and ultrarelativistic case, the differential cross-sections coincide with those corresponding to the photons, neutrinos, massless Rarita-Schwinger particles, gravitinos and gravitons, i.e., the gravitational particle scattering is spin independent, in agreement with many authors' results, obtained by other means.

As particularly interesting result, we point out that the differential cross-section for scattering of the vector particles in the backward direction and ultrarelativistic case is finite and the helicity is not conserved, while, for tensor and spin-3/2 particles in the same case the differential cross-section is clearly unlimited.

In this paper, using the S -matrix formalism and Gupta's linear approximation [1]

$$\sqrt{-g} g^{\mu\nu} = \eta^{\mu\nu} - k\gamma^{\mu\nu} \quad (1)$$

where $g^{\mu\nu}$, $\eta^{\mu\nu}$ and $\gamma^{\mu\nu}$ are the metric tensor, the Minkowski tensor - diag (+1, -1, -1, -1) - and the tensor of the weak gravitational field, respectively, $g = \det g_{\mu\nu}$ and $k = \sqrt{16\pi G}$ (in natural units, G being the Newton constant), the scattering of the massive 1, 2 and 3/2 spin particles in the external gravitational field described by Schwarzschild metric is studied. Also we discuss the differential backward-cross-section as an important particular case.

In order to obtain the first-order interaction Lagrangians between the gravitational and

* "Al I. Cuza" University, Department of Physics, 6600 Iassy, Romania

the massive vector, tensor and Rarita-Schwinger fields we use the principle of minimal coupling [2] According to this principle, for vector and tensor fields, we must add to the expression of the gravitational field Lagrangian the complex massive vector and tensor field Lagrangians written in the curved space [3, 4]

$$\mathfrak{L}_{vector} = \sqrt{-g} \left(-\frac{1}{2} g^{\mu\alpha} g^{\nu\beta} G_{\mu\nu}^* G_{\alpha\beta} + m^2 g^{\nu\alpha} B_\nu^* B_\alpha \right) \quad (2)$$

$$\mathfrak{L}_{tensor} = \sqrt{-g} g^{\mu\rho} g^{\nu\beta} \left(g^{\lambda\alpha} H_{\mu\nu\lambda}^* H_{\alpha\beta\rho} + m^2 \phi_{\mu\nu}^* \phi_{\rho\beta} \right) \quad (3)$$

It is easy to see that for the vector field we considered the Proca formalism Here $G_{\mu\nu} = B_{\nu,\mu} - B_{\mu,\nu}$ ($B_{\mu,\nu}$ being the covariant derivative of the vector field function) is the tensor of the massive vector field Concerning the tensor field we must emphasize that we followed a Schwinger's idea [5] using the third rank tensor

$$H_{\mu\nu\lambda} = \phi_{\nu\lambda,\mu} + \phi_{\mu\lambda,\nu} - \phi_{\mu\nu,\lambda} \quad , \quad (H_{\mu\nu\lambda} = H_{\nu\mu\lambda}), \quad (4)$$

where $\phi_{\mu\nu,\lambda}$ is the covariant derivative of the tensor field function We note in passing that a remarkable analogy between the massive tensor and linearized (weak) gravitational fields is revealed by this Lagrangian's choice In the case of the Rarita-Schwinger field, besides principle of minimal coupling, we also used the "vierbein" formalism [6], so that, the Lagrangian of this system can be written as follows

$$\mathfrak{L}_{R-S} = \sqrt{-g} g^{\mu\nu} \left[\frac{i}{2} \left(\bar{\psi}_\mu \nabla_\lambda \gamma^\lambda \psi_\nu - \bar{\psi}_\mu \gamma^\lambda \nabla_\lambda \psi_\nu \right) + m \bar{\psi}_\mu \psi_\nu \right] = \mathfrak{L}_1 + \mathfrak{L}_2, \quad (5)$$

where

$$\mathfrak{L}_1 = \sqrt{-g} g^{\mu\nu} \left[\frac{i}{2} \left(\bar{\psi}_{\mu,\lambda} \gamma^\lambda \psi_\nu - \bar{\psi}_\mu \gamma^\lambda \psi_{\nu,\lambda} \right) + m \bar{\psi}_\mu \psi_\nu \right] \quad (6)$$

$$\mathfrak{L}_2 = \frac{i}{8} \sqrt{-g} g^{\mu\nu} \bar{\psi}_\mu \left(\gamma_{\rho\lambda} \gamma^\rho \gamma^\lambda + \gamma^\lambda \gamma_{\rho\lambda} \gamma^\rho \right) \psi_\nu, \quad (7)$$

$\psi_{\mu,\lambda}$ being the usual derivative of the Rarita-Schwinger field function

The above expression for \mathfrak{L}_1 and \mathfrak{L}_2 have been obtained inserting the expression of the covariant of the spin-vectors:

$$\nabla_\mu \psi_\nu = \psi_{\nu,\mu} - \Gamma_\mu \psi_\nu, \quad \bar{\psi}_\nu \nabla_\mu = \bar{\psi}_{\nu,\mu} + \bar{\psi}_\nu \Gamma_\mu, \quad (8)$$

where Γ_μ are the Fock-Ivanenko spin coefficients of the affine connection [7] As it is known they have the following expression:

$$\Gamma_\mu = \frac{1}{4} \gamma_{\lambda,\mu} \gamma^\lambda, \quad (9)$$

where γ^μ are the generalized Dirac matrices [8,9].

$$\gamma^\mu = L^\mu(\alpha) \gamma(\alpha), \quad \gamma_\mu = L_\mu(\alpha) \gamma(\alpha), \quad (10)$$

$\gamma(\alpha)$ being the usual Dirac matrices. The expression for $\gamma_{\lambda,\mu}$ is

$$\gamma_{\lambda,\mu} = \gamma_{\lambda,\mu} - \gamma_\rho \Gamma_{\lambda\mu}^\rho \quad (11)$$

In relations (10) $L^\mu(\alpha)$ and $L_\mu(\alpha)$ are the "vierbein" coefficients satisfying the following constraints

$$L^\mu(\alpha) L^\nu(\alpha) = g^{\mu\nu}, \quad L_\mu(\alpha) L_\nu(\alpha) = g_{\mu\nu} \quad (12)$$

Since all our considerations refer only to the first-order approximation we give below the "linearized" relations for the quantities which appear in calculations [4,7]

$$g^{\mu\nu} = \eta^{\mu\nu} - k h^{\mu\nu} \quad (13)$$

$$g_{\mu\nu} = \eta_{\mu\nu} + k h_{\mu\nu} \quad (14)$$

$$h_i^\beta = \gamma_\lambda^\beta - \frac{1}{2} \delta_\lambda^\beta y, \quad h^{\mu\nu} = \frac{1}{2} \eta^{\mu\nu} y, \quad y = y_\alpha^\alpha \quad (15)$$

$$\Gamma_{\lambda\mu}^{\rho} = \frac{1}{2} k \left(h_{\lambda,\mu}^{\rho} + h_{\mu,\lambda}^{\rho} - h_{\mu,\mu}^{\rho} \right) \quad (\text{the Christoffel symbols}) \quad (16)$$

$$\gamma_{\lambda} = \gamma_{\lambda} + \frac{1}{2} k \gamma_{\beta} h_{\lambda}^{\beta}, \quad \gamma^{\lambda} = \gamma^{\lambda} - \frac{1}{2} k \gamma_{\beta} h^{\lambda\beta} \quad (17)$$

It is very simply to show that the \mathfrak{L}_2 term in (5) has no contribution in the first-order approximation. Indeed we have

$$\mathfrak{L}_2^{(1)}(k) = \frac{i}{16} k \bar{\psi}_{\mu} \gamma^{\lambda} \gamma_{\alpha} \gamma^{\rho} \psi^{\mu} \left(h_{\rho\lambda}^{\alpha} - h_{\lambda,\rho}^{\alpha} \right) = \frac{i}{16} k \bar{\psi}_{\mu} \gamma^{\lambda} \left(\gamma^{\alpha} \gamma^{\rho} - \gamma^{\rho} \gamma^{\alpha} \right) \psi^{\mu} h_{\alpha\rho,\lambda} = 0, \quad (18)$$

where the well known anticommutation rules have been used

$$\{ \gamma^{\lambda}, \gamma^{\nu} \} = \gamma^{\lambda} \gamma^{\nu} + \gamma^{\nu} \gamma^{\lambda} = 2 \delta^{\lambda\nu} \quad (19)$$

Taking into account the previous considerations the first-order interaction Lagrangian between the weak gravitational and the massive Rarita-Schwinger fields reads

$$\begin{aligned} \mathfrak{L}_{int}^{(1)}(k) &= -\frac{i}{4} k \left(\bar{\psi}_{\lambda,\mu} \gamma_{\nu} \psi^{\lambda} - \bar{\psi}_{\lambda} \gamma_{\nu} \psi_{\mu}^{\lambda} \right) h^{\mu\nu} - \\ &- \frac{i}{2} k \left(\bar{\psi}_{\mu\lambda} \gamma^{\lambda} \psi_{\nu} - \bar{\psi}_{\nu} \gamma^{\lambda} \psi_{\nu,\lambda} \right) \gamma^{\mu\nu} - k m \bar{\psi}_{\mu} \psi_{\nu} \gamma^{\mu\nu} \end{aligned} \quad (20)$$

Passing to the flat space

$$x^0 = t, \quad x^J, \quad (J = 1, 2, 3) \rightarrow x_j, \quad (j=1, 2, 3), \quad x_4 = it, \quad (21)$$

$$\gamma^{\mu} \rightarrow i \gamma_{\mu}, \quad \gamma^0 \rightarrow \gamma_4, \quad \eta^{\mu\nu} \rightarrow -\delta_{\mu\nu}, \quad (22)$$

the first-order interaction Lagrangians between the gravitational and massive vector, tensor and Rarita-Schwinger fields, respectively, are

$$\mathfrak{L}_{int}^{(1)}(k) = -k \left(G_{\mu\nu}^* G_{\mu\alpha}^{\nu} u_{\nu\alpha} + m^2 B_{\nu}^* B_{\nu}^{\alpha} v_{\nu\alpha} \right) \quad (23)$$

$$\begin{aligned} \mathfrak{L}_{int}^{(1)}(k) &= k \left[H_{\mu\nu\alpha}^* \left(H_{\alpha\nu}^{\mu} + H_{\alpha\nu}^{\mu} \right) + k_{\rho\sigma}^* H_{\rho\sigma}^{\mu\nu} - \gamma m^2 \phi_{\mu\nu}^* \phi_{\rho\sigma}^{\mu\nu} \right] v_{\rho\sigma}^{\mu\nu} - \\ &- k \left(H_{\mu\nu\lambda}^* H_{\lambda\nu\mu}^{\rho} - \frac{1}{2} m^2 \phi_{\mu\nu}^* \phi_{\mu\nu}^{\rho} \right) v^{\nu} + k \left[H_{\mu\nu\lambda}^* \phi_{\rho\mu}^{\nu} (h_{\rho,\nu}^{\lambda} + h_{\nu,\rho}^{\lambda} - h_{\rho,\nu}^{\lambda}) + \right. \end{aligned} \quad (24)$$

MASSIVE VECTOR, TENSOR AND SPIN-3/2 PARTICLES

$$\begin{aligned}
 & + \phi_{\rho\lambda}^* (h_{\mu\rho,\nu} + h_{\nu\rho,\mu} - h_{\mu\nu,\rho}) H_{\lambda\nu\mu} \Big] \\
 \mathcal{L}_{int}^{(1)}(k) = & \frac{1}{4} k (\bar{\psi}_{\alpha,\nu} \gamma_{\mu} \psi_{\alpha} - \bar{\psi}_{\alpha} \dot{\gamma}_{\mu} \psi_{\alpha,\nu}) \gamma_{\mu\nu} - \frac{1}{4} k m \bar{\psi}_{\alpha} \psi_{\alpha} \gamma_{\nu},
 \end{aligned} \tag{25}$$

where:

$$u_{\mu\nu} = \gamma_{\mu\nu} - \frac{1}{4} \delta_{\mu\nu} \gamma_{\alpha\alpha} \tag{26}$$

$$G_{\mu\nu} = B_{\nu\mu} - B_{\mu,\nu}; \quad H_{\mu\nu\lambda} = \phi_{\nu\lambda,\mu} + \phi_{\mu\lambda,\nu} - \phi_{\mu\nu,\lambda}, \tag{27}$$

$B_{\mu,\nu}$ and $\phi_{\mu\nu,\lambda}$ being the usual derivatives of the vector and tensor field functions, respectively

Also we have taken advantage of the Rarita-Schwinger field equation

$$\gamma_{\mu} \psi_{\alpha,\mu} = -m \psi_{\alpha} \tag{28}$$

and its adjoint

According to the standard quantum field theory the parts of the (23), (24) and (25) Lagrangians-casted into the normal form - which describe the interaction of the massive vector, tensor and 3/2-spin particles, respectively, with gravity are [4]

$$N[\mathcal{L}_{vec-g}^{(1)}(x)] = -k [G_{\mu\nu}^{*(-)}(x) G_{\mu\alpha}^{(+)}(x) u_{\nu\alpha}^{**}(x) + m^2 B_{\nu}^{*(-)}(x) B_{\alpha}^{(+)}(x) \gamma_{\nu\alpha}^{**}(x)] \tag{29}$$

$$\begin{aligned}
 N[\mathcal{L}_{int-g}^{(1)}(x)] = & k \{ \phi_{\alpha\nu,\mu}^{*(-)}(x) [3 \phi_{\lambda\nu,\alpha}^{(+)}(x) - \phi_{\lambda\alpha,\nu}^{(+)}(x) - \phi_{\nu\alpha,\lambda}^{(+)}(x)] + \phi_{\alpha\mu,\nu}^{*(-)}(x) \times \\
 & \times [\phi_{\lambda\nu,\alpha}^{(+)}(x) + \phi_{\lambda\alpha,\nu}^{(+)}(x) + \phi_{\alpha\nu,\lambda}^{(+)}(x)] + \phi_{\mu\nu,\alpha}^{*(-)}(x) [\phi_{\alpha\lambda,\nu}^{(+)}(x) + \phi_{\alpha\nu,\lambda}^{(+)}(x) - 3 \phi_{\lambda\nu,\alpha}^{(+)}(x)] - \\
 & - 2 m^2 \phi_{\mu\nu}^{*(-)}(x) \phi_{\lambda\nu}^{(+)}(x) \} \gamma_{\mu\lambda}^{**}(x) - k \{ [\phi_{\lambda\nu,\mu}^{*(-)}(x) + \phi_{\lambda\mu,\nu}^{*(-)}(x) - \phi_{\mu\nu,\lambda}^{*(-)}(x)] \times \\
 & \times [\phi_{\mu\nu,\lambda}^{(+)}(x) + \phi_{\mu\lambda,\nu}^{(+)}(x) - \phi_{\lambda\nu,\mu}^{(+)}(x)] - \frac{1}{2} m^2 \phi_{\mu\nu}^{*(-)}(x) \phi_{\mu\nu}^{(+)}(x) \} \gamma^{\mu\nu}(x) +
 \end{aligned} \tag{30}$$

$$\begin{aligned}
 & + k \left\{ \left[\phi_{\lambda\nu\mu}^{*(\prime)}(x) + \phi_{\lambda\mu\nu}^{*(\prime)}(x) \right] \phi_{\rho\sigma}^{(\prime)}(x) \left[h_{\lambda\sigma\nu}^{est}(x) + h_{\nu\sigma\lambda}^{est}(x) - h_{\lambda\nu\sigma}^{est}(x) \right] + \right. \\
 & \left. + \phi_{\alpha\lambda}^{*(\prime)}(x) \left[\phi_{\mu\nu\lambda}^{(\prime)}(x) + \phi_{\mu\lambda\nu}^{(\prime)}(x) - \phi_{\lambda\nu\mu}^{(\prime)}(x) \right] \left[h_{\mu\sigma\nu}^{est}(x) + h_{\nu\sigma\mu}^{est}(x) - h_{\mu\nu\sigma}^{est}(x) \right] \right\} \\
 N \left[\Xi_{R-S-\bar{g}}^{(1)}(x) \right] & = \frac{1}{4} k \left[\bar{\psi}_{\alpha\nu}^{(\prime)}(x) \gamma_{\mu} \psi_{\alpha}^{(\prime)}(x) - \bar{\psi}_{\alpha}^{(\prime)}(x) \gamma_{\mu} \psi_{\alpha\nu}^{(\prime)}(x) \right] \gamma_{\mu\nu}^{est}(x) - \\
 & - \frac{1}{4} km \bar{\psi}_{\alpha}^{(\prime)} \psi_{\alpha}^{(\prime)}(x) \gamma^{est}(x)
 \end{aligned} \tag{31}$$

The processes are described by the following Feynman's diagram type, where p and (r) and also p' and (s) are the four-momenta and polarization indices ($r, s = 1$ to $2s+1$, where s is the spin of the particle) of the initial and final particles, and q is the four momentum of the virtual graviton

Fig 1 The wavy line represents a graviton

The solid lines represent either vector, tensor or spin-3/2 quanta

Using the S -matrix formalism we deduced the Feynman-type rules for diagrams in the external gravitational field (described by Schwarzschild metric) which allowed us to calculate the matrix element $\langle p' | S | p \rangle$ in the mentioned approximation

Thus we find that [4]

$$u_{\mu\nu}^{est}(\vec{q}) = \left[\delta_{\mu'} \delta_{\nu'} - \frac{1}{4} \delta_{\mu\nu} \right] \gamma^{est}(\vec{q}) \tag{32}$$

$$\gamma_{\mu\nu}^{est}(\vec{q}) = \delta_{\mu'} \delta_{\nu'} \gamma^{est}(\vec{q}) \tag{33}$$

$$h_{\mu\nu,\alpha}^{est}(\vec{q}) = \left[\delta_{\mu'} \delta_{\nu'} - \frac{1}{2} \delta_{\mu\nu} \right] \gamma_{,\alpha}^{est}(\vec{q}) \tag{34}$$

$$\gamma_{,\alpha}^{est}(\vec{q}) = i \delta_{,\alpha} q_j \gamma_j^{est}(\vec{q}) ; (\iota = \sqrt{-1}) \tag{35}$$

Taking into account the Fourier transform of the static external gravitational potential

$$y^{\mu\nu}(\vec{q}) = \frac{1}{(2\pi)^{3/2}} \int e^{-i\vec{q}\vec{x}} \frac{kM}{4\pi|\vec{x}|} d^3x = \frac{kM}{(2\pi)^{3/2}|\vec{q}|^2}, \quad (36)$$

(where M is the mass of the central body that creates the gravitational field and $|\vec{x}|$ is the distance to this centre), the matrix elements in the external field approximation, corresponding to the diagram in fig 1 are respectively

$$S_{p'p}^{(1)} = \langle p' | S | p \rangle = \frac{-ik^2 M}{2(2\pi)^2 \sqrt{p'_0 p_0}} \int \frac{\delta(q_0)}{|\vec{q}|^2} \{ [e_\nu^{(j)}(\vec{p}') p'_\mu - 2\mu_\nu^{(j)}(\vec{p}') p'_\nu] [e_\alpha^{(j)}(\vec{p}) p_\mu - e_\mu^{(j)}(\vec{p}') p_\alpha] \times \\ \times \left(\delta_{\nu\alpha} \delta_{\alpha'} - \frac{1}{4} \delta_{\lambda\alpha} \right) + m^2 e_\nu^{(j)}(\vec{p}') e_\alpha^{(j)}(\vec{p}) \delta_{\nu\alpha} \delta_{\alpha'} \} \delta(\vec{p}' - \vec{p} - \vec{q}) d^3q = F(p', p) \delta(p'_0 - p_0) \quad (37)$$

$$S_{p'p}^{(2)} = \langle p' | S | p \rangle = \frac{-ik^2 M}{2(2\pi)^2 \sqrt{p'_0 p_0}} \int \frac{\delta(q_0)}{|\vec{q}|^2} \{ [e_{\alpha\nu}^{(j)}(\vec{p}') p'_\mu (3e_{\lambda\nu}^{(j)}(\vec{p}) p_\alpha - e_{\lambda\alpha}^{(j)}(\vec{p}) p_\nu - e_{\alpha\nu}^{(j)}(\vec{p}) p_\lambda) + \\ + e_{\alpha\mu}^{(j)}(\vec{p}') p'_\nu (e_{\lambda\nu}^{(j)}(\vec{p}) p_\alpha + e_{\lambda\alpha}^{(j)}(\vec{p}) p_\nu + e_{\alpha\nu}^{(j)}(\vec{p}) p_\lambda) + e_{\mu\nu}^{(j)}(\vec{p}') p'_\lambda (e_{\lambda\nu}^{(j)}(\vec{p}) p_\alpha + e_{\alpha\nu}^{(j)}(\vec{p}) p_\lambda) - \\ - 3e_{\lambda\nu}^{(j)}(\vec{p}) p_\alpha) - 2m^2 e_{\mu\nu}^{(j)}(\vec{p}') e_{\lambda\nu}^{(j)}(\vec{p}) \delta_{\mu\lambda} \delta_{\lambda'} - [(e_{\lambda\nu}^{(j)}(\vec{p}') p'_\mu + e_{\lambda\mu}^{(j)}(\vec{p}') p'_\nu - e_{\mu\nu}^{(j)}(\vec{p}') p'_\lambda) \times \\ \times (e_{\mu\nu}^{(j)}(\vec{p}) p_\lambda + e_{\mu\lambda}^{(j)}(\vec{p}) p_\nu - e_{\lambda\nu}^{(j)}(\vec{p}) p_\mu) - \frac{1}{2} m^2 e_{\mu\nu}^{(j)}(\vec{p}') e_{\mu\nu}^{(j)}(\vec{p})] + [(e_{\lambda\nu}^{(j)}(\vec{p}') p'_\mu + e_{\lambda\nu}^{(j)}(\vec{p}') p'_\nu - \\ - e_{\mu\nu}^{(j)}(\vec{p}') p'_\lambda) e_{\mu\alpha}^{(j)}(\vec{p}) \left(\left(\delta_{\lambda\alpha} \delta_{\alpha'} - \frac{1}{2} \delta_{\lambda\alpha} \right) \delta_{\nu j} + \left(\delta_{\nu\alpha} \delta_{\alpha'} - \frac{1}{2} \delta_{\nu\alpha} \right) \delta_{\lambda j} - \left(\delta_{\lambda\alpha} \delta_{\nu\alpha} - \frac{1}{2} \delta_{\lambda\nu} \right) \delta_{\alpha j} \right) - \\ - e_{\alpha\lambda}^{(j)}(\vec{p}') (e_{\mu\nu}^{(j)}(\vec{p}) p_\lambda + e_{\mu\lambda}^{(j)}(\vec{p}) p_\nu - e_{\lambda\nu}^{(j)}(\vec{p}) p_\mu) \left(\left(\delta_{\mu\alpha} \delta_{\alpha'} - \frac{1}{2} \delta_{\mu\alpha} \right) \delta_{\nu j} + \left(\delta_{\nu\alpha} \delta_{\alpha'} - \frac{1}{2} \delta_{\nu\alpha} \right) \times \right. \\ \left. \times \delta_{\mu\alpha} - \left(\delta_{\mu\alpha} \delta_{\nu\alpha} - \frac{1}{2} \delta_{\mu\nu} \right) \delta_{\alpha j} \right] \} \delta(\vec{p}' - \vec{p} - \vec{q}) d^3q = F(p', p) \delta(q_0) \quad (38)$$

$$\begin{aligned}
 S_{p'p}^{(32)} = \langle p' | S | p \rangle &= \frac{ik^2 m M}{4(2\pi)^2 \sqrt{p'_0 p_0}} \int \frac{\delta(q_0)}{|\vec{q}|^2} \{ [i p'_\mu \bar{u}_\alpha^{(s)}(\vec{p}') \gamma_\mu u_\alpha^{(r)}(\vec{p}) \delta_\mu \delta_\nu + \\
 &+ i \bar{u}_\alpha^{(s)}(\vec{p}') \gamma_\mu p_\nu u_\alpha^{(r)}(\vec{p}) \delta_\mu \delta_\nu + m \bar{u}_\alpha^{(s)}(\vec{p}') u_\alpha^{(r)}(\vec{p})] \delta(\vec{p}' - \vec{p} - \vec{q}) \} d^3 q = \\
 &= F(p', p) \delta(p'_0 - p_0),
 \end{aligned} \tag{39}$$

where $e_\mu^{(s)}(\vec{p})$, $e_{\mu\nu}^{(s)}(\vec{p})$, $u_\mu^{(s)}(\vec{p})$, $[\bar{u}_\mu^{(s)}(\vec{p}) = u_\mu^{(s)*}(\vec{p})\gamma_4]$ and p_0 on the one hand, and $e_\mu^{(s)}(\vec{p}')$, $e_{\mu\nu}^{(s)}(\vec{p}')$, $u_\mu^{(s)}(\vec{p}')$, $[\bar{u}_\mu^{(s)}(\vec{p}') = u_\mu^{(s)*}(\vec{p}')\gamma_4]$ and p'_0 on the other hand are the vectors, tensors, spin-vectors and the energy of the initial and final particles, respectively, and $q_0 = p'_0 - p_0 = 0$ states for the energy conservation law. We have denoted by the common notations m, p and p_0 the characteristic quantities (the mass, 4-momentum and the energy) for the all three fields respectively.

The differential cross-section is given by the well known expression

$$d\sigma = (2\pi)^2 \langle \sum_{f,sp} |F(p', p)|^2 \rangle_{i,sp} p_0^2 d\Omega, \tag{40}$$

where $d\Omega = 2\pi \sin\theta d\theta$, θ being the scattering angle. In order to evaluate the differential cross-section we must find the expression for $\langle \sum_{f,sp} |F(p', p)|^2 \rangle_{i,sp}$. For $|F(p', p)|^2$ we get from (37), (38) and (39) relations respectively

$$|F(p', p)|^2 = \left(\frac{k^2 M}{8(2\pi)^2 p_0 \vec{p}^2 \sin^2 \frac{\theta}{2}} \right) [Q_{vec}(p', p)]^2 \tag{41}$$

$$|F(p', p)|^2 = \left(\frac{k^2 M}{8(2\pi)^2 p_0 \vec{p}^2 \sin^2 \frac{\theta}{2}} \right)^2 [Q_{ten}(p', p)]^2 \tag{42}$$

$$|F(p', p)|^2 = \left(\frac{k^2 m M}{16(2\pi)^2 p_0 (p_0^2 - m^2) \sin^2 \frac{\theta}{2}} \right)^2 [Q_{sc}(p', p)]^2$$

where t is given by

$$t = 2i\gamma_1 p_0 - im$$

MASSIVE VECTOR, TENSOR AND SPIN-3/2 PARTICLES

Then, the expression $\langle \sum_{j_{sp}} |F(p', p)|^2 \rangle_{i_{sp}}$ for vector, tensor and respectively Rarita-Schwinger fields are.

$$\langle \sum_{j_{sp}} |F(p', p)|^2 \rangle_{i_{sp}} = \left(\frac{k^2 M}{8(2\pi)^2 p_0 (p_0^2 - m^2) \sin^2 \frac{\theta}{2}} \right)^2 \left(\frac{1}{3} \sum_{pol} Q_{vect}^2 \right) \quad (45)$$

$$\langle \sum_{j_{sp}} |F(p', p)|^2 \rangle_{i_{sp}} = \left(\frac{k^2 M}{8(2\pi)^2 p_0 (p_0^2 - m^2) \sin^2 \frac{\theta}{2}} \right)^2 \left(\frac{1}{5} \sum_{pol} Q_{tens}^2 \right) \quad (46)$$

$$\begin{aligned} \langle \sum_{j_{sp}} |F(p', p)|^2 \rangle_{i_{sp}} &= \left(\frac{k^2 m M}{16(2\pi)^2 p_0 (p_0^2 - m^2) \sin^2 \frac{\theta}{2}} \right)^2 \frac{1}{4} \sum_{r,s=1}^4 |\bar{u}_\alpha^{(r)}(\vec{p}') t u_\alpha^{(s)}(\vec{p})|^2 = \\ &= \left(\frac{k^2 m M}{16(2\pi)^2 p_0 (p_0^2 - m^2) \sin^2 \frac{\theta}{2}} \right)^2 \left(\frac{1}{4} \sum_{pol} Q_{R-S}^2 \right). \end{aligned} \quad (47)$$

where $\sum_{pol} Q_{vect}^2$, $\sum_{pol} Q_{tens}^2$ and $\sum_{pol} Q_{R-S}^2$ are the polarization sums for the vector, tensor and Rarita-Schwinger fields and because they have a long enough expressions we prefer not to give them here

In order to evaluate the polarization sums we take into account that the polarization vectors, tensors and spin-vectors, respectively, satisfy the relations [5, 10]

$$\sum_{\lambda=1}^3 e_{\mu}^{(\lambda)}(\vec{p}) e_{\nu}^{(\lambda)}(\vec{p}) = d_{\mu\nu}, \quad \mu, \nu = 1 \text{ to } 4 \quad (48)$$

$$\prod_{i,\nu,\lambda,\rho} e_{i\nu}^{(\lambda)}(\vec{p}) e_{\lambda\rho}^{(i)}(\vec{p}) = \frac{1}{2} (d_{\mu\lambda} d_{\nu\rho} + d_{\mu\rho} d_{\nu\lambda}) - \frac{1}{3} d_{\mu\nu} d_{\lambda\rho} \quad (49)$$

$$\sum_{r=1}^4 u_\mu^{(r)}(\vec{p}) \bar{u}_\nu^{(r)}(\vec{p}) = \frac{\gamma_\alpha p_\alpha + im}{2im} \left[\delta_{\mu\nu} - \frac{1}{3} \gamma_\mu \gamma_\nu + \frac{i}{3m} (\gamma_\mu p_\nu - \gamma_\nu p_\mu) + \frac{2}{3m^2} p_\mu p_\nu \right], \quad (50)$$

where $d_{\mu\nu}$ is given by: $d_{\mu\nu} = \delta_{\mu\nu} + \frac{p_\mu p_\nu}{m^2}$

After a laborious calculus, for the differential cross-section of the massive vector, tensor and Rarita-Schwinger particles one obtains the following expressions, respectively

$$d\sigma = \left(\frac{k^2 M}{16\pi}\right)^2 \frac{d\Omega}{\sin^4 \frac{\theta}{2}} \left[\left(\frac{1+v^2}{2v^2}\right)^2 - \frac{2}{3} \sin^2 \frac{\theta}{2} \left(\frac{2}{v^2} - \sin^2 \frac{\theta}{2}\right) \right] \quad (51)$$

$$d\sigma = \left(\frac{k^2 M}{16\pi}\right)^2 \frac{d\Omega}{\sin^4 \frac{\theta}{2}} \left\{ \left(\frac{1+v^2}{2v^2}\right)^2 - \frac{4}{v^2} \sin^2 \frac{\theta}{2} + \frac{2}{45(1-v^2)^4} \sin^4 \frac{\theta}{2} [9(31 - \right. \\ \left. - 108v^2 + 146v^4 - 92v^6 + 23v^8) + 48v^2(7 - 18v^2 + 19v^4 - 8v^6) \sin^2 \frac{\theta}{2} - \right. \\ \left. - 24v^4(5 - 6v^2 - 11v^4) \sin^4 \frac{\theta}{2} - 192v^6(1+v^2) \sin^6 \frac{\theta}{2} + 128v^8 \sin^8 \frac{\theta}{2}] \right\} \quad (52)$$

$$d\sigma = \left(\frac{k^2 M}{16\pi}\right)^2 \frac{d\Omega}{\sin^4 \frac{\theta}{2}} \left\{ \left(\frac{1+v^2}{2v^2}\right)^2 - \frac{1}{36v^4(1-v^2)^2} [v^2(15 - 41v^2 + 5v^4 + 21v^6) \sin^2 \frac{\theta}{2} + \right. \\ \left. + 4v^4(3 - 6v^2 - 5v^4) \sin^4 \frac{\theta}{2} + 8v^6(3+v^2) \sin^6 \frac{\theta}{2}] \right\}, \quad (53)$$

where we denoted by v the $\frac{|\vec{p}|}{p_0}$ ratio

We shall notice that in the small angle approximation the polarization sums become

$$\sum_{pol} Q_{vecl}^2 = 3\vec{p}^4 \left(\frac{1+v^2}{2v^2}\right)^2 \quad (54)$$

$$\sum_{pol} Q_{tens}^2 = 5\vec{p}^4 \left(\frac{1+v^2}{2v^2}\right)^2 \quad (55)$$

$$\sum_{\rho\sigma} Q_{R \rightarrow S}^2 = 4p_0^2 \frac{(1 + v^2)^2}{1 - v^2} \quad (56)$$

Taking into account the previous relations, the differential cross-sections in the small angle approximation become

$$d\sigma_{small\theta} = \left(\frac{k^2 M}{16\pi} \right)^2 \frac{d\Omega}{\sin^4 \frac{\theta}{2}} \left(\frac{1 + v^2}{2v^2} \right) = d\sigma_{Ruth}, \quad (57)$$

i.e., they are the differential cross-sections of Rutherford type. As we can see from (51), (52) and (53) the expression for $d\sigma_{Ruth}$ is contained by these relations as a first term. Since this term (i.e. $d\sigma_{Ruth}$) is quite the differential cross-section for the massive scalar particles (for instance the scalar mesons) we can interpret the second term in the (51), (52) and (53) relations as being the spin contribution of the vector, tensor and Rarita-Schwinger particles, respectively.

A particular interest is presented by the back-scattering limit case. In this special limit case we have worked out respectively

$$d\sigma_{scr}^* = \left(\frac{k^2 M}{16\pi} \right)^2 \left[\left(\frac{1 + v^2}{2v^2} \right)^2 - \frac{2}{3} \frac{2 - v^2}{v^2} \right] d\Omega^* \quad (58)$$

$$d\sigma_{ten}^* = \left(\frac{k^2 M}{16\pi} \right)^2 \frac{d\Omega^*}{180v^4(1-v^2)^4} \times \\ \times (45 - 810v^2 + 5067v^4 - 9228v^6 + 5475v^8 - 522v^{10} + 229v^{12}) \quad (59)$$

$$d\sigma_{R \rightarrow S}^* = \left(\frac{k^2 M}{16\pi} \right)^2 \frac{9 - 6v^2 + 5v^4}{36v^4(1-v^2)} d\Omega^* \quad (60)$$

where $d\sigma^* = d\sigma_{lab}^*$ and $d\Omega^* = 2\pi d\theta$

In the ultrarelativistic case ($v \rightarrow 1$) we get from (58)

$$\frac{d\sigma_{scr}^*}{d\Omega^*} = \frac{1}{3} (GM)^2 \quad (U R) \quad (61)$$

i.e., in the back-scattering and ultrarelativistic case, the differential cross-section $\frac{d\sigma^*}{d\Omega^*}$ for the vector field only (!) is constant (and non-zero), which means that in this case the helicity of the particles is not conserved, in agreement with [11].

Finally it's worthwhile to point out that in the small angle approximation, the differential cross-sections for scattering in Schwarzschild field of massive scalar, vector, spinor, Rarita-Schwinger and tensor particles have the same form and in ultrarelativistic case they coincide with those corresponding to the neutrinos, photons, gravitons and gravitinos, i.e., the gravitational particle scattering in this limit case is spin-independent [12, 13], in agreement with many authors' results, obtained by other means [14]

REFERENCES

1. S Gupta, Proc Phys Soc. A 65, 161, 608, 1952
2. De Witt B., Phys Rev, 160, 1113, 1967 162, 1195, 1967 162, 1239, 1967.
3. D Tatomir, An. sc Univ. "Al.I.Cuza" Iași (n.s.), section I b, phys, tom XXIV, p 91, 1978
4. D. Tatomir, "Contributions in Quantum Study of the Particles Interaction in the Presence of Gravitation" - Ph D. Thesis, "Al I Cuza" Univ, Iași, 1981 (to be published)
5. J. Schwinger, "Particles, Sources and Fields", Addison-Wesley Publishing Company, 1970 (printed in U.S.A.)
6. V. Fock and D Ivanenko. C r Acad. Sci, 188, 1470, 1929.
7. N Mitskevich, "Fiz polja v O.T.O", Izd.-vo "Nauka", Moskva, 1969.
8. R. Lias, Tr. Inst. fiz. astr., ANESSR, Nr 5, 25, 1957
9. Iu. Vladimirov, Izv. V.U Zov., Fizika, Nr 2, 133, 1963.
10. D Lurie, "Particles and Fields", J.Wiley & Sons, New-York, 1968
11. W De Logi and S.Kovacs, Phys. Rev, D, v. 16, Nr 2, 237, 1977.
12. D. Tatomir: "Abstracts of Contributed Papers for the Discussion Groups" Jena Univ, 14-19 July, 1980
13. D Tatomir, "10-th International Conference in G.R.G", Padova, 4-9 July, 1983, Contributed Papers, 140
14. K.Lotze, Acta Phys Pol., B 9, 665, 677, 1978.

FOURTH ORDER TORSION L -TENSOR FORMULAS FOR ANHARMONIC FORCE CONSTANT TRANSFORMATION

T.A. BEU*

Received 15 12 1993

ABSTRACT. - New fourth order analytical torsion L -tensors are reported, which complete previously published third order expressions. The formulas up to the third order are used in molecular normal mode analysis calculations for the nonlinear transformation of the force constants from internal coordinates to normal coordinates. Sample calculations are presented.

1. Introduction. Although, due to the advances in computer techniques, most of the computational effort of molecular normal mode analysis applications has been transferred to numerical methods, for large problems it may be still preferable to use analytical formulas for the L -tensors involved in the transformation of the force constants from internal- to normal coordinates, instead of numerically deriving the internal coordinates with respect to the normal coordinates, according to the definition of the L -tensors.

L -tensors formulas for all elementary internal valence coordinates are available. The torsional coordinates, however, require an especially delicate mathematical treatment, and give rise to the most complicated expressions. Formulas for planar equilibrium configurations [1], and more recently, general formulas [2] have been reported. Alternative torsion L -tensor formulas have been presented in [3] (hereafter referred to as Paper I), which, in contrast to the analytical results of [2], are more compact, implying scalar operations with trigonometric functions instead of cumbersome vector operations.

* "Babeș-Bolyai" University, Faculty of Physics, 3400 Cluj-Napoca, Romania

It is the purpose of this paper to present new fourth order torsion L -tensors, which complete the set reported in Paper I. Due to the complexity of the calculations, extensive use was made of the symbolic computation package *Mathematica*. The expressions up to the third order are equivalent to those of Paper I. Results for methanol and hydrazine, obtained by the numerical implementation of these expressions, are presented and compared with similar results from the literature.

2. Equations. The Taylor expansion of the potential energy with respect in terms of curvilinear internal displacement coordinates may be written as [1]

$$V = \frac{1}{2} \sum_{i,j} F_{ij} R_i R_j + \frac{1}{6} \sum_{i,j,k} F_{ijk} R_i R_j R_k + \frac{1}{24} \sum_{i,j,k,l} F_{ijkl} R_i R_j R_k R_l + \dots \quad (1)$$

where the force constants F_{ij} , F_{ijk} and F_{ijkl} are the 2nd, 3rd and 4th derivatives of the potential energy to the coordinates R_i , referred to the equilibrium configuration of the molecule. In order to perform a normal mode analysis, the vibrational-rotational Hamiltonian is, however, conveniently expressed in terms of the normal coordinates Q_r ,

$$V = \frac{1}{2} \sum_r \lambda_r Q_r^2 + \frac{1}{6} \sum_{r,s,t} \phi^{rst} Q_r Q_s Q_t + \frac{1}{24} \sum_{r,s,t,u} \phi^{rstu} Q_r Q_s Q_t Q_u + \dots \quad (2)$$

where $\lambda_r = 4\pi^2 c^2 \omega_r^2$

The internal coordinates R_i can be expressed in terms of normal coordinates Q_r nonlinear transformation

FOURTH ORDER TORSION L-TENSOR FORMULAS

$$R_i = \sum_r L_i^r Q_r + \sum_{r,s} L_i^{rs} Q_r Q_s + \sum_{r,s,t} L_i^{rst} Q_r Q_s Q_t + \dots \quad (3)$$

where the elements of the L -tensor, $L_i^r, L_i^{rs}, L_i^{rst}, \dots$, have to be interpreted as first-, second-, and third order derivatives of the internal coordinate R_i with respect to normal coordinates

The formulas for the transformation of the force constants from internal-, to normal coordinates (including only L -tensors up to the third order) may be readily obtained by substituting (3) in (1), and comparing the result with (2)

$$\begin{aligned} \lambda_r &= \sum_{i,j} F_{ij} L_i^r L_j^r \\ \phi^{rst} &= \sum_{i,j,k} F_{ijk} L_i^r L_j^s L_k^t + \sum_{i,j} F_{ij} \left(L_i^{rs} L_j^t + L_i^{rt} L_j^s + L_i^{st} L_j^r \right) \\ \phi^{rstu} &= \sum_{i,j,k,l} F_{ijkl} L_i^r L_j^s L_k^t L_l^u \\ &+ \sum_{i,j,k} F_{ijk} \left(L_i^{rs} L_j^t L_k^u + L_i^{rt} L_j^s L_k^u + L_i^{ru} L_j^s L_k^t \right. \\ &\quad \left. + L_i^{st} L_j^r L_k^u + L_i^{su} L_j^r L_k^t + L_i^{tu} L_j^s L_k^r \right) \\ &+ \sum_{ij} F_{ij} \left(L_i^{rs} L_j^{tu} + L_i^{rt} L_j^{su} + L_i^{ru} L_j^{st} \right. \\ &\quad \left. + L_i^{rs} L_j^{tu} + L_i^{rt} L_j^{su} + L_i^{ru} L_j^{st} \right) \end{aligned}$$

As stated above, it is only the case of torsional coordinates we are dealing with in what follows. The torsion coordinate involves four atoms. If the atoms $a, b, c,$ and d are linked by the bond vectors $r_i = ab, r_j = bc$ and $r_k = cd$, the torsion coordinate τ is defined as the dihedral angle between the planes abc and bcd . The torsion "displacement" coordinate $R_{y_{tk}}$, which is actually used as a normal coordinate, may then be defined as the difference

between the torsion coordinate and the corresponding equilibrium value τ_e ,

$$R_{ijk} = \tau - \tau_e = \arccos \left[\frac{(e_i \times e_j) \cdot (e_j \times e_k)}{\sin \phi_{ij} \sin \phi_{jk}} \right] - \tau_e, \quad (4)$$

where e_i, e_j, e_k are the unit vectors of the three bonds

The torsion L -tensor may be set up, as already pointed out, from the derivatives of the torsion displacement coordinate with respect to the normal coordinates. The relations for the first four orders are

$$L_{ijk}^r = \frac{\partial R_{ijk}}{\partial Q_r}, L_{ijk}^{rs} = \frac{\partial^2 R_{ijk}}{\partial Q_r \partial Q_s}, L_{ijk}^{rst} = \frac{\partial^3 R_{ijk}}{\partial Q_r \partial Q_s \partial Q_t}, L_{ijk}^{rstu} = \frac{\partial^4 R_{ijk}}{\partial Q_r \partial Q_s \partial Q_t \partial Q_u} \quad (5)$$

In order to avoid the complications implied by repeatedly deriving the mixed vector product from the expression of the torsion displacement given by (4), we transform R_{ijk} making use of the well-known Lagrange identity

$$(a \times b) \cdot (c \times d) = (a \cdot c)(b \cdot d) - (b \cdot c)(a \cdot d)$$

Relating the obtained scalar products of the unit vectors to the angles defined by them

$$e_i \cdot e_j = -\cos \phi_{ij}, \quad e_j \cdot e_k = -\cos \phi_{jk}, \quad e_i \cdot e_k = \cos \phi_{ik},$$

the torsion displacement coordinate becomes

$$R_{ijk} = \arccos \left(\frac{\cos \phi_{ij} \cos \phi_{jk} - \cos \phi_{ik}}{\sin \phi_{ij} \sin \phi_{jk}} \right) - \tau_e \quad (6)$$

As one may notice, the angle ϕ_{ik} between the non-adjacent bonds i and k appears in the above relation, as well

In performing the operations required to derive the expressions of the torsion L -

FOURTH ORDER TORSION L-TENSOR FORMULAS

tensors, it is useful to keep in mind the definition of the first order angle bending L -tensor

$$L_{ij}^r = \frac{\partial \phi_{ij}}{\partial Q_r} \quad (7)$$

which, coming from the derivatives of the angles ϕ_{ij} , ϕ_{jk} and ϕ_{ik} , respectively, will enter in the expression of all torsion L -tensor

In order to simplify the expressions of the torsion L -tensors, we define the following auxiliary tensors

$$S_{ij}^r = L_{ij}^r / \sin \phi_{ij}, \quad (8)$$

$$T_{ijk}^r = S_{ij}^r \cos \phi_{ij} + S_{jk}^r \cos \phi_{jk}, \quad (9)$$

$$U_{ijk}^{rs} = S_{ij}^r S_{ij}^s + S_{jk}^r S_{jk}^s, \quad (10)$$

$$V_{ijk}^{rst} = S_{ij}^r S_{ij}^s S_{ij}^t \cos \phi_{ij} + S_{jk}^r S_{jk}^s S_{jk}^t \cos \phi_{jk} \quad (11)$$

T_{ijk}^r , U_{ijk}^{rs} and V_{ijk}^{rst} are obviously symmetric with respect to the index pairs "ij" and "jk"

The formulas for the torsion L -tensors yielded by *Mathematica* (according to the definitions (5)) are obtained employing a rather elaborate set of expression manipulation rules, which allow for massive simplification of the relations, use being made of the expressions of the already determined lower order tensors. Here are the resulting formulas for the first order L -tensor

$$L_{ijk}^r = T_{ijk}^r \cot \tau_r + \csc \tau_r \left[L_{ij}^r \cot \phi_{jk} + L_{jk}^r \cot \phi_{ij} - \frac{L_{ik}^r \sin \phi_{ik}}{\sin \phi_{ij} \sin \phi_{jk}} \right], \quad (12)$$

the second order tensor

$$L_{ijk}^{rs} = -L_{ijk}^s T_{ijk}^r - \cot \tau_s \left(L_{ijk}^r L_{ijk}^s + U_{ijk}^{rs} \right) - \csc \tau_s \left[\frac{L_{jk}^r S_{ij}^s}{\sin \phi_{ij}} + \frac{L_{ij}^r S_{jk}^s}{\sin \phi_{jk}} + \frac{L_{ik}^r}{\sin \phi_{ij} \sin \phi_{jk}} \left(L_{ik}^s \cos \phi_{ik} - T_{ijk}^s \sin \phi_{ik} \right) \right], \quad (13)$$

the third order tensor

$$\begin{aligned}
 L_{ijk}^{rst} &= L_{ijk}^r L_{ijk}^s L_{ijk}^t + L_{ijk}^s U_{ijk}^{rt} + L_{ijk}^t U_{ijk}^{rs} - L_{ijk}^{st} T_{ijk}^r \\
 &- \cot\gamma_e \left[L_{ijk}^s L_{ijk}^t T_{ijk}^r + L_{ijk}^r L_{ijk}^{st} + L_{ijk}^s L_{ijk}^{rt} + L_{ijk}^t L_{ijk}^{rs} - V_{ijk}^{rst} \right] \\
 &+ \csc\gamma_e \left\{ 2 \cot\phi_{ij} L_{jk}^r S_{ij}^s S_{ij}^t + 2 \cot\phi_{jk} L_{ij}^r S_{jk}^s S_{jk}^t + \frac{L_{ik}^r}{\sin\phi_{ij} \sin\phi_{jk}} \right. \\
 &\left. \times \left[\cos\phi_{ik} \left(L_{ik}^t T_{ijk}^s + L_{ik}^s T_{ijk}^t \right) + \sin\phi_{ik} \left(L_{ik}^s L_{ik}^t - T_{ijk}^s T_{ijk}^t - U_{ijk}^{st} \right) \right] \right\}, \tag{14}
 \end{aligned}$$

and finally, the fourth order L -tensor

$$\begin{aligned}
 L_{ijk}^{rstu} &= L_{ijk}^r \left(L_{ijk}^s L_{ijk}^{tu} + L_{ijk}^t L_{ijk}^{su} + L_{ijk}^u L_{ijk}^{st} \right) + L_{ijk}^s \left(L_{ijk}^t L_{ijk}^{ru} + L_{ijk}^u L_{ijk}^{rt} \right) \\
 &+ L_{ijk}^t L_{ijk}^u L_{ijk}^{rs} + \left(L_{ijk}^s L_{ijk}^t L_{ijk}^u - L_{ijk}^{stu} \right) T_{ijk}^r + L_{ijk}^{st} U_{ijk}^{ru} + L_{ijk}^{su} U_{ijk}^{rt} + L_{ijk}^{tu} U_{ijk}^{rs} \\
 &+ \cot\gamma_e \left[L_{ijk}^r L_{ijk}^s L_{ijk}^t L_{ijk}^u - L_{ijk}^{rs} L_{ijk}^{tu} - L_{ijk}^{rt} L_{ijk}^{su} - L_{ijk}^{ru} L_{ijk}^{st} - L_{ijk}^r L_{ijk}^{stu} \right. \\
 &- L_{ijk}^s L_{ijk}^{rtu} - L_{ijk}^t L_{ijk}^{rsu} - L_{ijk}^u L_{ijk}^{rst} - \left(L_{ijk}^s L_{ijk}^{tu} + L_{ijk}^t L_{ijk}^{su} + L_{ijk}^u L_{ijk}^{st} \right) T_{ijk}^r \\
 &- 2 \left(1 + 2 \cos^2\phi_{ij} \right) S_{ij}^r S_{ij}^s S_{ij}^t S_{ij}^u - 2 \left(1 + 2 \cos^2\phi_{jk} \right) S_{jk}^r S_{jk}^s S_{jk}^t S_{jk}^u \\
 &+ L_{ijk}^s L_{ijk}^t U_{ijk}^{ru} + L_{ijk}^s L_{ijk}^u U_{ijk}^{rt} + L_{ijk}^t L_{ijk}^u U_{ijk}^{rs} \left. \right] - L_{ijk}^r V_{ijk}^{tu} - L_{ijk}^t V_{ijk}^{su} - L_{ijk}^u V_{ijk}^{st} - L_{ijk}^u V_{ijk}^{rst} \\
 &+ \csc\tau_e \left\{ -2 \left(1 + 2 \cos^2\phi_{ij} \right) \csc\phi_{ij} L_{jk}^r S_{ij}^s S_{ij}^t S_{ij}^u - 2 \left(1 + 2 \cos^2\phi_{jk} \right) \csc\phi_{jk} L_{ij}^r S_{jk}^s S_{jk}^t S_{jk}^u \right. \\
 &+ \frac{L_{ik}^r}{\sin\phi_{ij} \sin\phi_{jk}} \left[\cos\phi_{ik} \left(L_{ik}^s L_{ik}^t L_{ik}^u - L_{ik}^u T_{ijk}^s T_{ijk}^t - L_{ik}^t T_{ijk}^s T_{ijk}^u - L_{ik}^s T_{ijk}^t T_{ijk}^u \right) \right. \\
 &- L_{ik}^u U_{ijk}^{st} - L_{ik}^s U_{ijk}^{tu} - L_{ik}^t U_{ijk}^{su} \left. \right] + \sin\phi_{ik} \left(-L_{ik}^t L_{ik}^u T_{ijk}^s - L_{ik}^s L_{ik}^u T_{ijk}^t - L_{ik}^s L_{ik}^t T_{ijk}^u \right. \\
 &\left. \left. + T_{ijk}^s T_{ijk}^t T_{ijk}^u + T_{ijk}^u U_{ijk}^{st} + T_{ijk}^t U_{ijk}^{su} + T_{ijk}^s U_{ijk}^{tu} + V_{ijk}^{rstu} \right) \right\} \tag{15}
 \end{aligned}$$

As it is apparent from Eqs (12-15), all torsion L -tensor elements depend on the angle bending tensor elements L_{ij}^r , and on the torsion L -tensor elements of lower order. It should

also be emphasized the explicit dependence of the torsion L -tensors on the equilibrium value of the torsion displacement coordinate τ_e only through the factors $\cot \tau_e$ and $\cos \tau_e$.

Another point worth discussing is the appearance of the "angle bending" L -tensor elements, L'_{ik} , corresponding to the angle ϕ_{ik} defined by the non-adjacent bond vectors. The significance of the mentioned elements may be regarded as purely mathematical, and for their computation the formulas for usual angle bending may be employed [1]

3. Sample calculations. We present in what follows fundamental frequency results for two sample cases involving torsional coordinates: methanol and hydrazine. In both cases there have been used only L -tensors up to the third order.

The harmonic frequencies and normal coordinates have been calculated by the Wilson F-G method. The anharmonicity correction is accomplished by employing the approach of Hoy, Mills and Strey [1] (briefly discussed in section 2) embedded in an original FORTRAN 77 computer code for general normal mode analysis, run both under the UNIX and DOS operating systems.

The geometry and internal coordinates used to describe methanol are those of [4]. The force constants are taken from the same reference, where all cubic force constants of the type F_{ijk} , with i, j and k all different, and all quartic force constants other than the diagonal stretching ones are neglected. It should be noted that the calculations reported in [4] are performed strictly numerically, no use being made of analytical L -tensor formulas.

Table 1 shows the computed fundamental frequencies of [4], the ones computed by means of our L -tensor formulas, along with the observed frequencies reported in [5]. One may

notice the fair agreement between our frequency values and those of [4]. Both sets of computed frequencies exhibit the same overestimating tendency as compared to the experimental values, however, the overall better agreement of our results (with a smaller maximum relative error of 6.7%) is obvious. Exceptions are τ_2 (C-H bond stretching) and τ_9 (C-O-H angle bending), for which the errors are small anyway. For the three torsion modes of methanol (τ_{10} , τ_{11} and τ_{12}) our relative errors are significantly smaller.

Table I. Fundamental vibration frequencies of methanol. ν^{obs} are the experimental values of [5], ν' are the calculated values of [4] and ν'' are the frequencies computed in this work (in cm^{-1} , the corresponding relative errors being expressed in %).

	ν^{obs}	ν'	$(\nu' - \nu^{obs})/\nu'$	ν''	$(\nu'' - \nu^{obs})/\nu''$
A'					
ν_1	3682	3730	1.3	3728	1.2
ν_2	2999	3009	0.3	3011	0.4
ν_3	2844	2919	2.6	2865	0.7
ν_4	1478	1611	8.3	1583	6.6
ν_5	1455	1571	7.4	1559	6.7
ν_6	1334	1391	4.1	1364	2.2
ν_7	1075	1113	3.5	1080	0.5
ν_8	1034	1046	1.1	1.39	0.5
A''					
ν_9	2970	2988	0.6	3006	1.2
ν_{10}	1465	1583	7.5	1537	4.7
ν_{11}	1145	1234	7.2	1190	3.8
ν_{12}	271	262	3.4	263	1.0

FOURTH ORDER TORSION L-TENSOR FORMULAS

All relevant data for the hydrazine molecule (geometry, internal coordinates and force constants) are taken from [2] Table II shows besides the calculated frequencies of [2] and of the present work, experimental data of [6] One should again notice the fair agreement between the two sets of computed frequencies The discrepancies between our frequencies and those of [2] (with maxima for the τ_7 N-N stretching mode and τ_{12} antisymmetric NH_2 wagging mode) are probably due less accurate force constants listed in [2] and used in our calculations, than the ones actually used to produce the frequencies of [2]

Table II. Fundamental vibration frequencies of hydrazine ν^{obs} are experimental data, ν' are computed values of [2], and ν'' are the frequencies computed in this work (in cm^{-1} , the corresponding relative errors being expressed in %)

	ν^{obs}	ν'	$(\nu' - \nu^{\text{obs}})/\nu'$	ν''	$(\nu'' - \nu^{\text{obs}})/\nu''$
A					
ν_1	3390 ^a	3413	0.7	3397	0.2
ν_2		3300		3297	
ν_3	1628 ^b	1659	1.9	1671	2.6
ν_4	1324 ^c	1344	1.5	1361	2.7
ν_5	1098 ^b	1121	2.0	1119	1.9
ν_6	780 ^b	840	7.1	843	7.5
ν_7	377 ^d	398	5.3	350	-7.7
B					
ν_8	3398 ^a	3402	0.1	3440	1.2
ν_9	3297 ^e	3287	-0.3	3331	1.0
ν_{10}	1587 ^b	1645	3.5	1655	4.1
ν_{11}	1283 ^e	1320	2.8	1318	2.6
ν_{12}	937 ^f	1045	10.3	1058	11.4

^a [6], ^b [7], ^c [8], ^e [10], ^f [11]

4. Conclusions. New torsion L -tensor formulas up to the fourth order are presented, which, in contrast to some previous analytical results, are more compact, implying scalar operations with trigonometric functions instead of cumbersome vector operations. The numerical results which have been subject to comparison, although affected by the employed set of force constants and the adopted numerical strategy, compare favourably with one another and with experimental data from the literature.

Acknowledgements The autor is indebted to Prof U Buck for his kind hospitality and many helpful discussions during the two visits at the Max-Planck-Institut für Stromungsforschung from Göttingen, where essential parts of the reported research have been accomplished. The author would like to thank Dr B Schmidt for many suggestions of substance.

R E F E R E N C E S

- 1 Hoy, A R , Mills, I M , Strey, G Mol Phys **24**, 1265 (1972)
- 2 Tanaka, N , Hamada, Y , Sugawara, Y , Tsuboi, M J Mol Spectrosc **99**, 245 (1983)
- 3 Beu, T A Z Phys D **27**, 263-266 (1993)
- 4 Schlegel, H B , Wolfe, S , Bernardi, F J Chem Phys, **67**, 4181 (1977)
- 5 Serrallach, A , Meyer, R , Gunthard, Hs H J Mol Spectrosc , **52**, 94 (1974)
- 6 Tipton, T , Stone, D A , KuBulat, K , Person, W J Phys Chem , **93**, 2917 (1989)
- 7 Giguère, P A , Liu, I D J Chem Phys **20**, 136 (1952)
- 8 Durig, J , Bash, S F , Mercer, E E J Chem Phys **44**, 4238 (1966)
- 9 Yamaguchi, A , Ichushima, I , Shimanouchi, T , Mizushima, S spectrochim Acta **16**, 1471 (1960)
- 10 Catalano, E , Sanborn, R H , Frazer, J W J Chem Phys **38**, 2265 (1963)
- 11 Hamada, Y , Hirakawa, A Y , Tamagake, K , Tsuboi, M J Mol Spectrosc **35**, 420 (1970)

EXCITATION OF A LOWER HYBRID WAVES IN A WARM PLASMA BY A WARM RELATIVISTIC ELECTRON BEAM

J. KARÁCSONY and Z. KISS*

Received 2 08 1993

ABSTRACT. - The linear theory of excitation of electrostatic lower hybrid waves into a warm magnetized plasma by a warm relativistic electron beam is presented. It is found that electrostatic lower hybrid waves can be excited by Cherenkov resonance. The frequencies and growth rates for excited waves are calculated.

1. Introduction. Absorption of a lower hybrid waves seems to be a very efficient method for heating ions in a plasma [1,2]. In recent years, considerable attention has been focused on theoretical and experimental studies of lower hybrid waves for plasma heating and current generation in tokamaks. These waves have been successfully employed to heat electrons and to drive plasma current in a number of tokamaks [3-8].

On the other hand, it has been demonstrated that lower hybrid waves generated by auroral electrons can produce transversally accelerated ions in ionospheric plasmas [9, 10].

In the space physics context a great attention has been accorded to the lower hybrid drift instability generated by density and magnetic field inhomogeneities [11, 12]. The lower hybrid wave can be also excited by an electromagnetic pump wave [13] and by electron beams. The linear theory of the lower hybrid waves excited by a nonrelativistic electron beam streaming through a cold plasma along the magnetic field has been discussed in detail by Papadopoulos and Palmadesso [14]. The relativistic electron beam temperature effects on this

* *University of Cluj-Napoca, Faculty of Physics, 3400 Cluj-Napoca, Romania*

instability has been studied in [15]. In the present paper we demonstrate that such waves can be generated by a warm relativistic electron beam into a warm magnetized plasma

In our model a warm relativistic electron beam with density n_{ob} and a velocity \vec{v}_e streams through a plasma with warm electrons and cold ions along a magnetic field B_0 . The unperturbed plasma density is considered to be $n_{op} \gg n_{os}$. Because we are interested with lower hybrid waves excitation we will study the almost perpendicular propagation of plasma waves to the magnetic field

2. Dispersion equation. The general dispersion equation for longitudinal waves can be written as [19]

$$\epsilon_{11} \sin^2\theta + \epsilon_{33} \cos^2\theta + 2\epsilon_{13} \cos\theta \sin\theta = 0 \quad (1)$$

where ϵ_{ij} ($i, j = 1, 3$) are the dielectric tensor components of the system and θ represents the angle between the wave vector k and the direction of the external magnetic field B_0 . (One assumes that the wave vector k lies in the xOz-plane and Oz-axis is oriented parallel to the external magnetic field)

The dielectric tensor can be expressed by means of the conductivity tensor σ in the following way [19]

$$\epsilon_{ij} = \delta_{ij} + \frac{4\pi i}{\omega} \sigma_{ij} \quad (2)$$

We will use the expressions calculated in [17] for the conductivity tensor components of the warm relativistic electron beam and the expressions calculated in [16] for the conductivity tensor components of the warm plasma with temperature anizotropy. Considering cold plasma ions and using relation (2) we can write the dielectric tensor components under

EXCITATION OF LOWER HYBRID WAVES

the form

$$\epsilon_{xx} = 1 - \frac{\omega_{pi}^2}{\omega^2 - \omega_{ci}^2} - \frac{\omega_{pe}^2}{\omega^2} \left\{ 1 - \sum_n n^2 \frac{A_n(\lambda_e)}{\lambda_e} \left[\frac{n\omega_{ce}}{k_x^2 v_{1e}} Z(s_{ne}) + \frac{T_{1e}}{T_{1e}} Y(s_{ne}) \right] + \sum_n n^2 \frac{A_n(\lambda_b)}{\lambda_b} P_n \right\} \quad (3)$$

$$\epsilon_{xx} = \frac{\omega_{pe}^2}{\omega^2} \text{tg} \theta \left\{ \sum_n n \frac{A_n(\lambda_e)}{\lambda_e} \frac{T_{1e}}{T_{1e}} \left[\frac{\omega}{\omega_{ce}} + n \left(\frac{T_{1e}}{T_{1e}} - 1 \right) \right] Y(s_{ne}) + \frac{\eta}{\gamma_o} \sum_n n \frac{A_n(\lambda_b)}{\lambda_b} Q_n \right\} \quad (4)$$

$$\epsilon_{xx} = 1 - \frac{\omega_{pi}^2}{\omega^2} + \frac{\omega_{pe}^2}{\omega^2} \text{tg}^2 \theta \left\{ \left(\frac{\omega}{\omega_{ce}} - n \right) \frac{T_{1e}}{T_{1e}} \left[\frac{\omega}{\omega_{ce}} + n \left(\frac{T_{1e}}{T_{1e}} - 1 \right) \right] \right\} \times Y(s_{ne}) + \frac{\eta}{\gamma_o} \sum_n \left(\frac{\omega \gamma_o}{\omega_{ce}} - n \right) \frac{A_n(\lambda_b)}{\lambda_b} Q_n \quad (5)$$

where the following notations have been used

$$P_n = 1 - \frac{n\omega_{ce}}{\gamma_o k_x v_{1b}} Z(s_{nb}) - \frac{T_{1b}}{T_{1b}} Y(s_{nb}) \quad (6)$$

$$Q_n = n \left[\frac{v_o}{v_{1b}} Z(s_{nb}) + \left(1 - \frac{T_{1b}}{T_{1b}} \right) Y(s_{nb}) \right] + \frac{\omega \gamma_o}{\omega_{ce}} \frac{T_{1b}}{T_{1b}} Y(s_{nb}) \quad (7)$$

and

$$A_n(\lambda) = e^{-\lambda} I_n(\lambda) \quad (8)$$

$I_n(\lambda)$ are the Bessel functions of the first kind of imaginary argument with

$$\lambda_e = \frac{k_x^2 v_{1e}^2}{\omega_{ce}^2} \quad (9)$$

for the plasma and

$$\lambda_b = k_x \frac{\bar{v}_{\perp b}^2 \gamma_o^2}{\omega_{ce}^2} \quad (10)$$

for the beam

The quantity ω_{pe} represents the electron plasma frequency and ω_{pi} the ion plasma frequency, while ω_{ce} and ω_{ci} are the electron and ion cyclotron frequencies, respectively. The perpendicular and parallel mean square velocity for beam electrons have been defined by the following relations [18].

$$T_{\perp b} = m_e \bar{v}_o^{\perp 2} b \quad (11)$$

$$T_{\parallel b} = m_e \bar{v}_o^{\parallel 2} b \quad (12)$$

where $T_{\perp b}$ and $T_{\parallel b}$ are the perpendicular and parallel beam temperature, respectively $\gamma_o = (1 - v_o^2/c^2)^{-1/2}$ is the usual relativistic factor and $\eta = n_{ob}/n_{op} \ll 1$.

In the expressions (3)-(7) we used the plasma dispers in functions [18]

$$Z(s_n) = (2\pi)^{-1/2} \int_{-\infty}^{\infty} \frac{\exp(-t^2/2)}{t - s_n} dt \quad (13)$$

and

$$Y(s_n) = (2\pi)^{-1/2} \int_{-\infty}^{\infty} \frac{t \exp(-t^2/2)}{t - s_n} dt \quad (14)$$

with

$$s_{ne} = \frac{\omega - n\omega_{ce}}{k_x \bar{v}_{1e}} \quad (15)$$

for the plasma and

$$s_{nb} = \frac{\omega - k \bar{v}_o - n\omega_{ce} \gamma_o}{k_x \bar{v}_{1b}} \quad (16)$$

for the beam

The perpendicular and parallel mean square velocity for the plasma electrons have been defined by the relations [16]

$$T_{\perp,1,e} = m_e \bar{v}_{\perp,1,e}^2 \quad (17)$$

EXCITATION OF LOWER HYBRID WAVES

where $T_{\perp e}$ and $T_{\parallel e}$ are the perpendicular and parallel electron plasma temperature, respectively

Since we will be interested with almost perpendicular wave propagation with respect to plasma return current direction, in expressions (3)-(5) we neglected plasma return current effects

Substituting the expressions (30)-(5) in (10 and taking into account that [18]

$$Y(s_n) = 1 + s_n Z(s_n) \quad (18)$$

the electrostatic dispersion relation becomes

$$\begin{aligned} D(K, \omega) = & 1 - \frac{\omega_{pe}^2 \cos^2 \theta}{\omega^2} - \frac{\omega_{pe}^2 \sin^2 \theta}{\omega^2 - \omega_{ci}^2} + \frac{\omega_{pe}^2}{k^2 \bar{v}_{1e}^2} \left[1 + \sum_n A_n(\lambda_e) Z(s_{ne}) \right] \times \\ & \times \left(s_{ne} + \frac{n \omega_{ce}}{k_x \bar{v}_{1e}} \frac{T_{\parallel e}}{T_{\perp e}} \right) + \frac{\eta}{\gamma_o^3} \frac{\omega_{pe}^2}{k^2 \bar{v}_{1b}^2} \left[1 + \sum_n A_n(\lambda_b) Z(s_{nb}) \right] \times \\ & \times \left(s_{nb} + \frac{n \omega_{ce}}{k_x \bar{v}_{1b} \gamma_o} \frac{T_{\parallel b}}{T_{\perp b}} \right) = 0 \end{aligned} \quad (19)$$

3. Excitation of lower hybrid waves. For electrostatic waves with $\omega_{ci} \ll \omega \ll \omega_{ce}$ and $\cos \theta \leq m_e/m_i$, some simplification of equation (19) is possible because $s_{ne} > 1$ Using the asymptotic values of $Z(s_{ne})$ [18]

$$Z(s_{ne}) = -\frac{1}{s_{ne}} - \frac{1}{s_{ne}^3} - + i \sqrt{\frac{\pi}{2}} e^{-\frac{S_{ne}^2}{2}} \quad (20)$$

and neglecting the higher order terms, the dispersion equation (19) reduces to

$$\begin{aligned} D(K, \omega) = & 1 - \frac{\omega_{pe}^2}{\omega^2} - \frac{\omega_{pe}^2}{\omega^2} A_o(\lambda_e) \cos^2 \theta - \frac{\omega_{pe}^2}{k^2 \bar{v}_{1e}^2} \sum_n A_n(\lambda_e) \frac{n \omega_{ce}}{\omega - n \omega_{ce}} \frac{T_{\parallel e}}{T_{\perp e}} + \\ & + i \sqrt{\frac{\pi}{2}} \frac{\omega_{pe}^2 \omega}{k^2 k_x \bar{v}_{1e}^3} A_o(\lambda_e) e^{-\frac{\omega^2}{2k_x^2 \bar{v}_{1e}^2}} - \frac{\eta}{\gamma_o^3} \frac{\omega_{pe}^2}{k^2 \bar{v}_{1b}^2} \left[1 + \sum_n A_n(\lambda_b) \right] \times \end{aligned} \quad (21)$$

$$\times Z(s_{nb}) \left(s_{nb} + \frac{n\omega_{ce}}{k_z v_{1b} \gamma_o} \frac{T_{1b}}{T_{1b}} \right) = 0$$

Now, taking into account that for lower hybrid waves we can use for $A_n(\lambda_e)$ the expression [19]

$$A_n(\lambda_e) = \frac{\lambda_e^{|n|}}{2^{|n|} |n|!} \quad (22)$$

and we finally have the dispersion relation in the form

$$D(\vec{k}, \omega) = 1 - \frac{\omega_{pe}^2}{\omega^2} - \frac{\omega_{pe}^2}{\omega^2} \cos^2 \theta + \frac{\omega_{pe}^2}{\omega_{ce}^2} + i \sqrt{\frac{\pi}{2}} \frac{\omega_{pe}^2 \omega}{k^2 k_z \bar{v}_{1e}^3} e^{-\frac{\omega}{2k_z \bar{v}_{1e}}} - \frac{\eta}{\gamma_o^3} \frac{\omega_{pe}^2}{k^2 \bar{v}_{1b}^2} \left[1 + \sum_n A_n(\lambda_e) Z(s_{nb}) \left(s_{nb} + \frac{n\omega_{ce}}{k_z v_{1b} \gamma_o} \frac{T_{1b}}{T_{1b}} \right) \right] = 0 \quad (23)$$

With the purpose to investigate this dispersion equation, we will follow the usually applied procedure in plasma physics [19] According to this, when $\text{Im } \omega \ll \text{Re } \omega$, the excited wave frequencies can be calculated from the equation

$$\text{Re } D(\vec{k}, \omega) = 0 \quad (24)$$

and the corresponding growth rates from the relation

$$\text{Im } \omega = - \frac{\text{Im } D(\vec{k}, \omega_e)}{\partial \text{Re } D(\vec{k}, \omega_k) / \partial \omega_k} \quad (25)$$

where $\omega_k = \text{Re } \omega(\vec{k})$

Writing the $Z(s_{nb})$ function under the form [18]

$$Z(s_{nb}) = -\exp\left(-\frac{S_{nb}}{2}\right) \left[\int_0^{s_{nb}} \exp\left(\frac{\xi^2}{2}\right) d\xi - i \left(\frac{\pi}{2}\right)^{1/2} \right] \quad (26)$$

and taking into account that in $\text{Re } D(\vec{k}, \omega)$ the contribution of the beam terms are of order η , we obtain for the excited wave frequencies the expression

EXCITATION OF LOWER HYBRID WAVES

$$\omega_k^2 = \frac{1}{1 + \alpha^2} (\omega_{pl}^2 + \omega_{pe}^2 \cos^2 \theta) \quad (27)$$

where

$$\alpha^2 = \frac{\omega_{pe}^2}{\omega_{ce}^2} + \frac{\eta}{\gamma_o^3} \frac{\omega_{pe}^2}{k^2 v_{1b}^2} \left[1 + \sum_n A_n(\lambda_b) \cdot \right. \quad (28)$$

with

$$\left. \cdot \operatorname{Re} Z(s_{nb}) \left(s_{nb} + \frac{n \omega_{ce}}{k_z v_{1b} \gamma_o} \frac{T_{1b}}{T_{1e}} \right) \right]_{s = \omega_k} \quad (29)$$

The growth rate for the instability can be found from (24) using for $D(K, \omega)$ the expression (23)

Taking into account that $\operatorname{Im} Z(s_{nb})$ with $n \neq 0$ are small compared with $\operatorname{Im} Z(s_{nb})_s$, we obtain for $\operatorname{Im} \omega$ the following expression

$$\operatorname{Im} \omega = - \frac{\sqrt{\pi}}{2^{3/2}} \frac{\omega_{pe}^2}{k^2} \frac{\omega_k}{1 + \alpha^2} \left[\frac{\omega_k}{k_z v_{1e}^3} e^{-\frac{\omega_k^2}{2k_z^2 v_{1e}^2}} + \right. \quad (30)$$

$$\left. + \eta \sqrt{\frac{\pi}{2}} A_o(\lambda_b) \frac{\omega_k - K v_o}{k_z v_{1b}^3 \gamma_o} e^{-\frac{(\omega_k - K v_o)^2}{2k_z^2 v_{1b}^2}} \right]$$

The fastest growing instability of the lower hybrid wave is then obtained when

$$\omega_k \approx K \cdot v_o \quad (31)$$

with the beam electron speed just a little faster than the phase velocity of the wave in the beam direction. This is necessary to assure $\operatorname{Im} \omega > 0$

The first factor in the bracket characterizes the damping of excited waves due to plasma electrons

4. Conclusions. The above results show that a warm relativistic electron beam can excite lower hybrid waves in warm magnetized plasma. These waves can be excited by Cherenkov resonance when $\omega_k \approx k \cdot \vec{v}_0$. We calculated the frequencies and growth rate for excited waves. The obtained growth rate expression contains also the damping effects due to the plasma electrons [first term in the bracket of expression (30)] on the excited waves. When the Cherenkov resonance condition is satisfied the damping term becomes small compared with the term which is responsible for the growth of the wave amplitudes [the second term in the bracket of expression (30)]. Thus it results an instability for the lower hybrid waves.

Another important conclusion can be also drawn for beam electron temperature effect. The expression which was derived for the growth rate shows that parallel beam temperature has an stabilizing effect on the instability.

REFERENCES

1. Porkolab M, Nucl Fusion 12, 329 (1972)
2. Allen G R et al., Phys Rev Lett 41, 1045 (1978)
3. Fisch N J, Rev Mod Phys. 59, 175 (1987)
4. Bell R E et al, Phys Rev: Lett 60, 1294 (1988)
5. Yamamoto T et al, Phys Rev. Lett 63, 1148 (1989)
6. Nemoto M et al, Phys Rev Lett 67, 70 (1991)
7. Fisch N J, Rax J M, Phys Rev Lett. 69, 612 (1992)
8. Maekawa T et al, Phys Rev Lett 70, 2561 (1993)
9. Chang T, Coppi B, Geophys Rev Lett 8, 1253 (1981)
10. Kintner P M et al, Phys Rev Lett. 68, 2448 (1992).
11. Huba J D, Papadopoulos K, Phys Fluids 21, 121 (1978)
12. Huba J D, Gladd N T, Papadopoulos K, J Geophys Res, 83, 5217 (1978)
13. Hasegawa A, Chen L, Phys Fluids 19, 1321 (1975)
14. Papadopoulos K, Palmadesso P, Phys Fluids 19, 605 (1976)
15. Karacsony J, Rev Roum Phys 29, 705 (1984)
16. Alexandrov A F, Bogdankevic L S, Ruhadze A a, Osnovy Elektrodinamiki Plasmy, Moskva, 1978
17. Karacsony J, Selinger V, Bull Math Soc Sci Math R S R, 24 363 (1980)
18. Bludman S A, Watson K M, Rosenbluth M N, Phys Fluids 3, 747 (1960)
19. Akhiezer A I, Stepanov K N, Akhiezer I A, Polovin R V, Sitenko A G, Elektrodinamika Plazmy, Nauka, Moskva, 1974

ANALYSIS OF THE PHYSICAL CHARACTERISTICS
OF A DUSTY PLASMA I. THE GRAIN CHARGES
AND THEIR EFFECTS

Speranța COLDEA*

Received 5 09 1993

ABSTRACT. - The charge of a dust in a plasma is not a fixed one, depending on the characteristics of the plasma, on other phenomena as secondary and field emission, photoemission, etc. By supposing the grains being at rest in a Maxwellian plasma, an analysis for the properties of grain charges in a dusty plasma is made. The corresponding effects are shortly discussed. In the second part of the paper other effects of the electrostatics of dusty plasmas will be analysed.

1. Introduction. A dusty plasma can be defined as a plasma with a phase of solid objects (grains or dusty particles), that usually exist in laboratory plasmas, planetary and cosmic plasmas. For the understanding of the ionosphere properties and of the consequences for earth atmospheric pollution, a modern knowledge of the dusty plasmas characteristics is needed. Generally, the method of study such plasmas characteristics is based on the theory of the composite plasma dynamics (kinetic model or fluid model). Experimentally, the Ionospheric Radar Scatter Technique is used, based on the analysis of the statistical properties of radar returns from ionosphere. Measurements of physical properties of dusty plasma in ionosphere or planetary ring (magnetosphere) are also made by satellites. The conclusion of the experiments is that the present of dust may change the structure and properties of the plasma. The present paper deals with the study of fundamental properties of a dusty plasma with impurities, that are electrically charged. A short analysis of the grain charging and of the

* "Babeș-Bolyai" University, Faculty of Physics, 3400 Cluj-Napoca, Romania

corresponding effects in a dusty plasma is given, based on the fundamental equations of such a plasma and on some quantitative considerations

2. The basic equations. Firstly we shall present the equations that describe the charging of dust grains in a plasma, process driven by plasma currents, photoelectron and secondary emission currents [1]-[7]. The basic equations for all these currents in the case of a number of grains in a plasma comparatively with those of a single grain in plasma or in vacuum will be presented

By considering that a grain is at rest in a Maxwellian plasma with electron and ion temperatures T_e and T_i ($T_e \sim T_i$) and by neglecting the other charging effects, the potential of the grain ϕ is obtained to be negative (if $\text{Flow}_i \ll \text{Flow}_e$). The currents to the surface of the grain are [1]-[3], [7]:

$$I_e = - \frac{4\pi a^2 n_e e}{(2\pi\beta_e m_e)^{1/2}} \cdot \exp(e\beta_e \phi) \quad (1)$$

$$I_i = \frac{4\pi a^2 n_i Z e}{(2\pi\beta_i m_i)^{1/2}} \cdot (1 - \beta_i Z e \phi) \quad (2)$$

where $\beta = 1/kT$ and a is the grain radius, m_e , m_i being the electron and ion mass and T_e , T_i the corresponding temperatures, ϕ is the grain surface potential

If $\phi > 0$ then $I_i = \exp(-eZ\beta_i \phi)$ and $I_e \sim (1 - e\beta_e \phi)$. The equilibrium potential is found from the condition.

$$I_i + I_e = 0 \quad (3)$$

and it is independent of plasma density

Because the charging time is nonzero and it is proportional to $1/a$ a specific

gyrophase drift motion of grain in plasma takes place

The secondary and photo-emissions determine a positive current to the grain Two cases could be discussed

(a) If $\phi < 0$, all the released electrons by secondary emission escape and the corresponding electron current is of the form

$$I_{sec} = 3.7 \delta_m \cdot n_e \left(\frac{kT_e}{2\pi m_e} \right)^{1/2} \cdot F_5 \left(\frac{E_m}{4kT_e} \right) \cdot e^{-\frac{e\phi}{kT_e}} \quad (4)$$

where

$$F_5 \left(\frac{E_m}{4kT_e} \right) = \frac{E_m^2}{16k^2 T_e^2} \cdot \int du \cdot u^5 \cdot \exp \left[- \left(\frac{E_m \cdot u^2}{4kT_e} + u \right) \right] \quad (5)$$

and δ_m is a material parameter of value $0.5 < \delta_m < 30$ and E_m is the value $E_m(\delta_m) \in (0.1 - 2) \text{ keV}$

(b) If $\phi > 0$, several electrons are reabsorbed in the secondary emission process and then we have

$$I_{sec} = 3.7 \delta_m n_e \left(\frac{kT_e}{2\pi m_e} \right)^{1/2} \cdot \left(1 + \frac{e\phi}{kT_e} \right) \cdot \exp \left[- \frac{e\phi}{k} \left(\frac{1}{T_s} - \frac{1}{T_e} \right) \right] \cdot F'_5(x) \quad (6)$$

where $x = \frac{B_m}{4kT_e}$, $T_s \sim 10^4 K$, $B = \left(\frac{e\theta}{E_m} \right)^{1/2}$ and

$$F'_5 = x^2 \int du \cdot u^5 \cdot e^{-xu^2 + u} \quad (7)$$

The photoelectrons flow is of the following form [9]

$$I_p = \pi a^2 \cdot K \quad \text{if } \phi < 0$$

$$I_p = \pi a^2 \cdot K \cdot \exp \left(- \frac{2\phi}{2T_f} \right) \quad \text{if } \phi > 0 \quad (8)$$

where T_i is the temperature of photoelectrons ($T_f \sim 1 \text{ eV}$) and $K = \eta \cdot x$ is the flow of photons (η being the photoefficiency of value $\in (0 \text{ } 1 - 1)$)

When a grain of $a = 1 \mu \text{ m}$ in a plasma of $T_f = 1 \text{ eV}$ is taken, and the plasma and secondary emission currents are considered, three steady states are possible (if $I_{\text{total}} = 0$), the middle one is unstable and the other two ones stable. From some considerations that we don't introduce here it could be seen that this behaviour leads to a coagulation of dust grains effect [6], that will be discussed elsewhere.

The case of a moving grain in plasma can be also assumed, the corresponding electron and ion currents being given by

$$I_e = - \frac{2\sqrt{2\pi} a^2 e n_e}{(\beta_e \cdot m_e)^{1/2}} \cdot \exp(e\beta_e \phi) \quad (9)$$

and

$$I_i = \pi a^2 n_i Z e \left[\left(1 + \frac{T_{ihl}}{2\mu^2} - \frac{2Ze\phi}{m_i \mu^2} \right) + \frac{\alpha}{\omega \sqrt{\pi}} \cdot \exp\left(-\frac{\omega^2}{T_{ihl}^2}\right) \right] \quad (10)$$

where $T_{ihl} = \left(\frac{2kT_i}{m_i} \right)$ is the ion thermal velocity and ω is the grain velocity. Because $\omega \ll T_{ihl}$, the grain may be considered at rest and I_e is the same as (1). From the equilibrium condition $I_e + I_i = 0$ the potential $\phi = \phi(\omega)$ could be obtained.

At this point a qualitative discussion must be made the capacitance of a grain in vacuum $C_g \sim a$, if the grain is introduced in a plasma, the potential around it is $\phi = Q \cdot \frac{\exp[-k(r-a)]}{r(1+ka)}$ where $k = \frac{1}{\lambda_D}$, r is the distance between grains [3]. The effect of this like a spherical capacitor grain surrounded by positive sheaths (outer conducting shells) is the following: when $r \sim \lambda_D$, the positive shell is pushed closer to grain surface and its capacitance increases. If grains are in a neutral plasma they become negatively charged and there are

excess ions in plasma, the condition $I_e \approx I_i$ at the grain surface is satisfied

3. The effects of grain charge in a dusty plasma. The relation for ion and electron densities $n_i(\vec{r})$ are given by the Boltzmann factor.

$$n_i(\vec{r}) = C_i \cdot \exp[-q_i \beta_i \phi(\vec{r})] \quad (11)$$

where C_i ($i = e, i$) is taken from the condition $\int n_i(\vec{r}) d^3r = N_i$, N_i being the total number of "i" species, ϕ - the potential around the grain and q_i is the charge

The Poisson equation that will be used in this case is

$$\begin{aligned} \nabla^2 \phi + 4\pi \rho_g(\vec{r}) &= -4\pi \sum_i n_i \cdot q_i = \\ &= -4\pi \sum_i \frac{N_i q_i \exp[-\beta_i q_i (\phi(\vec{r}) - \phi)]}{\int d^3r' \cdot \exp[-\beta_i q_i (\phi(\vec{r}') - \phi)]} \end{aligned} \quad (12)$$

with $\rho_g(\vec{r})$ being the charge density on the grain. After using the method of expansion of electric potential in $\beta_i q_i (\phi - \bar{\phi})$ ($\bar{\phi} \ll 1$), we obtain to the lower order the relation

$$\begin{aligned} \nabla^2 \phi - k^2 \phi + 4\pi q_e(\vec{r}) &= -4\pi \sum_i \bar{n}_i \cdot q_i \\ &- \frac{k^2}{V} \int d^3r' (\phi - \bar{\phi}) - k^2 \bar{\phi} \end{aligned} \quad (13)$$

where

$$k = 4\pi \sum_i \bar{n}_i q_i^2 \cdot \beta_i \quad (14)$$

and

$$\bar{n}_i = \frac{1}{V} \int d^3r \cdot n_i(\vec{r}) \quad (15)$$

with V - the volume of integration, $\bar{\phi}$ being the averaged value of ϕ over V

The final Poisson equation is gauge invariant

$$\nabla^2(\phi - \bar{\phi}) - k^2(\phi - \bar{\phi}) + 4\pi \rho_e(\vec{r}) = -4\pi \sum_i \bar{n}_i q_i \quad (16)$$

It can be observed that the currents on the grain are driven by the difference $(\phi - \bar{\phi})$. The solution of the last equation could be obtained under the following form if a neutral grains-plasma system ($Q (< 0) = Q_p (> 0)$), with N grains of same radius a and charge Q, is considered:

$$\phi - \bar{\phi} = \phi(\vec{r}) + \frac{4\pi}{k^2} \sum_i \bar{n}_i \cdot q_i \tag{17}$$

where $\phi(\vec{r})$ is the solution of the boundary condition

$$\nabla^2 \phi(\vec{r}) - k^2 \phi(\vec{r}) + 4\pi \rho_s(\vec{r}) = 0 \tag{18}$$

that could be written as an integral equation using the Green's theorem

$$\phi(\vec{r}) = \frac{1}{4\pi} \sum_j \int dr'_j \left[\frac{\exp(-k|\vec{r}-\vec{r}'_j|)}{|\vec{r}-\vec{r}'_j|} \cdot \frac{\vec{r}_j - \vec{r}'_j}{|\vec{r}-\vec{r}'_j|} \cdot \nabla' \phi(\vec{r}') - \phi(\vec{r}') \frac{\vec{r}_j - \vec{r}'_j}{|\vec{r}_j - \vec{r}'_j|} \cdot \nabla' \frac{\exp(-k|\vec{r}-\vec{r}'_j|)}{|\vec{r}-\vec{r}'_j|} \right] \tag{19}$$

The center of ith-grain is chosen as the origin of the system and only the ith term $\phi_i(\vec{r})$ of the above sum \sum_i is considered. The grain surface potential is $\phi(a)$ and the electric field $-\nabla\phi(\vec{r}')$ is the same over the grain surface. From Gauss' theorem it can be obtained

$$\frac{(\vec{r}_i - \vec{r}')}{|\vec{r}_i - \vec{r}'|} \cdot \nabla' \phi(\vec{r}') = \frac{Q_i}{a^2} \tag{20}$$

By integrating the equation (19) the following result is obtained

$$\phi(\vec{r}) = \frac{Q_i}{r} \exp(-kr) \frac{\exp(ka) - \exp(-ka)}{2ka} + \frac{\phi(a)}{2kr} \exp(-kr) [\exp(-ka)(1 + ka) - \exp(ka)(1 - ka)] \tag{21}$$

Further the other grains ($j \neq i$) are considered and the collective effects between grains may be taken into account and then the potential $\phi(r)$ is given after integration of eq (19), for any distribution function

ANALYSIS OF THE PHYSICAL CHARACTERISTICS I

$$\sum_{j=1}^3 f(\vec{r}_i, \vec{r}_j) = N \int d^3 r_j \cdot f(\vec{r}_i, \vec{r}_j) \quad (22)$$

If $f = 1$, this condition is of the form $4\pi R^3/3 = N$, that defines a distance $R \sim \frac{r}{2}$ In

this case the potential is

$$\phi(r) = \frac{Q}{r} \exp[-k(r-a)] \cdot \frac{1 + 2\pi N k^{-3} \exp(-kR) (1+kR) (\exp(2kr) - 1)}{1 + ka - 2\pi N k^{-3} \exp(-kR) \cdot [(1+ka) - (1-ka) \exp(2ka)]} \quad (23)$$

and then

$$\phi(r) - \bar{\phi} = \phi(r) - \frac{4\pi N Q}{k^2 \left(1 - \frac{4\pi a^3 N}{3}\right)} \quad (24)$$

For equilibrium the condition $I_e + I_i = 0$ is imposed, and in above equation the currents are given by the eq (1) - (2), with the $\bar{n}_e, \bar{n}_i, \phi(a) \rightarrow \bar{\phi}$ and $\bar{n}_e \neq \bar{n}_i, \bar{n}_i - \bar{n}_e = -\frac{Q}{e} \cdot \frac{N}{\left(1 - 4\pi a^3 \frac{N}{3}\right)}$

The ion charge is taken as unity and $\beta_e = \beta_i$. Then the equilibrium grain charge is deduced

from the equation

$$1 - e\beta[\phi(a) - \bar{\phi}] = \left(\frac{m_i}{m_e}\right)^{1/2} \frac{\bar{n}_e}{\bar{n}_i} \cdot \exp[e\beta(\phi(a) - \bar{\phi})] \quad (25)$$

A dimensionless parameter $A(N)$ that contains the dependence of ϕ on grain and plasma parameters is introduced, defined by

$$A(N) = \frac{4\pi N \frac{Q(N)}{(\phi(a) - \bar{\phi})}}{k^2 \left(1 - \frac{4\pi a^3 N}{3}\right)} \quad (26)$$

with the aim to write the equilibrium charge equation (23) as follows

$$\begin{aligned}
 & 1 - e\beta[\phi(a) - \bar{\phi}][1 - e\beta(\phi(a) - \bar{\phi})A(N)] = \\
 & = \left(\frac{m_i}{m_e}\right)^{1/2} [1 + e\beta(\phi(a) - \bar{\phi}) \cdot A(N)] \cdot \exp[e\beta(\phi(a) - \bar{\phi})]
 \end{aligned} \tag{27}$$

It can be seen that $A(N) \propto N$ If the ratio $\frac{Q(N)}{Q(0)}$ of grain charges (for a number of $\frac{N}{V}$ grains in plasma) and the charge of a single grain in the considered plasma are introduced, this ratio is

$$\frac{Q(N)}{Q(0)} = \frac{\phi(a) - \bar{\phi}}{[\phi(a) - \bar{\phi}]_{N=0}} \cdot \frac{C(N)}{C(0)} \tag{28}$$

where $\frac{\phi(a) - \bar{\phi}}{[\phi(a) - \bar{\phi}]_{N=0}} < 1$ but $\frac{C(N)}{C(0)} > 1$

As an example the F-ring of the Saturn, that contains a dusty plasma, may be considered The specific parameters are in this case $a = 1\mu\text{m}$, $R = 0,2\text{ cm}$, $T = 10\text{ }\mu\text{eV}$, $n = 100\text{ cm}^3$ (O^+ ions) and $\lambda_D = 166\text{ cm}$ The result for the value of capacitance ratio is

$$\frac{C(N)}{C(0)} = 10009 \text{ and } \frac{[\phi(a) - \bar{\phi}]}{[\phi(a) - \bar{\phi}]_{N=0}} = 2,7 \cdot 10^{-4}$$

From the presented analysis two conclusions could be deduced for the present state of the considered problem

a) The grain charge, under the given conditions, is not so large as we could expect if the plasma temperature $T = 10\text{ eV}$ is taken $Q(N) = 270243 \cdot 10^{-4} Q(0)$

b) The corresponding electromagnetic forces are smaller in the considered example, for the evaluated smaller grain charge

The same discussion could be made for dense dusty plasmas [9] and also for high

ANALYSIS OF THE PHYSICAL CHARACTERISTICS I

dust-grain density by using the same kind of analysis

The other effects on a charged grain in a dusty plasma, as drag on a moving grain, the motion of such a dust and coagulation of grain in plasma will be discussed in the second part of the paper

REFERENCES

- 1 Hill J R and Mendis D A , Moon and Plan., 21, 3, (1979)
- 2 Hill J R and Mendis D A , Can J Phys , 59, 897, (1980)
- 3 Whipple E C , Rep Progr Phys , 44, 1197, (1981)
- 4 Mendis D A , Houps H L F and Hill J R , J Geophys Res , 87, 3449, (1982)
- 5 Ikezi H , Phys Fluids, 29, 1764, (1986)
- 6 Northrop T G and Hill J R , J Geophys Res , 87, 661, 1982, 88, 1, 6102, 1989
- 7 de Angelis U , Physics of dusty plasmas, Spring College on Plasma Physics, ICTP, Trieste, Italy, (1991)
- 8 Goertz C K and Ip W H , a) Geophys Res Lett, 11, 349, 1984, b) Geophys Res Lett, 15, 84, 1988
- 9 Goertz C K , rev Geophys , 27, 271, (1990)



ANALYSYS OF THE PHYSICAL CHARACTERISTICS OF A DUSTY PLASMA II. THE COLLECTIVE EFFECTS FOR THE DRAG ON A MOVING DUST GRAIN

Speranța COLDEA*

Received: 5 09 1993

ABSTRACT. - The plasma collective effects are included to analyse the process of the plasma drag on a charged dust grain moving through a plasma, due to Coulomb collisions. The conclusion of the analytical discussion is that the forces among the ions modify the grain influence on the ions trajectories, which is the source of the collective effects and that the drag on a grain is independent of the presence or absence of plasma particles moving faster than the dust.

1. Introduction. The effects of a charged particle on the grains in a dusty plasma can be considered from two points of view

(a) the effects of electric and magnetic forces on the dynamics of the grains in the plasma, and

(b) the effects of the grain charge on the properties of a plasma waves propagation, instabilities and new modes

In the case (a) the electromagnetic force should be added to the gravitational or radiation pressure forces and the orbits of the grains in plasma could be altered

The equation of motion of a grain is of the form [1]-[2]

$$m \cdot \nabla \vec{v} = e Z_g \left(E + \frac{1}{c} \cdot (\vec{v} \times B) \right) + F_g - \pi \alpha^2 \cdot P \quad (1)$$

where F_g is the gravitational force and P is the radiation pressure. Such a theory is called gravito-electrodynamics [1]-[2]. The plasma physics is modified by the presence of some

* "Babeș-Bolyai" University, Faculty of Physics, 3400 Cluj-Napoca, Romania

charged dusty particles

Depending on the considered particular phenomenon that is discussed two kinds of theories could be used

(i) the dust-grain can be taken as another plasma component (heavy ions) and then the known results of many-component plasma theory could be applied

(ii) the grains could be considered as external fixed impurities, acting as local and strong perturbations for plasma particles

Grains moving through the plasma could be also considered

For a dusty plasma, without the case when the grain radius $a(\mu) \leq 1$ and when it contains very low frequency oscillation modes, the grain dynamics can be neglected with respect to the plasma ion electron dynamics. The following simple physical model for a dusty plasma can be taken into account a nonneutral plasma ($n_e \neq n_i$) in the presence of a distribution of fixed charged centers that determines a stationary potential distribution of the system, being the solution of the Poisson equation

$$\nabla^2 \phi = -4\pi \left[\sum_{\alpha} q_{\alpha} \int f_{\alpha 0}(\vec{r}, \vec{u}) d^3u + \rho_g(\vec{r}) \right] \quad (2)$$

where $f_{\alpha 0}(\vec{r}, \vec{u})$ $\alpha = i, e, h$ are the distribution functions of the plasma components in the presence of grains and the charge density of the grain ρ_g is given as

$$\rho_g(\vec{r}) = e \cdot \sum_{\beta} Z_{\beta}^{\beta} \delta(\vec{r} - R_{\beta}) \quad (3)$$

$\rho_g(\vec{r})$ is a given function and does not change the plasma response in the presence of a wave or of any other perturbation

This is the simplest model for a dusty plasma, but other more complex physical models are used, such as the spherical capacitor model, where the spherical symmetry

assumption is made and for which the nearest neighbor approximation is not needed. Other two models are those of impermeable grains and of permeable grains in a plasma, the last being artificial because it was considered that plasma permeates the grain and the system is overall neutral.

The collective effects could be included or not in the theory of dusty plasmas. In this second part of the paper [3] the collective effects in the plasma drag process on a charged grain are analysed. We take into account only the effects of electric forces due to ion Coulomb collisions on the grains in the plasma.

2. Collective effects on a dust grain in the case of drag process. A charged grain interacts with the other charged dusty plasma particles. The collective effects occur because there are forces among the plasma particles that are altered by the presence of a grain charge. The inclusion of collective effects requires the use of the Vlasov - Maxwell equations. Usually a linearization is needed, giving an inexact solution.

A more complex collective effect, the drag on a grain in a dusty plasma, when the grains move through the plasma, is analysed in the paper, the collective effects between the plasma ions exist due to their interaction and are considered here. The interaction of the grains among themselves is not considered. The charging currents could be calculated, the factor by which the grain charge and the electromagnetic force on such a particle are altered by the presence of the other grains in a dusty plasma may be also evaluated. The plasma is considered as a perturbed reservoir (with $n_e \neq n_i$, because some charges are given to the grains). The velocity distribution of such a plasma is a Maxwellian one and the plasma has

an average potential $\bar{\phi}$, the difference $\phi(a) - \bar{\phi}$, where $\phi(a)$ is the grain surface potential determines the ion and electron currents to a grain [1]-[2], all the other charging processes are neglected here. It is considered that $\beta_e = \beta_i$. An analysis could be made by considering a gauge-invariant Poisson equation

$$\nabla(\phi(a) - \bar{\phi}) - k^2(\phi(a) - \bar{\phi}) + 4\pi \cdot \rho_e(r) = -4\pi \sum_{\alpha} n_{\alpha} \cdot q_{\alpha} \quad (4)$$

The solution of this equation can be given for the different earlier considered models. The detailed theory of the motion of a charged grain in a plasma and of the collective effects on such a grain is not given here. The analysis for the electrostatics of a dusty plasma, with the study only of the drag on a dust grain moving in the plasma is made.

The drag force on a moving grain in a plasma is a phenomenon due to direct ions impact and to the grain-ion collisions and is defined as the product of the acceleration of grains (of velocity v_0) and of the grain mass m_g , e.g. $m_g \cdot \underline{a}(v_0)$ (we will adopt the Chandrasekhar approximation of finite m_g). The direct ion impact drag is given by an equation of the form [4], if the collective effects are neglected

$$F_{id} = -n_i \cdot \pi a^2 m_i \cdot \alpha^2 \left[\frac{\omega}{\sqrt{\pi} \cdot \alpha} \cdot (\exp - \omega^2) + \left(\frac{\omega}{\alpha} + \frac{1}{2} \right) \cdot J_{er} \left(\frac{\omega}{\alpha} \right) \right] \quad (5)$$

where $m_i \alpha^2 = 2kT_i$.

There are two cases that may be taken into consideration

(i) if $\omega \leq \alpha$ the grain is moving slowly and in this case.

$$F_{id} = -2\sqrt{\pi} n_i \cdot a^2 m_i \alpha \omega \quad (6)$$

and

(ii) if $\omega \geq \alpha$ the grain is moving faster and then

$$F_{id} = \pi n_i \cdot a^2 \cdot m_i \cdot \omega^2 \quad (7)$$

The assumption that the dusty grains do not interact is made. The collective effects among the ions could be or not considered, the force among the ions modifies the grain influence on the ion trajectory. It is necessary to linearize the ion distribution by assuming that $b/a \ll 1$, e.g. the force is slightly changed in the presence of a grain charge, that means to not consider the smallness of scattering angles. This is the same as expanding the product of grain and ion charges in Qe , this product being proportional to the grain-ion coupling.

The expressions for F_{id} in the case of no large scattering angles (for the limit of small product Qe) can be given under the following form

$$F_g = \frac{4\pi Q^2 e^2}{m_i} \cdot \ln \frac{\lambda_D}{a} \cdot \int d^3v \cdot \frac{f(v) \vec{v}}{v^3} \quad (8)$$

that is the expression given by eq (5) if $f(v)$ is taken as a Maxwellian distribution and for the case of large scattering angles is given by the relation [5]

$$F_g = \frac{2\pi Q^2 e^2}{m_i} \int d^3v \cdot \frac{f(v) \cdot \vec{v}}{v^3} \cdot \ln \frac{1 + \frac{m_i v^4}{Q^2 e^2} \lambda_D^2}{1 + \frac{m_i v^4}{Q^2 e^2} b^2} \quad (9)$$

where the impact parameters are $b_{max} = \lambda_D$ and $b_{min} = b$

With the aim to include all effects discussed above, the equations given for the drag force in the considered approximations are coupled and it is possible to give a more realistic result. The difference between the eqs (8) and (9) is a measure of the errors that appear due to linearization of the Vlasov-Maxwell equations, if the impact parameters satisfy the condition $a \leq b \leq \lambda_D$. This correction is used together with the drag force obtained with the inclusion of collective effects in the set of Vlasov-Maxwell equations (for $a \leq b \leq \infty$)

$$F_g = -\frac{Q^2}{2\pi^2} \int d^3k \frac{k'}{k^2} \frac{1 - K(k, \omega)}{k(k, \omega)} \quad (10)$$

where $K(k, \omega)$ is the plasma dispersion function [6] Only for the condition $b > \lambda_D$ (the scattering angles are small) a correction is not needed Then for $a \leq b \leq \lambda_D$ the collective effects are not so important and only the grain charge imposes the ion trajectory and not the other ions

A possibility to find the radial motion velocity of dust in a magnetospheric (planetary) plasma (the migration motion), that is due to the drag effect, appears as the result of the earlier made analysis The rotating plasma gives then to a grain a large circular orbit added to its angular momentum motion Inside of synchrotronous radius a dust grain overtakes the plasma and falls towards any considered planet Usually the ions are not influenced by the other neighbours (ions) are describe hyperbolic orbits. The forces among ions modify the grain influence on the ion trajectories, this fact being the source of the collective effects

The conclusion of this short analysis is that we can choose some particular data for a given plasma, as the density n_i of ions, the temperature T_i , the Landau wavelength λ_D , the charge Q of the grain and the grain velocity ω , then the force F_{id} could be evaluated for a specific case, this fact giving the possibility to see the correct comportament of the dusty grains in a planetary plasma Some numerical evaluations of the drag force in a particular case will be done elsewhere

R E F E R E N C E S

- 1 Mendis D A , Houpsis H L F , Hill J R , J Geophys Res , 87, 3449, (1982)
- 2 de Angelis U , Physica Scripta 45, 465 (1992)
- 3 Coldea S , Studia Univ Babeş-Bolyai, ser, Physica 38 nr 2, (1993)
- 4 Chandrasekhar S , Ap J , 97, 255 (1943)
- 5 Morfill G E , Goerts C K , Planet Space Sci, 28, 1087, (1980), Icarus, 55 111 (1983)
- 6 Krall N A and Trivelpiece A W , Principles of Plasma Physics McGraw-Hill ed , New York (1973)

VIBRATIONAL AND ROTATIONAL RELAXATION IN PYRROLE PURE LIQUID AND SOLUTIONS STUDIED BY RAMAN SPECTROSCOPY

T. ILIESCU, A. SIKE*

Received 5 06 93

ABSTRACT. - Rotational and vibrational relaxation of pure liquid pyrrole at temperatures 283, 293, 303, 313, 333 K and in CS₂ solution at 283 K have been studied by Raman bande shape analysis. The activation energy for molecular reorientation of pyrrole molecule was determined. The experimental vibrational correlation functions were compared with the Kubo-Rothschild and Oxtoby relations.

1. Introduction. Different spectroscopic techniques (IR, depolarised Rayleigh, Raman, NMR) are used for the study of molecular dynamics in condensed phases [1,2]

Rotational relaxation was studied first for the molecules in which vibrational relaxation appeared as an additional and often very weak phenomenon.

Therefore in order to test the different theories of vibrational relaxation, heavy molecules in which vibrational relaxation has an important contribution, should be preferred.

Recently Navarro and al [3] were obtained the IR relaxations from the molecules of biological interest.

Among the different spectroscopic techniques, Raman Spectroscopy has the advantage to separate the contributions of rotational and vibrational relaxation, in the line hope.

From the experimental spectra I_{VV} and I_{VH} (the indexes refer to the polarisations of incident and scattering light, respectively) we can obtain the isotropic line profil (I_{iso}) which

* "Babeș-Bolyai" University, Faculty of Physics, 3400 Cluj-Napoca, Romania

offers information only on the vibrational relaxation and anisotropic one (I_{aniso}) from which we obtain information about rotational relaxation [4]

$$I_{\text{iso}}(\omega) = I_{\text{VV}}(\omega) - \frac{1}{3} I_{\text{VH}}(\omega) \quad (1)$$

$$I_{\text{aniso}}(\omega) = I_{\text{VH}}(\omega) \quad (2)$$

By eliminating the contribution of the slit width of the spectrometer and by assuming a lorentzian shape line, we can obtain the real vibrational widths of the line (full widths at half maximum, fwhm)

$$\Gamma_{\text{iso}} = \Gamma_{\text{V}} \quad (3)$$

$$\Gamma_{\text{aniso}} = \Gamma_{\text{iso}} + \Gamma_{\text{2R}} \quad (4)$$

(Γ_{2R}) being the line width of the rotational contribution

Vibrational (τ_{V}) and rotational (τ_{2R}) correlation times are obtained by using

$$\tau_{\text{V,2R}} = 1/h\pi\Gamma_{\text{V,2R}} \quad (5)$$

The vibrational ($G_{\text{V}}(t)$) and rotational ($G_{\text{2R}}(t)$) correlation functions, offer another possibility to estimate the different relaxation mechanisms

$$G_{\text{V}}(t) = \int I_{\text{iso}}(\omega) \exp(i\omega t) d\omega \quad (6)$$

$$G_{\text{2R}}(t) = \int I_{\text{aniso}}(\omega) \exp(i\omega t) d\omega / G_{\text{V}}(t) \quad (7)$$

The main purpose of the present work is the Raman study of vibrational and rotational relaxations for ring breathing vibration (1144 cm^{-1} , A_1 , $\rho \approx 0.05$) of liquid pyrrole and carbon disulfide solutions and to compare the experimental correlation function with theoretical Kubo-Rothschild and Oxtoby equations

2. Experimental. Raman spectrum was excited with 488 nm line (0.3-0.4 w) of a Ar

VIBRATIONAL AND ROTATIONAL RELAXATION

laser type ILA 120-1 the radiation being passed beforehand through a Glann-Thomson prism. The scattered light collected at 90° was analysed with a double monochromator GDM 1000 and I_{VV} and I_{VH} components were obtained by a 90° rotation of the polaroid situated in the gathering optics.

One of the Raman spectra in liquid pyrrole is shown in figure 1

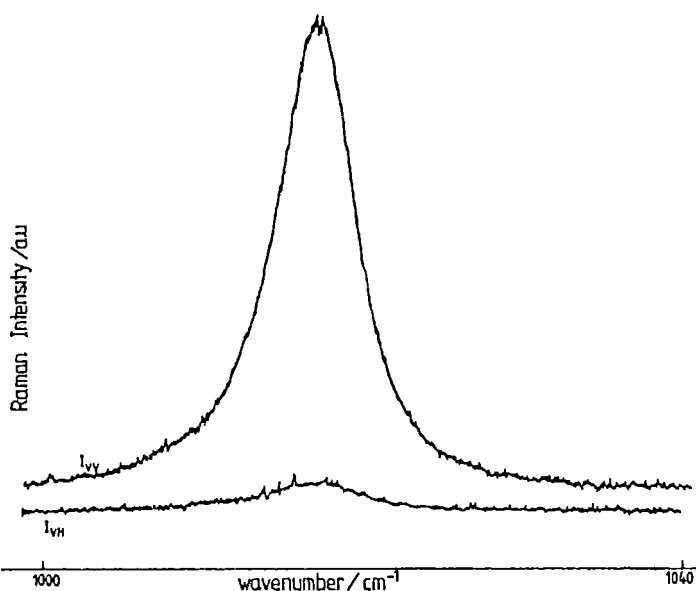


Figure 1 I_{VV} and I_{VH} Raman spectra for $\nu_{nu8}(A_1)$ mode of liquid pyrrole at 283K, slit width of 0.6 cm^{-1} . The intensity are expressed in arbitrary units.

The monochromator slit width was set at $0.6-0.8 \text{ cm}^{-1}$ (fwhm) for both scattering components. The ratio between the slit width and apparent band width of I_{VV} component was 0.1, so that the finite slit width effect on the determined Γ_{ν_8} and $\Gamma_{\nu_{nu8}}$ values could be neglected. In order to avoid a weak asymmetry of the band, I_{VV} and I_{VH} spectra were measured at every 0.4 cm^{-1} on the high wave number side of the band. A distance of 5.5 half-

widths from the peak center was used in order to insure a flat base line

Fourier transforms of I_{iso} and I_{anis} spectra were deconvoluted with the triangle slit function (obtained with Ar⁺ plasma laser lines). The experimental vibrational second moment Λ_2^v was obtained by using the formula [5]

$$\Lambda_2^v = \int I_{iso}(\omega) (\omega - \omega_0)^2 d\omega - \int S(\omega) (\omega - \omega_0)^2 d\omega \quad (8)$$

where $I_{iso}(\omega)$ and $S(\omega)$ are the normalised isotropic Raman spectra and experimental triangle slit function respectively

The pyrrole was purified by distillation and used immediately. Solvent of "Merk" uvasol type was used without purification. Only CS₂ was utilised because in other solvents (like CCl₄, C₂H₅OH, CH₃CN) the modification of the colour solution during the illumination with the laser light was noticed.

During the measurements the temperature was constant within ± 0.5 K.

3. Results and discussion. The Raman band parameters obtained for ν_{ring} mode of pure liquid pyrrole using the relations (1-5) and neglecting the influence of slit width, are summarized for different temperatures in table 1.

In the limit of the experimental errors ± 0.5 cm⁻¹ there is a coincidence of both scattering components.

The τ_v values calculated from the slope of $\ln G_v(t)$ are very close to values obtained from Γ_v without slit correction. The computation of τ_{2R} from the slope of $\ln G_{2R}(t)$ is very difficult because $G_{2R}(t)$ oscillate after 1.5 ps.

Fig. 2 presents vibrational and rotational correlation functions on logarithmic scale at

VIBRATIONAL AND ROTATIONAL RELAXATION

303 K for pure liquid pyrrole

From τ_{2R} values (see table 1) is evident that the reorientational contribution to the band shape increases with temperature, as expected. On the other hand, in the limit of experimental errors the vibrational correlation times τ_V are temperature independent.

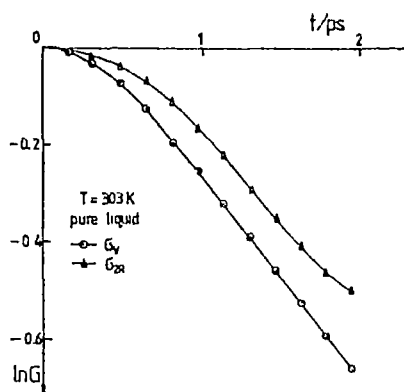


Fig 2 Vibrational, reorientational correlation functions of $\nu_{nmg}(A_1)$ mode for pure liquid pyrrole for $T = 283$ K

Table 1 Raman line parameters for ν_{nmg} mode pure liquid pyrrole at several temperatures (line width (fwhm) correlation time τ)

T/K	Scattering component	Γ/cm^{-1}	τ_V ps	τ_{2R}/ps
283	I_{150}	57	18	8.1
	I_{4150}	70		
	I_{150}	56		
293	I_{4150}	74	19	5.9
	I_{150}	57		
303	I_{4150}	77	18	5.3
	I_{150}	56		
313	I_{4150}	80	19	4.4
	I_{150}	57		
333	I_{150}	57	18	3.9
	I_{4150}	84		

Assuming an Arrhenius type relationship for temperature dependence of the rotational correlation time [6]

$$\tau_{2R} = A \exp(E_a/RT) \quad A = \text{const} \quad (6)$$

The activation energy E_a for the reorientation of pyrrole molecule is estimated to be

9.5 KJ/mol (fig 3)

We will use the τ_{2R} values in order to conclude about the relative importance of different relaxation mechanisms. For all the temperatures studied, the vibrational relaxation is the most important mechanism in forming the band shape.

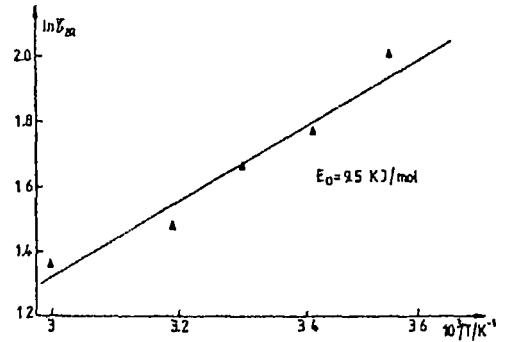


Fig 3 The logarithm of the reorientational correlation times (τ_{2R}) for $\nu_{ring}(A_1)$ mode vs $1/T$

In order to understand the evolution of relaxation times and the interactions between pyrrole molecules and solvents, the experimental vibrational (G_V) and rotational (G_{2R}) correlation functions were determined for different concentrations of pyrrole in the carbon disulfide solutions. Fig 4 presents the rotational and vibrational correlations functions for pyrrole in CS_2 at concentrations (molar fractions m.f) 0.72, 0.46, 0.22.

In solution at short times G_V decays faster than G_{2R} , and therefore the vibrational relaxation is the main mechanism, responsible for the band shape broadening. A parabolic character of the vibrational correlations functions (Fig 2 and 4) is noticed at short times and the function becomes

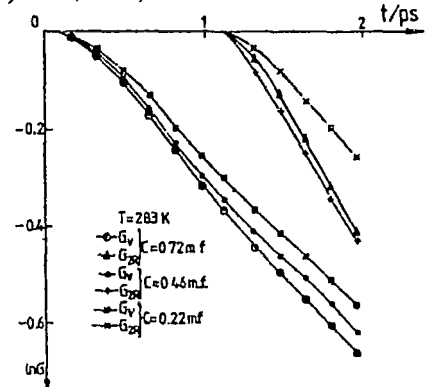


Fig 4 Vibrational and reorientational correlation functions of ν_{ring} mode of pyrrole CS_2 solution

almost linear in logarithmic scale at long time. This character corresponds respectively to Lorentzian function in the central section of the line and to a Gaussian in the wings. In this situation, we can apply the relation (4) even if the profile is not a pure Lorentzian shape.

VIBRATIONAL AND ROTATIONAL RELAXATION

The application of the vibrational dephasing theory developed by Kubo and Rothschild [7] supplies some additional informations concerning the vibrational relaxation processes of the ν_{ring} mode in pyrrole. According to this theory the vibrational correlations functions is expressed by

$$G_v(t) = \exp\left[-\langle \omega^2(0) \rangle \left\{ \tau_c^2 [\exp(-t/\tau_c) - 1] + \tau_c t \right\}\right] \quad (10)$$

This vibrational correlation function is essentially determined by a measurement of vibrational second moment M_2^V (in cm^{-2}), which gives the mean-square frequency displacement of the instantaneous vibrational frequency $\omega_0 + \omega(t)$

$$\langle \omega^2(0) \rangle = 4\pi^2 c^2 M_2^V \quad [\rho_s^{-2}] \quad (11)$$

and the modulation time τ_c , which characterizes the correlation decay of the stochastic perturbation of $\omega(t)$

$$\langle \omega(t) \omega(0) \rangle / \langle \omega^2(0) \rangle = \exp(-t/\tau_c) \quad (12)$$

Two typical situations are distinguished, depending on whether,

$$\langle \omega^2(0) \rangle^{1/2} \tau_c < 1 \text{ or } > 1 \quad (13)$$

the processes which modulate $\omega(t)$ are either "fast" or "slow"

Equation (10) describes the vibrational dephasing process and the two limiting cases can be examined. For extremely low modulation ($\tau_c \rightarrow \infty$) or for short times ($t \ll \tau_c$) eq (10) leads to a gaussian vibrational function

$$G_v(t) = \exp[-\langle \omega^2(0) \rangle t^2/2] \quad (14)$$

The half width corresponding to a gaussian spectrum being

$$\Gamma_v^G = (2 \ln 2)^{1/2} \langle \omega^2(0) \rangle^{1/2} / \pi c \quad (15)$$

For a very fast modulation ($\tau_c \rightarrow 0$) or for long times ($t \gg \tau_c$) eq (10) becomes a simple

exponential relaxation function

$$G_{\nu}(t) = \exp[-\langle \omega^2(0) \rangle \tau_c t] \tag{16}$$

The half width for a lorentzian spectrum being

$$\Gamma_{\nu}^L = \langle \omega^2(0) \rangle \tau_c / \pi \tag{17}$$

Another expression for relation (12) has been proposed by Oxtoby [8]

$$\langle \omega(t)\omega(0) \rangle / \langle \omega^2(0) \rangle = \text{sech}^2(t/\tau_c) \tag{18}$$

which gives the correlation function

$$G_{\nu}(t) = \exp[-\langle \omega^2(0) \rangle \tau_c^2 \ln \cosh(t/\tau_c)] \tag{19}$$

Theoretical equations (10) and (19) were applied to our experimental correlations functions. The experimental second moments M_2^{ν} , obtained from isotropic Raman spectra (eq 8) were used to calculate $\langle \omega^2(0) \rangle$ (eq 11)

The theoretical vibrational correlations functions were computed according to eq (10,19) by inserting experimental $\langle \omega^2(0) \rangle$ and adjusting τ_c for the best agreement between the theoretical and experimental correlation functions

Table 2 present the application of Kubo-Rothschild's and Oxtoby's equations to ν_{ring} mode of pyrrole pure liquid at different temperatures and for solutions at 283K

Table 2 Application of Kubo-Rothschild's and Oxtoby's equations to ν_{ring} mode pyrrole pure liquid and solutions

System	T (K)	Oxtoby					Kubo-Rothschild				Γ_{ν} (cm ⁻¹) exp
		$\langle \omega^2(0) \rangle$ (ps ⁻²) exp	τ_c (ps) O λ	$\langle \omega^2(0) \rangle^{1/2}$ * τ_c (cm ⁻¹) O λ	$\Gamma_{\nu}^O = \Gamma_{\nu}^O$ (cm ⁻¹) O λ	Γ_{ν}^O (cm ⁻¹) O λ	τ_c ps KR	$\langle \omega^2(0) \rangle^{1/2}$ * τ_c (cm ⁻¹) KR	Γ_{ν}^O (cm ⁻¹) KR		
pure pyrrole	285	1.14	0.41	0.43	13.3	4.9	0.44	0.46	5.3	5.6	
	293	0.97	0.48	0.47	12.3	4.9	0.52	0.51	5.3	5.9	
	303	0.65	0.71	0.57	10.0	4.8	0.80	0.64	5.5	5.7	
	313	0.90	0.70	0.66	11.8	6.6	0.84	0.79	8.02	5.6	

VIBRATIONAL AND ROTATIONAL RELAXATION

Solution m.f.										
0.72	283	0.94	0.46	0.44	12.1	4.5	0.50	0.48	4.9	5.0
0.46	283	0.92	0.41	0.39	11.9	4.0	0.43	0.41	4.2	4.8
0.22	283	0.72	0.52	0.44	8.9	3.7	0.56	0.47	4.2	4.4

With experimental vibrational second moment $\langle \omega^2(0) \rangle_{exp}$, Γ_V^G (eq 15) and Γ_V^L (eq 17) were calculated. These values were compared with the experimental $\Gamma_V^{exp} = \Gamma_{iso}$.

Inspection of table 2 shows that Γ_V^L values are very close to Γ_V^{exp} which implies an important contribution of lorentzian part in the band shape.

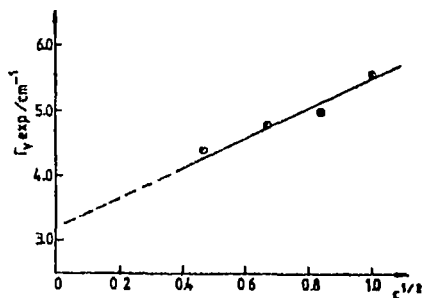
The τ_c values for pure liquid pyrrole are 0.4-0.8 ps and increase as the temperature is raised. Thus the correlation decay of stochastic perturbation is slow at high temperatures. At high temperatures a polymerization of pyrrole molecules take probably place. In general, for solution, τ_c values decrease with dilution due to the decrease of the velocity of fluctuation.

The vibrational second moment $\langle \omega^2(0) \rangle$ decrease with increasing dilution. It is known that an increase in the $\langle \omega^2(0) \rangle$ appears in the systems where the oscillators interact strongly with the neighboring molecules. This means that in our case the interaction between pyrrole molecule and surrounding molecules is larger in concentrated solution than in diluted one, as expected, CS_2 molecule being nonpolar molecule.

In condensed phase at low concentration the main mechanism of vibrational relaxation is the phase relaxation (vibrational dephasing) [9]. In addition to the above mentioned mechanism, in concentrated solution, two other mechanisms may contribute to the broadening of the isotropic Raman spectra: resonance energy exchange [10] and concentration fluctuation [11].

These theories predict a concentration dependence of the line widths of the $\nu_1 - \nu_2$

type From table 2 we noticed a decrease of $\Gamma_v(\text{exp})$ values with dilution Fig 5 present, this linear dependence By extrapolating $C^{1/2} \rightarrow 0$, the line width due to pure dephasing for CS_2 solution to be 3.2 cm^{-1} .



From relation (13) and inspection of table 2 we observe that Kubo product $\langle \omega^2(0) \rangle^{1/2} \tau_c$ is approximately similar for both equation (10,19) and its value for different temperatures in pure liquid pyrrole 0.43 - 0.7 indicate an intermediate modulation regime for vibrational dephasing τ_{vng} mode of pyrrole. The fact that the Kubo product values are ~ 0.4 in dilution is an indication that there is a faster modulation regime than in pure liquid.

In fig 6 the experimental vibrational correlation function is compared with the theoretical Kubo-Rothschild's and Oxtoby's correlation functions for pure liquid pyrrole and diluted in CS_2 .

Particularly for short times, the Oxtoby equation fits better than Kubo-Rothschild equation the experimental data.

Particularly for short times, the Oxtoby equation fits better than Kubo-Rothschild equation the experimental data.

4. Conclusions. The results obtained indicate that for the entire time scale studied, the vibrational relaxation is the most important mechanism for ν_{vng} vibrational mode of pure pyrrole and in CS_2 solution. From Arrhenius type dependence of τ_{2R} vs $1/T$, an activation energy of 9.5 KJ/mol for pyrrole molecule was determined.

VIBRATIONAL AND ROTATIONAL RELAXATION

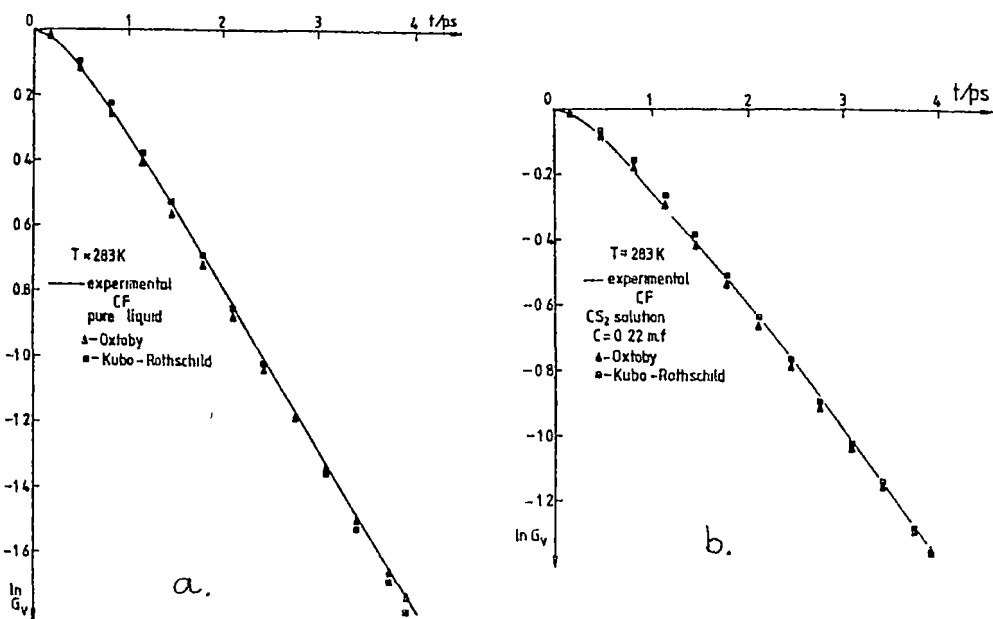


Fig 6 Experimental vibrational correlation functions fitted with Kubo and Oxtoby equations

a-pure liquid

b-carbon disulfide solutions

To simplify the figure only one temperature for pure and CS₂ solution are presented To simplify the figure only one temperature for pure and CS₂ solution are presented

A pure dephasing line width of 3.2 cm⁻¹ was obtained from the linear dependence $\Gamma_V(\text{exp})$ vs $C^{1/2}$

A better fit with the experimental data is obtained using the Oxtoby equation instead of Kubo-Rothschild equation. The Kubo product corresponds to an intermediate modulation regime. In diluted solutions this regime is faster than in pure liquid pyrrole.

To simplify the figure only one temperature for pure and CS₂ solution are presented

R E F E R E N C E S

- 1 W G Rothschild, "Dynamics of Molecular Liquids", John Wiley New York 1984
- 2 S Bratos, R M Pick (Eds) "Vibrational Spectroscopy of Molecular Liquids, Plenum Press, New York, 1980
- 3 R Navarro, I Bratu, A Hernanz, J Phys Chem 97 9081(1993)
- 4 F J Bartoli, T A Litovitz, J Chem Phys 56 404(1972)
- 5 T Kato, T Takemaka, Chem Phys Lett 62(1978)
- 6 T Kato, T Takemaka J Chem Phys 84 3405(1986)
- 7 W G Rothschild, J Chem Phys 65 455(1976)
- 8 D W Oxtoby, J Chem Phys 74 1503(1981)
- 9 I Bratu, K Klosterman, T Iliescu, S Astilean, J Molec Liquids 45 57(1990)
- 10 M Kakimoto, T Fujiyama, Bull Chem Soc Japan 47 1983(1974)
- 11 A F Bondarev, Opt i spectr 35 350(1977)

TOTAL CROSS SECTION DETERMINATION BY FAST NEUTRONS SPECTROMETRY ON AN ISOTOPICALLY ENRICHED ^{15}N TARGET USING AN ^{241}Am - ^9Be NEUTRON SOURCE

L. DĂRĂBAN*, T. FIAT*, E. VARI-NAGY*

Received 10.07 1993

ABSTRACT. - We have build a method, for measuring the excitation function, based on the analysis of the transmitted spectrum of the fast neutrons generated by ^{241}Am - ^9Be isotopic source and using a spectrometer with recoil protons and pulse - shape discrimination. We have demonstrated that, in case of ^{15}N nucleus as target, acceptable values of the total cross sections can be obtained by means of this method.

1 Introduction. In the field of nuclear reactions induced by fast neutrons, a lot of interest is concentrated on the problems which refer to the mechanism of the fast neutrons interaction with the nucleus, and on the information that can be inferred about the nuclear structure from these interactions.

Analysing the experimental data from a statistic point of view, we may observe that the nucleus of the stable isotopes with little natural abundance are of a special interest. These nucleus been less research subject, but, because of the more unstable nuclear structure, they have a spectacular behaviour during the nuclear processes.

2. Experimental. The experimental methodology for measuring total cross sections is presented. Lately, there have been used "white" neutron sources, based on cyclotrons, linear accelerators or tandem generators, to measure excitation functions $\sigma_1(E)$. We used for the first time the ^{241}Am - ^9Be source spectrum. It should be mentioned that these kind of measurements can be realised only with a fast neutrons spectrometer and the use of the Am-Be source needs a good n- γ discrimination.

The probability of interaction between the fast neutrons and the nucleus is

* "Babeș-Bolyai" University, Faculty of Physics, 3400 Cluj-Napoca, Romania

characterized by the cross section σ_T and is defined in the following way [1]

$$\sigma_T = \frac{dN}{Nnd}$$

where dN is the number of interactions between the neutrons and the target nucleus, N is the neutrons number that fall on 1 cm^2 of target area, n is the nucleus concentration per target volume unit of pure element and d is the target thickness. In the case of a molecular target the relation (1) became much complex like in relation (16)

When using a thick target, the density of the flux changes with thickness "x". In order to find out the number of the neutrons penetrating the target, one should give the differential equation of the layer fulfilling the following requirement for a given thin layer having a thickness dx at a depth X in the sample the following equation is valid

$$dN = -N(x)n \sigma_T dx$$

The solution of the equation (2) has this form

$$N(x) = N_0 \exp(-n \sigma_T x)$$

where N_0 is the initial neutron flux. This means that, for finding out the cross section of the neutrons interaction with the nucleus is sufficient to measure in one experiment the decrease of the neutrons flux $N(d)/N_0$, during the penetration of the target

$$\sigma_T = \frac{\ln \frac{N_0}{N(d)}}{nd}$$

This formula can be turned into another one containing more accessible experimental parameters. In this way

$$n = \frac{N'}{V}, \quad V = Sd \quad \wedge \quad N' = \frac{m}{A} N_A c$$

It results the next formula

$$\sigma_T = \frac{A \ln \frac{N_0}{N(d)}}{N_A c \frac{m}{S}}$$

where $N(d)$ is the number of the neutrons which are left after the penetration of the target, A is the atomic mass of the target isotope, N_A is the Avogadro's number, c is the isotopical concentration, m is the mass of the pure element and S is the transversal section of the target. The relation $N/N_0 = T$ is called transmission factor.

TOTAL CROSS SECTION DETERMINATION

If we have the possibility to verify the energy of the neutrons with a neutron spectrometer, then we can measure the total cross sections corresponding to already known values of the neutrons energy

Measurements are done through the transmission method, by means of the so-called "good geometry arrangement" We place the sample in the way of a collimated bundle of monoenergetic neutrons We measure N_0 and N in order to be able to calculate T [2]

If we want to extract an excitation function having the following form $\sigma_1=f(E_n)$, then we register the spectrum of neutrons, measuring both with and without sample, on the whole energy field, and we calculate, by means of the formula (6), σ_T for every value of the energy of the spectrum

Our purpose was to determine the excitation function for ^{15}N For that purpose we used a sample of $^{15}\text{NH}_4^{15}\text{NO}_3$ (double marked), enriched by isotopes up to the concentration of 98,5% in ^{15}N

In order to measure the cross sections, we use an $^{241}\text{Am}-^9\text{Be}$ source of neutrons of 1Ci, generating 10^6n/s , enclosed in a collimator of borate paraffine, a fast neutron spectrometer with stilbene crystals and a pulse-shape discrimination circuit (fig 1), studied in [3-8]

To extract the laterally scattered neutrons, we used a beam stopper The common method is to put a long metal bar (of Fe, Cu, or Pb) in the place of the sample, through which the neutrons cannot enter Then, the transmission factor corrected by the background is

$$T = \frac{N - N_b}{N_0 - N_b}$$

where N_b is the laterally scattered neutrons intensity, which arrives in the detector

We have performed preliminary studies on the ^{12}C nucleus using the spectrum of the Am-Be source, for improving the measurement method of the total cross section at fast neutrons and we obtained the excitation function of ^{12}C nucleus This shows broader and thicker resonances The purpose of these measurements was to see if we could collect nuclear data in a 10^6 n/s total pencil (the Am-Be source gives 10^6 n/s in 4π) Another purpose was to estimate the neutrons spectrometer resolution depending on resonances separation

We collimated the neutrons source with a borated paraffine collimator and we placed

a neutron detector to 0,5 m distance of the collimator. A graphite sample with $m/s=3,78 \text{ g/cm}^2$ was placed in the middle, between the detector and the collimator. We registered the incident neutron spectra $N_0(E_n)$ and the transmitted spectra $N(E_n)$ in 2 hours each other, to have a good statistic. We made the calibration of the multichannel analyser's channels in protons energies and operated the neutron spectrometer with stilbene in the same conditions, but with the gate in anticoincidence, this means opposite to the neutron signal of the pulse-shape discrimination circuit (fig 1). Using the method of calibration in electronic energies with

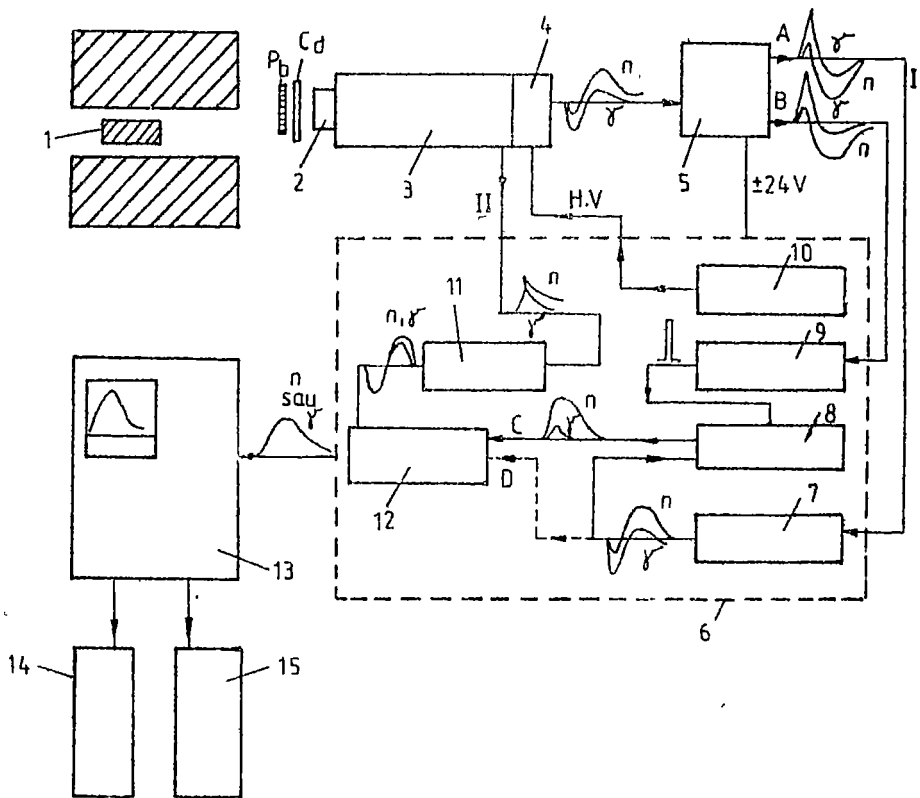


Fig 1 The scheme of neutron spectrometer with n- γ discrimination I-The PSD input, II Spectrometric input, A,B identical output, C -double discrimination, D - simple discrimination

1 The Am-Be source in borated parafine collimator, 2 Stilbene scintillation crystal 20x30 mm, 3 Fotomultipliator $\psi \gamma$ 19, 4 The PSD circuit, 5 The charge preamplifier type 1141 FAN, 6 Power source with cadre for NIM modules type ST 614, 7 Mixer reversor type NE 4618, 8 Linear gate (I) type 1183 FAN, 9 Energy analyser type NE 4664, 10 High voltage power supply type 1135, 11 Spectrometric amplifier type NE 4698, 12 Linear gate (II) type 1183 FAN, 13 Multichannel analyser ICA-70, 14 Printer, 15 Potentiometric recorder

TOTAL CROSS SECTION DETERMINATION

γ sources, these have been turned in proton energies with a luminosity function having the next form $L(E_p)=C_1 E_p^{C_2}$

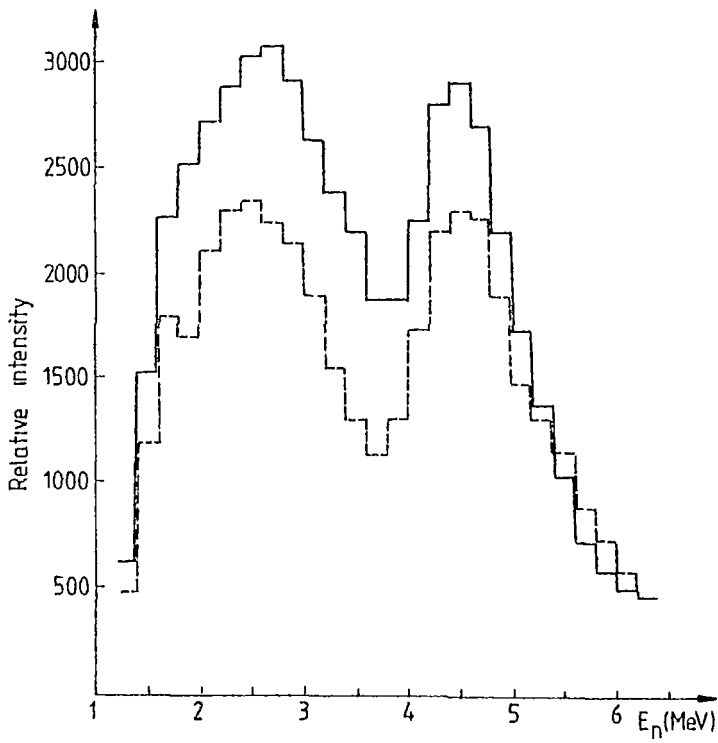


Fig 2 The transmission neutrons of the ^{241}Am - ^9Be source neutrons through carbon

The data were transferred in one computer CORAL 4021 that was working in tandem with a multichannel analyser ICA-70. Using a program named SPEC-N, we obtained the incident neutron spectrum $N_0(E_n)$, and in a carbon sample transmitted neutrons spectrum $N(E_n)$ (fig 2)

Using the relation (6), we calculated point by point, the values of the function $\sigma_1(E)$ and in order to find the transmission factor T, we divided the two spectras. Fig 3 shows the results, in comparison with the results obtained in [9]. In conclusion, we have

a. After the calibration of the Am-Be source spectrum with gamma sources, (without control by the monoenergetics neutrons), there are appearing deviation from the real energy of the neutrons until 0,5MeV. This is illustrated by the position of the carbon's resonances

b. The absolute values of the cross section are not in accordance with the data given in literature [9], these have the tendency to be systematically less in the two neutron peaks region and systematically greater where we have less neutrons

The "good geometry" condition require that the value of the transmission factor to be cc 0,5 for each energetics group. So, in order to determine the excitation function, we can't use the continuous spectrum the way it's shaped in fig 3, so only by measuring the transmission factor in the energy region

Also, introducing a set of changed values set (I_1, E_1) in the SPEC-N program, we

TOTAL CROSS SECTION DETERMINATION

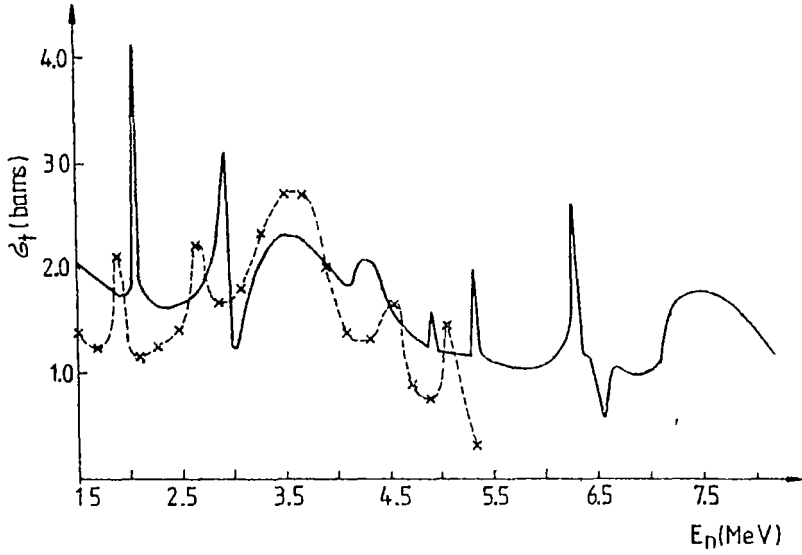
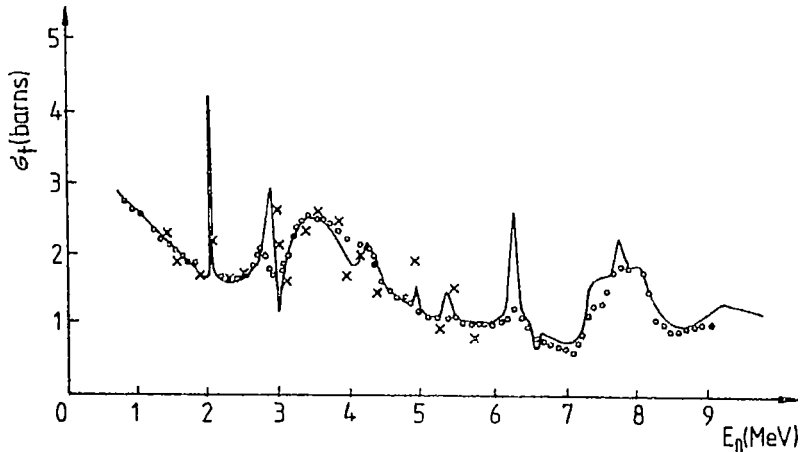


Fig 3 The continuous line - the results indicated by [10] The broken line - the measurements effectued on the Am-Be source

adjusted the luminosity function $L(E_p)$ depending on the shift established comparatively with the carbon's resonances. In that way, we used the carbon resonances for the recalibration of the neutron spectrometer, we obtained for a stilbene crystal with 3 cm diameter and 2 cm thickness

$$L(E_p) = 0,184 E_p^{1,4044}$$

With this measurement technique, perfected on the ^{13}C nucleus, we obtained the total



correct values of the excitation function (using an Am-Be source) (fig 4)

By using fig 4, we can study the resolution of our neutron spectrometer with the stilbene crystal. By the way this spectrometer solves the carbon resonances at 2,08 MeV or 2,45 MeV, you can see that the equipment (built and perfected in our laboratory) has a resolution of 0,2 MeV, we can estimate the equipment measurement error, by using the results from the fig 4, too 10%

3 Total cross section determination of ^{15}N In order to calculate the total cross section of ^{15}N , we measured the initial neutronic spectrum of the $^{241}\text{Am-}^9\text{Be}$ source and the spectrum transmitted through the sample double marked with ^{15}N (enriched at 98,5% in ^{15}N)

TOTAL CROSS SECTION DETERMINATION

In order to verify the contribution of the oxygen and hydrogen of the NH_4NO_3 sample, we also registered the spectrum transmitted through the natural sample, having the same mass and containing ^{14}N , as well as the spectrum of the laterally scattered neutrons (fig 5)

It is true that the curves of fig 5 are close, but, as a result of our experience with the program SPEC-N, we found that the difference was still there, because the sample marked with ^{15}N absorbs more intensive the neutrons than the natural sample

Knowing these curves, the excitation function of ^{14}N , as well as the major isotopical concentration $C_{^{15}\text{N}}$, $C_{^{14}\text{N}}$ and respectively, the minor isotopical concentration $C_{^{15}\text{N}}$, $C_{^{14}\text{N}}$ of the ^{15}N and ^{14}N from the sample, we are able to calculate the microscopic cross section of ^{15}N for the maximal values of the spectrum in fig 5, where we had a better statistics

The macroscopic cross section of the chemical compound NH_4NO_3 , can be defined in accord with [3], in the following way

$$\Sigma_i(E_n) = n_{^{15}\text{N}} \sigma_{^{15}\text{N}}(E_n) + n_H \sigma_H(E_n) + n_O \sigma_O(E_n) + n_{^{14}\text{N}} \sigma_{^{14}\text{N}}(E_n)$$

where n_i is the concentration of the i nucleus in 1 cm^3 , n_i' is the concentration of the minor isotope, and $\sigma_i(E_n)$ is the cross section according to the value E_n of the neutrons

From the relations (3) and (9), we can obtain the next relation

$$\Sigma_i(E_n) = \frac{1}{d} \ln \frac{N_0(E_n)}{N(E_n)}$$

We can extract the neutron background, which is exactly the spectrum measured with the beam stopper, using the relation (7)

$$\Sigma_i(E_n) = \frac{1}{d} \ln \frac{N_0(E_n) - N_0(E_n)}{N(E_n) - N_0(E_n)}$$

If we couple the relations (9) and (11), then we will obtain a relation for the microscopic

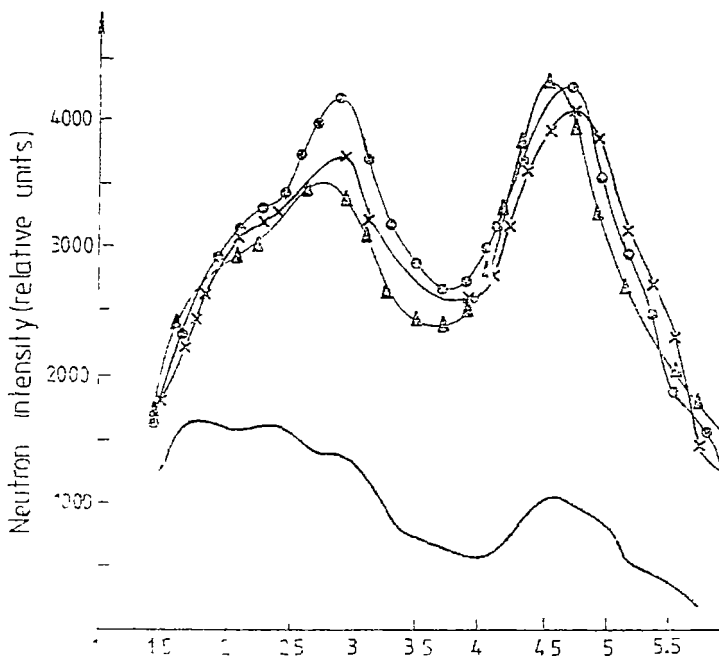


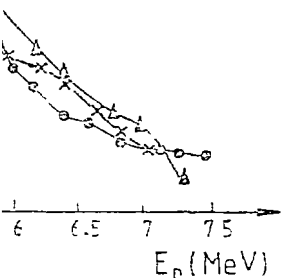
Fig 5 Neutron spectra used in cross section determination.

L DARABAN, T FIAT, E VARI-NAGY

cross section of ^{15}N

$$\sigma_{^{15}\text{N}}(E_n) = \frac{1}{N_{^{15}\text{N}}} \left\{ \left[1 - \frac{N_0(E_n)}{N(E_n)} - \frac{N_0(E_n)}{N_0(E_n)} \right] - \left[n_{\text{H}^2\text{O}}(E_n) + n_{\text{O}}(E_n) + n'_{^{14}\text{N}}(E_n) \right] \right\}$$

- ⊙ Incident spectra
- × Transmitted spectra in ^{15}N
- △ Transmitted spectra in ^{14}N
- Spectra with beam stopper



TOTAL CROSS SECTION DETERMINATION

We need to know the excitation functions of the oxygen, hydrogen and nitrogen - 14 (minor in this sample on this energetic domain) and the nucleus numbers in one volume unit n_{14N} , n_0 and n'_{14N}

But the utilisation of relation (12) is not the most comfortable way to measure the cross section of the ^{15}N with minimum error Therefore, we made a measurement in the same conditions on one natural sample NH_4NO_3 , having the same mass and geometrical form (the natural isotopical concentration of ^{15}N is 0,37%). We wrote for this sample a similar relation to (12) After that, we made the differences of the two relations

$$\begin{aligned} \sigma_{15N}(E_n) = & \sigma_{14N}(E_n) + \frac{1}{d n_{15N}} \ln \frac{N_0(E_n) - N_b(E_n)}{N_{15N}(E_n) - N_b(E_n)} - \\ & - \frac{1}{d n_{14N}} \ln \frac{N_0(E_n) - N_b(E_n)}{N_{14N}(E_n) - N_b(E_n)} + \left(\frac{n_H^{14}}{n_{14N}} - \frac{n_H^{15}}{n_{15N}} \right) \sigma_H(E_n) + \\ & + \left(\frac{n_0^{14}}{n_{14N}} - \frac{n_0^{15}}{n_{15N}} \right) + \frac{n'_{15N}}{n_{14N}} \sigma_{15N}(E_n) \frac{n'_{14}}{n_{15}N} \sigma_{14N}(E_n) \end{aligned}$$

Because we worked with samples having the same mass, we can prove that

$$\left(\frac{n_H^{14}}{n_{14N}} - \frac{n_H^{15}}{n_{15N}} \right) \sigma_H(E_n) = 0,03 \sigma_H(E_n)$$

(it will be neglected)

$$\left(\frac{n_0^{14}}{n_{14N}} - \frac{n_0^{15}}{n_{15N}} \right) \sigma_0(E_n) = 0,06 \sigma_0(E_n)$$

Relation (13) becomes

$$\begin{aligned} \left(1 - \frac{C'_{15N}}{C_{14N}} \right) \sigma_{15N}(E_n) = & \left(1 - \frac{C'_{14N}}{C_{15N}} \right) \sigma_{14N}(E_n) + \\ & + \frac{1}{d n_{15N}} \ln \frac{N_0(E_n) - N_b(E_n)}{N_{15N} - N_b(E_n)} - \frac{1}{d n_{14N}} \ln \frac{N_0(E_n) - N_b(E_n)}{N_{14N}(E_n) - N_b(E_n)} \end{aligned}$$

In that way, knowing the microscopic cross section of ^{14}N , we can find the microscopic cross section of ^{15}N . If we consider that the thicknesses of the sample are the same, using formula (2) we can turn relation (15) into another one, more useful

$$\begin{aligned} \left(1 - \frac{C'_{15N}}{C_{14N}}\right) \sigma_{15N}(E_n) &= \left(1 - \frac{C'_{14N}}{C_{15N}}\right) \sigma_{14N}(E_n) + \\ &+ \frac{1}{N_A} \frac{m_N^{\text{enriched}}}{S} \frac{A_{15N}}{C_{15N}} \ln \frac{N_0(E_n) - N_b(E_n)}{N_{15N}(E_n) - N_b(E_n)} - \\ &- \frac{1}{N_A} \frac{m_n^{\text{natural}}}{S} \frac{A_{15N}}{C_{15N}} \ln \frac{N_0(E_n) - N_b(E_n)}{N_{14N}(E_n) - N_b(E_n)} \end{aligned}$$

where $N_b(E_n)$ represented the spectrum measured by means of the beam stopper, $N_{14N}(E_n)$ is the spectrum transmitted through the natural sample, and A_{15N} and A_{14N} are the respective isotopical masses

We have made the calculation with relation (16), using the spectras from fig 5. We found out that the only sure values are those from the region of the two intense groups of the neutrons. This value is fulfilled the "good geometry" condition for the transmission factor.

The values obtained by, using formula (16) were placed over the excitation function given by [11, 12], our points being marked by *. Regarding the order of magnitude the results proved to be in accordance with the results given by [11, 12] (fig 6).

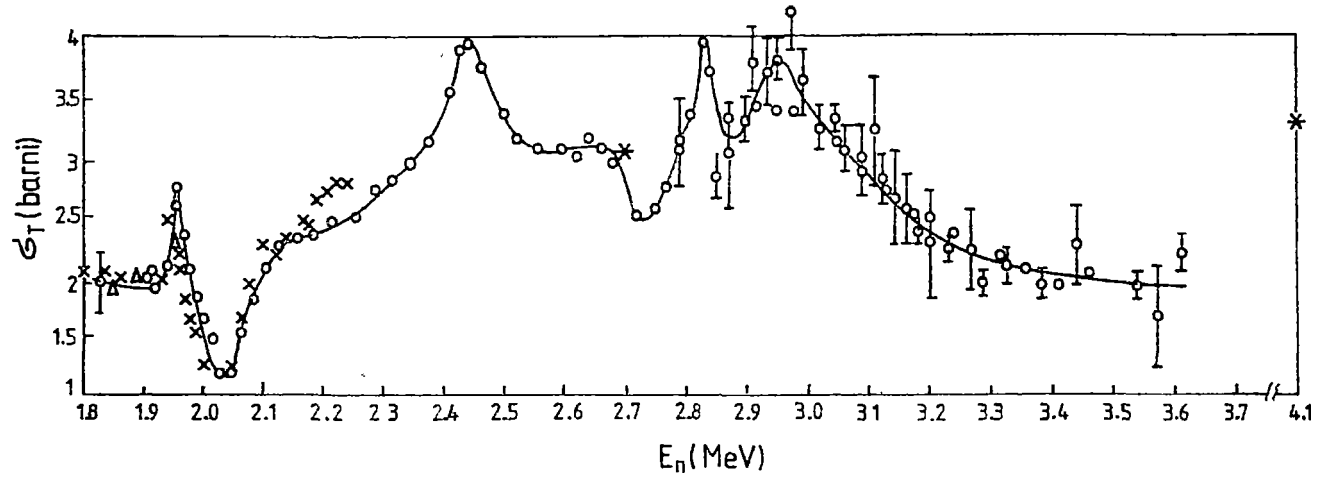


Fig 6 The excitation function of ^{15}N given by /11/, /12/ and our measurements are marked by *



TOTAL CROSS SECTION DETERMINATION

REFERENCES

- 1 K N Muhun, Fizică nucleară experimentală, vol I, Ed Tehnică, București, 1981
- 2 L Bratenahl et al , Phys Rev ,**110**,927 (1958)
- 3 Yu A Egorov, Scintilationu metod spectrometri gama izlucenu i bistrîh neutronov, Gostatomizdat, Moskva, 1963
- 4 M Bormann et al , Nucl Instr Meth., **92**, 61 (1971)
- 5 G Dietze, H Klein, Nucl Instr Meth , **193**, 549 (1981)
- 6 H W Broek, C E Anderson, Rev Sci Instr., **31**, 1063 (1960)
- 7 M Sîrbu, St Cerc Fiz , **38**, 714 (1986)
- 8 N M.N Wasson, The use of stilbene with decay time discrimination, as a fast neutron spectrometer, reprint AERE-R, 4169, U K , G B Harwele, Berkshire, 1963
- 9 V I Kuhtevich et al , At energia, **23**, 191 (1967)
- 10 J B Marion, J L Fowler, Fizica bistrîh neutronov, 231, Gostatomizdat, Moskva, 1963
- 11 A Ajzenberg-Selove, Nucl Phys , **A152**,6,43 (1970)
- 12 B N L 325, Neutron cross sections, supl 1, no 2, vol 1, z=1 to 20 (1964)

SPECTROSCOPIC INVESTIGATION OF THE INFLUENCE OF MELTING TEMPERATURE ON THE REDOX EQUILIBRIUM OF URANIUM IONS IN 0.95Na₂B₄O₇-0.05Al₂O₃-0.02UO₃ GLASS

E. CULEA and I. MILEA*

Received 15.06.1993

ABSTRACT. - The influence of the melting temperature on the redox equilibrium of uranium ions in the 0.93Na₂B₄O₇-0.05Al₂O₃-0.02UO₃ glass was studied using optical spectroscopy. The obtained optical data prove that increasing melting temperature determine the reduction of the U⁶⁺ ions to U⁴⁺ ions in the studied glass.

1. Introduction. Since glass is used to immobilization of nuclear waste [1,2] the study of glasses containing radionuclides becomes important. Uranium is one of the important radionuclides that appears in nuclear wastes. As was previously reported [3,4] uranium ions appear in oxide glasses in different valence state, such as U⁶⁺, U⁵⁺ and U⁴⁺. The study of redox equilibrium between these valence states is of considerable interest.

This paper presents the results of a spectroscopic investigation of the influence of the melting temperature on the redox equilibrium of uranium ions in the 0.93Na₂B₄O₇-0.05Al₂O₃-0.02UO₃ glass.

2. Experimental Method. Samples were prepared using reagent grade borax Na₂B₄O₇·10H₂O, Al₂O₃ ("Reactivul" Romania) and uranyl nitrate UO₂(NO₃)₂·6H₂O ("Chemapol" Czechoslovakia). First a borax glass was obtained by melting borax at 1000°C for 30 minutes. UO₃ was obtained by thermal decomposition of the uranyl nitrate. Then, adequate amounts of Na₂B₄O₇ (powdered glass), UO₃ and Al₂O₃ were melted to obtain the

* Technical University of Cluj-Napoca, 3400 Cluj-Napoca, Romania

0.93Na₂B₄O₇-0.05Al₂O₃-0.02UO₃ glass The samples were prepared using five different melting temperatures, namely 800, 900, 1000, 1100 and 1200°C The melts were equilibrated at these temperatures for 2 hours Glass samples were obtained as slabs (20x8x3 mm) by pouring the melts in a stainless steel piece having an appropriate groove

Optical absorption spectra for the visible and UV region(10,000-30,000cm⁻¹) were recorded using a Specord UV-VIS(Germany) spectrometer To obtain the optical spectra the glass slabs were polished on two opposite sides

3. Results and Discussion. All the samples containing UO₃ were yellow This suggests the presence of uranium ions mainly as U⁶⁺, probably in UO₂²⁺ (uranyl) form

The 0.02UO₃ content of the studied samples permits to obtain optical absorption spectra with well resolved spectral features A representative absorption spectrum of the 0.93Na₂B₄O₇-0.05Al₂O₃-0.02UO₃ glass for the UV and visible region is presented in figure 1 (spectrum 1)

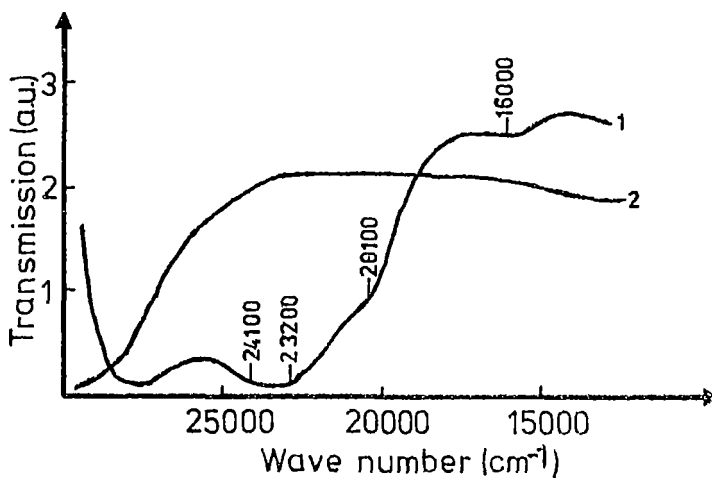


Fig 1 Optical spectra of 0.93Na₂B₄O₇-0.05Al₂O₃-0.02UO₃ (curve 1) and 0.93Na₂B₄O₇-0.05Al₂O₃ (curve 2) glasses

SPECTROSCOPIC INVESTIGATION

Spectrum 2 in this figure corresponds to the basic $0.93\text{Na}_2\text{B}_4\text{O}_7-0.05\text{Al}_2\text{O}_3$ glass. The comparison of the two spectra proves that the spectral features exhibit by spectrum 2 belong to the uranium ions. The spectroscopic features evidenced by this spectrum are characteristic for oxide glasses containing uranium ions[3,4]

The most important features of the $0.93\text{Na}_2\text{B}_4\text{O}_7-0.05\text{Al}_2\text{O}_3-0.02\text{UO}_3$ glass appear at about $16,000\text{cm}^{-1}$ (assigned to U^{4+} ions), $20,700\text{cm}^{-1}$ (assigned mainly to U^{6+} ions), $23,200\text{cm}^{-1}$ (assigned mainly to U^{4+} ions), and from $24,100\text{cm}^{-1}$ (assigned to U^{6+} ions). The assignments were made according to some previously reported data concerning some borosilicate and borate glasses[3,4]. We note that the positions of the absorption bands belonging to the U^{4+} and U^{6+} ions observed for the $0.93\text{Na}_2\text{B}_4\text{O}_7-0.05\text{Al}_2\text{O}_3-0.02\text{UO}_3$ glass are close to those reported for other borate and borosilicate glasses. This suggests the fact that the coordination sites of uranium valence states seem to be independent of glass composition.

The variation of the melting temperature generates some changes of the spectral features. These changes are shown in figure 2.

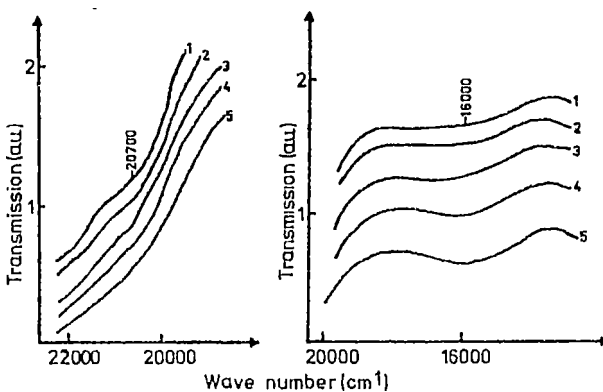
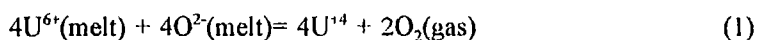
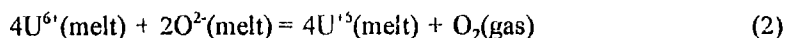


Fig 2 Changes produced in the optical spectra of the $0.93\text{Na}_2\text{B}_4\text{O}_7-0.05\text{Al}_2\text{O}_3-0.02\text{UO}_3$ glass by increasing the melting temperature (1 for 800°C , 2 for 900°C , 3 for 1000°C , 4 for 1100°C and 5 for 1200°C)

Thus increasing melting temperature generates the increase of the bands from 16,000 and 23,200 cm^{-1} and the decrease of the shoulder from 20,700 cm^{-1} . These changes indicate an increase of the amount of U^{4+} ions in the samples with increasing the melting temperature. The increase of the melting temperature of the samples seem to determine the reduction of the uranium ions according to the equation



It is possible that this process implies not only U^{6+} and U^{4+} ions but also U^{5+} ions and follows a two step process, according to the equations



Our spectroscopic data did not permit to evidentiate the presence of U^{5+} ions. However we do not exclude the possibility of appearance of U^{5+} ions, but we estimate that the 5+ valence state is probably less stable in the studied glass than 6+ and 4+ ones.

4. Conclusions. An optical spectroscopic investigation was made on the 0.93 $\text{Na}_2\text{B}_4\text{O}_7$ -0.05 Al_2O_3 -0.02 UO_3 glass in order to study the influence of the melting temperature on the redox equilibrium of the uranium ions. The obtained data indicate that the increasing melting temperatures determine the reduction of the U^{6+} ions to U^{4+} ions.

REFERENCES

- 1 J.L. Crandall, *Scient Basis Nucl Waste Mgmt*, 2(1980) 39
- 2 M.J. Plodinec, *Scient Basis Nucl Waste Mgmt*, 1, (1979) 31
- 3 H.D. Schreiber and G.B. Balasz, *Phys Chem Glasses* 23, 5(1982) 139 and H.D. Schreiber, G.B. Balasz, P.L. Jamison and A.P. Shaffer, *Phys Chem Glasses* 23, 5(1982) 147
- 4 E. Culea, I. Milea and I. Bratu, *J Molec Struct* 291 (1993) 271

In cel de al XXXVIII-lea an (1993) *Studia Universitatis Babeş-Bolyai* apare în următoarele serii:

matematică (trimestrial)
fizică (semestrial)
chimie (semestrial)
geologie (semestrial)
geografie (semestrial)
biologie (semestrial)
filosofie (semestrial)
sociologie-politologie (semestrial)
psihologie-pedagogie (semestrial)
ştiinţe economice (semestrial)
ştiinţe juridice (semestrial)
istorie (semestrial)
filologie (trimestrial)
teologie ortodoxă (semestrial)
educaţie fizică (semestrial)

In the XXXVIII-th year of its publication (1993) *Studia Universitatis Babeş-Bolyai* is issued in the following series

mathematics (quarterly)
physics (semesterly)
chemistry (semesterly)
geology (semesterly)
geography (semesterly)
biology (semesterly)
philosophy (semesterly)
sociology-politology (semesterly)
psychology-pedagogy (semesterly)
economic sciences (semesterly)
juridical sciences (semesterly)
history (semesterly)
philology (quarterly)
orthodox theology (semesterly)
physical training (semesterly)

Dans sa XXXVIII-e année (1993) *Studia Universitatis Babeş-Bolyai* paraît dans les séries suivantes:

mathématiques (trimestriellement)
physique (semestriellement)
chimie (semestriellement)
géologie (semestriellement)
géographie (semestriellement)
biologie (semestriellement)
philosophie (semestriellement)
sociologie-politologie (semestriellement)
psychologie-pédagogie (semestriellement)
sciences économiques (semestriellement)
sciences juridiques (semestriellement)
histoire (semestriellement)
philologie (trimestriellement)
théologie orthodoxe (semestriellement)
éducation physique (semestriellement)

CONTENTS

Molecular Physics and Spectroscopy

- P. ARDELEAN, F. DUNCA, C. CUNA, D. IOANOVICIU, A. PAMULA, C. ARDELEAN, L. MALZ. Medium Size Normal Cicle Bounded Homogenous Magnetic Field Single Focusing Mass Spectrometer with Improved Resolution 3
- M. CULEA, N. PALIBRODA, S. NICOARĂ, O. COZAR, I. OPREAN, I. FENEȘAN. Electron Impact Fragmentation of Some Thionic - Dioxo - Phosphorinan-Arylsulphonamidic Derivatives 11
- T. ILIESCU, S. SIMON, I. ARDELEAN, N. MARTON. Raman Spectroscopic Study of the Structure of B₂O₃ -Li₂O-CuO Glasses 23
- G.V. DAMIAN. Comparison of Interaction Energies for Methane Using Buckingham and Lennard-Jones Potentials 31

Plasma Physics

- S. D. ANGHEL. A RF - Generator for Capacitively Coupled Plasma at Atmospheric Pressure 39
- S. COLDEA. Application of the Simulation Method for a Gyrotron Amplifier 53

Theoretical Physics

- D. JALOBEANU, L. TĂȚAR. The BRST-BV Symmetry in Classical Mechanics 63
- I. ARDELEAN. Thermodynamic Theory of Cross - Polarization in a NMR - Moist Experiment 69
- S. CODREANU. The Reconstruction of the State Space from Chaotic Time Series 75
- A. MIHALY. The Behaviour of the Nucleon Spin in a Periodic Phase of the Nuclear Matter 89